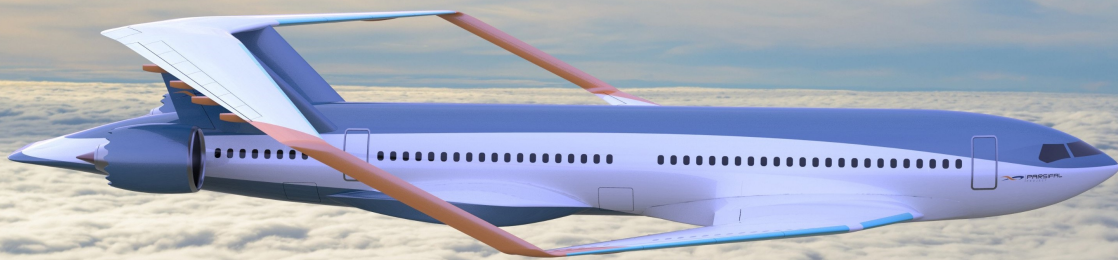


The Impact of Control Allocation on Optimal Control Surface Positioning and Sizing

A comparative study for a PrandtlPlane

N.F.M. Wahler



Front page image: Artist impression of the PARSIFAL box wing project,
see <https://parsifalproject.eu/>

The Impact of Control Allocation on Optimal Control Surface Positioning and Sizing

**A comparative study
for a PrandtlPlane**

by

N.F.M. Wahler

to obtain the degree of Master of Science
at the Delft University of Technology,
to be defended publicly on Friday February 19, 2021 at 09:00.

Student number:	4446976
Project duration:	May 20, 2020 – February 19, 2021
Thesis committee:	Dr. ir. G. la Rocca, TU Delft
	Dr. F. Oliviero, TU Delft
	C. Varriale MSc TU Delft
	Dr. ir. E. van Kampen TU Delft

Executive Summary

Classically, aircraft controls are designed such that every distinct type of control effector primarily influences a single degree of freedom by creating a moment. Increased availability of computational resources and novel aircraft configuration allow a deviation from this approach and to utilize every control surface as an individual effector to generate moments around multiple axes. Control allocation, the combination of control effector functions, is especially interesting for a PrandtlPlane. The unique geometry of two full wings allows more flexibility in control surface (CS) placement while retaining control effectiveness. Where a conventional aircraft is restricted in position for effective ailerons and elevators, the PrPs wings allow the placement of extra control surfaces.

This research aims to investigate the impact of control allocation algorithms on the required control surface span and area for a PrandtlPlane. A new optimization system for automatic control surface sizing under the constraints of adequate handling qualities has been developed. Three options are implemented for the control allocation: mechanical gearing (MG), constrained pseudo inverse (CPI) and direct allocation (DA). MG uses a predetermined gearing matrix to determine the deflections. CPI is a simple allocation algorithm using a linear least squares approach. DA uses an optimisation routine to find the control vector. The framework consists of the optimizer, an aerodynamics and a handling and flying quality evaluation module. The current framework has two objective functions implemented for the studies, minimum total CS span and minimum total CS area. For the aerodynamic calculations the linear solver AVL is used. The flight mechanics discipline is evaluated using the in-house developed Performance, Handling Qualities and Load Analysis toolbox (PHALANX), which is programmed in Matlab and Simulink. The model created by PHALANX is used to investigate a selection of different handling and flying quality criteria, that are typically required for the certification of a full aircraft design. The selected tests and their target values are extracted from the MIL-F-8785C. Tests are run at two design points of the aircraft, at cruise and at the approach phase, as well as two different wind conditions.

Results show that the advanced control allocation methods achieve smaller control surface layouts with respect to classic mechanical gearing, in terms of total control surface span or area. Regarding the minimum span objective function, MG requires the largest overall CS span. CPI reduces the total required span width by about 9.5%. DA reduces the required span width further, achieving a reduction of about 17% compared to MG. A sensitivity analysis showed that different CS layouts can be equally optimal. Regarding the minimum area optimization results, MG again requires the largest CS. CPI reduces this area about 8%. DA is able to reduce the required size further, achieving a reduction of about 26% compared to MG. An application example shows that the classic layout is not optimal. Improvements can be seen if the inner rear surface is positioned further mid-wing compared to the initial layout. This can reduce the required CS span width by another 14%.

The results show that the PrP configuration can benefit from the use of control allocation algorithms. The second full size wing gives flexibility to the positioning of the control surfaces. Hence, effectors can be placed in such a way that they are very efficient in providing both a pitching and rolling moment. The improved capabilities are only harnessable because of the control allocation, classic mechanical gearing would be unable to operate these surfaces in the most efficient way.

Preface

This thesis marks the conclusion of five and a half years of aerospace studies in Delft. It was a laborious time, but I learned a lot about aviation and the engineering challenges it poses. I was always fascinated by new and unconventional aircraft configurations. Hence the PrandtlPlane specifically sparked my interest.

I am very grateful to Prof. Gianfranco La Rocca for giving me the opportunity to perform my Master research project on this concept in the Flight Performance research group and for his guidance and support. My gratitude extends to Carmine Varriale, who helped me shape the topic. I am especially grateful to him for his time investments and the many very helpful discussions we had. I am also very thankful to Prof. van Kampen and Dr. Oliviero for being on my defense committee and their willingness to join it on such short notice.

Furthermore, I would like to thank my parents for their continuing support and patience during the whole study period. I am thankful to my friends Maria, Andy and the team from the SSVOB Lambach Aircraft for their friendship, mental support and a lot of fun time throughout all of my studies.

*N.F.M. Wahler
Delft, February 2021*

Contents

List of Figures	ix
List of Tables	xiii
Nomenclature	xv
1 Introduction	1
1.1 Research context	1
1.2 Research Objective	2
1.3 Research Questions.	3
2 The Box-wing aircraft	5
2.1 Aerodynamic background	5
2.2 The PrandtlPlane	9
2.2.1 Stability and control considerations	10
2.3 Conceptual Design Studies	11
2.3.1 The PARSIFAL project	12
2.4 Control surface design in boxwings.	14
2.5 Handling Qualities	17
2.5.1 Handling qualities overview	17
2.5.2 Handling qualities in box-wings.	19
3 Control Allocation	21
3.1 Pseudo Inverse	24
3.2 Direct allocation	25
4 The optimisation framework	29
4.1 The optimiser.	29
4.1.1 Objective functions	30
4.1.2 Constraints.	30
4.1.3 Optimiser settings.	31
4.1.4 Implementation overview	31
4.2 PrandtlPlane geometry	33
4.3 Aerodynamics	33
4.3.1 Vortex lattice method.	34
4.3.2 Implementation	36
4.4 Flight mechanics.	38
4.5 Handling and flying qualities	39
4.6 Hardware and Software.	41
5 Verification	43
5.1 Aerodynamics	43
5.2 Control allocation	43
5.3 System test	44

6 Results and Discussion	47
6.1 Minimum span objective function	48
6.1.1 Optimiser behaviour	49
6.2 Sensitivity analysis	54
6.3 Minimum area objective function	56
6.4 Proposed improved CS placement on the rear wing	59
6.5 Attainable moment set	62
7 Conclusions and Recommendations	65
Bibliography	66
A Detailed optimisation results	71
A.1 Detailed optimisation results for minimum span objective function.	71
A.2 Detailed optimisation results for minimum area objective function	74
A.3 Detailed optimisation results for improved rear CS placement minimum span objective function	76
B Exploring the effect of higher control surface numbers	79

List of Figures

2.1	Drag efficiency for different span ratio and vertical spacing [4]	7
2.2	Lift distribution on ideal boxwing [3]	7
2.3	Ideal pressure distribution on a boxwing according to Prandtl [4]	7
2.4	Drag reduction for boxwing compared to other multiplanes [4]	8
2.5	Comparison between Frediani's and Prandtl's results [19]	8
2.6	Demasi's solution to an unequal lift distribution [21]	9
2.7	Forces and moments on a boxwing [22]	10
2.8	3-side view of the PARSIFAL PrandtlPlane ¹	13
2.9	Classical control surface layout applied to PrP [15]	14
2.10	Trade-off independent versus combined controls from van Ginneken et al. [12]	15
2.11	Control surface effectiveness results from Varriale [14]	16
2.12	Longitudinal and lateral sizing criteria overview for control surfaces [31]	18
3.1	Control system structure including control allocation [18]	22
3.2	Mapping of the admissible control set to the attainable moment set through control effectiveness matrix B [36]	23
3.3	Comparison of a 2-dimensional moment set with pseudo-inverse (dashed lines) as subset of the AMS (solid lines) [35]	24
3.4	Comparison of greatest attainable moment set (GAMS) with attainable moment sets from pseudo-inverse (PSINV) and direct allocation (DCA). Note that the GAMS and DCA are not distinguishable graphically as they are equal. [36]	26
3.5	Direction preserving solution for an unattainable moment command [35]	27
4.1	XDSM diagram of developed framework	29
4.2	Overview scheme of control surface sizing optimisation system	32
4.3	Parsifal Milestone 1 geometry shape used for this study	33
4.4	Vortex distribution on a flat surface in VLM solver [40]	35
4.5	Detailed view on horseshoe vortex [41]	36
4.6	Top level overview of PHALANX workflow [14]	39
5.1	Steady aerodynamic coefficient comparison between VSAero and AVL for a Cessna Citation II	44
5.2	Geometry and CS layout of Varriale [14]	45
5.3	Verification comparison of mean MG layout to results from Varriale [14]	45
6.1	Initial layout of the study case showing the non-dimensional CS span widths and bounds	48
6.2	CS size comparison for minimum span objective	49
6.3	Objective function development for minimum span for mechanical gearing (MG), constrained pseudo inverse (CPI) and direct allocation (DA)	50
6.4	Non-dimensional span width design variables behaviour for MG	50
6.5	Non-dimensional span width design variables behaviour for CPI	51
6.6	Non-dimensional span width design variables behaviour for DA	51

6.7	Scaled trim and OEI constraints for MG	52
6.8	Scaled trim and OEI constraints for CPI	52
6.9	Scaled trim and OEI constraints for DA	52
6.10	Scaled HFQ constraints for MG	53
6.11	HFQ constraints behaviour for CPI	53
6.12	HFQ constraints behaviour for DA	53
6.13	CS size comparison using MG for minimum span objective	55
6.14	CS size comparison using CPI for minimum span objective	55
6.15	CS size comparison using DA for minimum span objective	55
6.16	CS total span width objective development using MG for minimum span objective	56
6.17	CS total span width objective development using CPI for minimum span objective	56
6.18	CS total span width objective development using DA for minimum span objective	56
6.19	CS results for minimum area objective	57
6.20	CS total wing area objective development for minimum area objective	58
6.21	CS layout for the cases A, B and C. Both inner and the outer rear CS are equal for all cases	60
6.22	Final CS layout comparison of cases A, B and C using DA for minimum span	61
6.23	CS total span width objective development using DA for minimum span objective with improved layout	61
6.24	Comparison of AMS for initial and optimised CS span for the MG algorithm	62
6.25	Comparison of AMS for initial and optimised CS span for the CPI algorithm	63
6.26	Comparison of AMS for initial and optimised CS span for the DA algorithm	63
6.27	Volume of the AMS for initial and end points of all minimum span optimisations as function of CS span width: MG (blue), CPI (red), DA (green) and improved cases (grey)	64
A.1	CS span development for MG 2	71
A.2	Trim and OEI constraints for MG 2	71
A.3	HFQ constraints for MG 2	72
A.4	CS span development for MG 3	72
A.5	Trim and OEI constraints for MG 3	72
A.6	HFQ constraints for MG 3	72
A.7	CS span development for CPI 2	72
A.8	Trim and OEI constraints for CPI 2	72
A.9	HFQ constraints for CPI 2	73
A.10	CS span development for CPI 3	73
A.11	Trim and OEI constraints for CPI 3	73
A.12	HFQ constraints for CPI 3	73
A.13	CS span development for DA 2	73
A.14	Trim and OEI constraints for DA 2	73
A.15	HFQ constraints for DA 2	74
A.16	CS span development for DA 3	74
A.17	Trim and OEI constraints for DA 3	74
A.18	HFQ constraints for DA 3	74
A.19	CS span development for MG	75
A.20	Trim and OEI constraints for MG	75
A.21	HFQ constraints for MG	75
A.22	CS span development for CPI	75
A.23	Trim and OEI constraints for CPI	75
A.24	HFQ constraints for CPI	75

A.27 HFQ constraints for DA	76
A.25 CS span development for DA	76
A.26 Trim and OEI constraints for DA	76
A.28 CS span width development for case B	77
A.29 Trim and OEI constraints for case B	77
A.30 HFQ constraints for case B	77
A.31 CS span width development for case C	77
A.32 Trim and OEI constraints for case C	77
A.33 HFQ constraints for case C	77
B.1 Initial layout for the three CS investigation	80
B.2 Resulting layout of three individual CS using DA for minimum area	81
B.3 Resulting layout of four individual CS using DA for minimum area	81
B.4 Aerodynamic moment coefficients from AVL for a CS at ± 30 degrees deflection as function of non-dimensional span width	81
B.5 CS span width development for three individual CS per wing	82
B.6 CS inboard position development for three individual CS per wing	82
B.7 Trim and OEI constraints for three individual CS per wing	82
B.8 HFQ constraints for three individual CS per wing	82
B.9 Resulting layout of three connected CS using DA for minimum area	83
B.10 Resulting layout of four connected CS using DA for minimum area	83
B.11 CS span width development for three connected CS per wing	84
B.12 CS inboard position development for three connected CS per wing	84
B.13 Trim and OEI constraints for three connected CS per wing	84
B.14 HFQ constraints for three connected CS per wing	84

List of Tables

2.1	Mil-F-8785C Aircraft classes [28]	19
2.2	Mil-F-8785C Levels of acceptability [28]	19
4.1	Options for fmincon	31
4.2	Geometric input parameters defining the main wings of the aircraft	34
4.3	Geometric input parameters defining the tailplanes of the aircraft	34
4.4	Coefficients obtained from AVL analysis	37
4.5	Handling and flying quality test matrix used as constraints in the optimisation	40
4.6	Sample computational time breakdown for one function evaluation	41
6.1	Initial values for the design variables and bounds	47
6.2	Resulting objective function values for minimum span objective function	48
6.3	Resulting CS sizes as fraction of wing span for the minimum span optimisation	49
6.4	Sensitivity analysis for minimum span objective function. The initial layout described the initial point with the distribution: inner front/outer front/inner rear/outer rear	54
6.5	Resulting objective function values for minimum area objective function	57
6.6	Resulting CS sizes as fraction of wing span for minimum area objective function	57
6.7	Initial values for the design variables and bounds for the three cases A,B and C	59
6.8	Span objective result comparison between cases A, B and C	60
6.9	CS size comparison between the cases A,B and C	60
B.1	Initial value and bounds for three surface individual optimisation	80
B.2	Resulting CS position and sizes as fraction of span of three connected surfaces for minimum area	83
B.3	Resulting CS position and sizes as fraction of span of four connected surfaces for minimum area	83

Nomenclature

List of Abbreviations

AMS	Attainable Moment Set
AVL	Athena Vortex Lattice
CG	Center of Gravity
CPI	Constrained Pseudo Inverse
CS	Control Surface
DA	Direct Allocation
EASA	European Aviation Safety Authority
FAA	Federal Aviation Authority
GAMS	Greatest Attainable Moment Set
HFQ	Handling and FlyingQualities
MG	Mechanical Gearing
MTOM	Maximum Take-Off Mass
PrP	PrandtlPlane

List of Symbols

η_i	Normalised control surface inboard location	[–]
Γ	Circulation	[–]
κ	ratio of biplane and monoplane induced drag	[–]
λ	LaGrange multiplier for pseudo inverse allocation	[–]
Φ	Attainable moment set	[–]
ρ	Air density	$[kg/m^3]$
α	Angle of attack	$[rad]$

ϵ	Downwash angle	[rad]
τ_c	Commanded virtual control force vector	[–]
τ	Virtual control force vector	[–]
A_s	State matrix	[–]
B_s	Control effectiveness matrix	[–]
C_L	Lift coefficient	[–]
C_M	Pitching moment coefficient	[–]
C_s	Output matrix	[–]
$C_{L\alpha^2}$	Lift curve slope of isolated aft wing	[1/rad]
$C_{L\alpha}$	Lift curve slope of whole aircraft	[1/rad]
D	Drag	[N]
D_i	Induced drag	[N]
G	Vertical distance between the wings	[m]
L	Lift	[N]
M	Wing pitching moment	[Nm]
N	Placeholder matrix for generalised inverse	[–]
P	Generalised inverse matrix	[–]
\bar{c}	Average chord	[m]
b	Wing span	[m]
g	Gravitational acceleration	[m/s ²]
h	Location of center of gravity as fraction of forward wing chord $\frac{x_{cg}}{\bar{c}}$	[–]
l	Distance from center of gravity to rear wing aerodynamic center	[m]
l'	Distance from front to rear wing aerodynamic center	[m]
l_v	Length of vortex filament	[m]
n	Load factor	[–]
n_0	Maximum load factor	[–]

p, q, r	aerodynamic rates roll, pitch, yaw	[–]
q_∞	Dynamic pressure	[Pa]
r	Distance between vortex and control point	[m]
r_w	Ratio of wing spans $\frac{b_2}{b_1}$	[–]
s	Relative wing reference area	[m ²]
w	Normal velocity	[m ³ /s]
w_i	Normalised control surface span width	[–]
x_w	Fraction of top wing lift of total lift	[–]
$\dot{\mathbf{x}}$	Time derivative of state vector	[–]
\mathbf{m}_{des}	Desired aerodynamic moment	[Nm]
\mathbf{u}	Control vector	[–]
$\mathbf{u}_{min,max}$	Lower/Upper limit of control effector deflection	[rad]
\mathbf{x}	State vector	[–]
\mathbf{y}	Output vector	[–]

Introduction

1.1. Research context

Global aviation used to be a growing economy. With an average annual growth rate of 3.6%, forecasts predicted that the amount of air transport passengers will nearly double to 7.8 billion travelers per year by 2036 [1]. While the current COVID 19 pandemic is severely impacting the global travel industry and the aviation market, this sector will eventually recover to the previous levels [2]. Global warming and its implications are becoming increasingly relevant. With this increasing ecological awareness, it is imperative for the global aviation industry to invest in research and development of novel airframe configurations and engine technologies.

A potential contender in the search for unconventional configurations is the PrandtlPlane (PrP) aircraft [3]. This layout uses two wings that are connected at the wing tips in a way to create a closed box. Prandtl has shown that this wing layout can yield the lowest possible induced drag when properly designed [4, 5]. However, the concept has never been used in commercial transport aircraft. With increasing pressure to make aviation more sustainable, the concept has gained new interest in the scientific and professional community [3, 6, 7]. Different concept studies were performed which have shown the aerodynamic advantages of such a layout over the conventional design. They have also shown that these aircraft are most efficient in high density, short-to-medium range flights [8–10]. For these flights, a larger fraction of the mission is spent in climbing and descending phases, where induced drag is typically of higher relevance. Hence, a reduction in this drag component would yield the largest benefits. This study is based on the Parsifal project, which was funded by the European Commission within the Horizon 2020 program to design a medium-sized PrP.

A distinguishing feature of the PrandtlPlane concept are the two wings and their implications [11]. Having two full size wings allows additional control surface space and freedom regarding the placement of control surfaces [12]. These can now be spread over both wings, hence the control surface function is not determinate anymore. The geometry allows new configurations, such as outboard surfaces on both wings for roll control, or elevators on the front wing as well. Effective Additional surfaces can be placed to increase redundancy in case of failure, alleviate gust loads or improve the overall aerodynamic efficiency in maneuvering flight [13]. Another potential benefit is the possible implementation of direct lift or pure moment control, where the surfaces on both wings are deflected in the same or opposite direction respectively. While many studies have performed preliminary sizing of the aerodynamic shape and its dynamic behavior, the newly available design space for control surface placement and design has rarely been investigated [12]. Current PrP studies are limited to a deterministic approach in control surface design, by assigning explicit roll, pitch and yawing moment generation to distinct and

individual control surfaces [14–16]. This classic layout is imposed on the box-wing concept by both wings having elevator surfaces at the wing roots and ailerons at the wing tips. For this, a mechanical gearing approach is used. The control surfaces are ganged together such that all pitch control surfaces move together to create the pitching moment. The roll control surfaces are ganged similarly.

Gearing is the simplest method of control allocation. This classic approach however may not be optimal anymore with the given wing geometry. Modern control allocation algorithms can utilise all control surfaces in a given set independently, hence allowing each surface to contribute to each aerodynamic moment [17, 18]. The use of these algorithms increases the attainable moment set of the control surface layout as conventional gearing constraints are removed. For a given moment set, the total size of the required control effectors is expected to be reduced.

1.2. Research Objective

The research objective of this thesis is to assess the impact of control allocation methods on optimal control surface arrangements. The comparison is made between a classic control system using mechanical gearing and two different modern control allocation methods. With application to a PrP aircraft configuration, the control surface layout is optimised to obtain required levels of handling qualities.

The methodology for this research is derived from a software framework developed by Varriale [14], which automatically sizes the control surfaces under the constraints of adequate handling qualities. The study has only investigated separate control surfaces using mechanical gearing. The new research presented in this thesis will focus on expanding this framework and formalizing a more general approach to the optimisation system that allows more flexibility on the control surface assignments.

The formulation will allow each control surface to deflect independently, and the inclusion of a control allocation algorithm determines the optimal deflection of all control effectors to achieve the desired motion. This increased flexibility in control surface deflection and combination will allow the PrP design to fully show the strength of having a full-size second wing for the placement of additional control surfaces.

As a first step, the computational optimisation framework needs to be created. This framework will consist of two main modules: an aerodynamic solver to provide the aerodynamic coefficients for a given set of control surfaces and a flight mechanics toolbox that can analyse the handling quality criteria. An overarching optimisation function provides a wrapper for the two disciplines. The framework should be able to update its aerodynamic database for every function evaluation. Thus, an aerodynamic solver shall be implemented that is simple enough to be fast, yet providing reliable results of the actual aerodynamic behavior. The handling quality analysis is the main criteria by which the sizing is performed. For this, the use of a toolbox that can adequately model dynamic behavior is required. This must include an integrated control allocation method to determine control surface deflections for each maneuver.

Once the actual framework is completed, it will be used to investigate aspects of the overall control surface layout. Investigations will analyse the obtainable reductions in control surface size, compared to the mechanical gearing. A comparison of control allocation methods and classic gearing for a given number of control surfaces is performed. This will show the differences in layout that can be achieved when the control surfaces are not geared anymore, but free to deflect individually. As an application, a modified control surface position is proposed showing the flexibility that the PrP layout can provide using control allocation.

The motivation of investigating this novel application of control allocation is to analyse and highlight the benefits of the PrP concept, and to challenge the currently used control surface

arrangement and use.

1.3. Research Questions

The proposed research question resulting for this study is hence:

What is the effect of control allocation methods on the design of the control surface arrangement of a box-wing aircraft?

1. How does the control surface layout change using control allocation for given handling quality requirements?
 - (a) How much does the minimum required total control surface span change for different control allocation algorithms?
 - (b) How much does the minimum required total control surface area change for different control allocation algorithms?
2. To what extent does the inherent attainable moment set of different control allocation methods influence the control surface layout?
3. Is the classic arrangement of control surfaces optimal for a box-wing aircraft?

Finding answers to these questions requires the creation and use of the optimisation framework. Chapter 2 gives background information on the box-wing concept and the current state of design and research regarding control surface placement. Control allocation and the specific algorithms used in this study are described in chapter 3. Next, the actual framework layout and all disciplines within are explained in chapter 4. Chapter 5 shows the performed verification to the framework. This framework is then applied to the PrP geometry and the results of the investigations are shown and discussed in chapter 6. Lastly, chapter 7 states the conclusions drawn from the discussion and presents some recommendations for future research.

2

The Box-wing aircraft

In the past years, scientific interest in the box-wing aircraft concept has risen again. Albeit not a new concept, it was never really taken as a serious competitor to the currently dominant tube-and-single-wing designs. This is of course due to the increasing complexity of such a configuration and the associated risks in development of new airframe technology. This chapter aims to give a background in the aerodynamic peculiarities and potential benefits of the box-wing, as well as the current state of research in control surface design.

2.1. Aerodynamic background

In 1924, German aerodynamicist Ludwig Prandtl researched the drag behavior of multiplanes of different configurations [4]. He concluded that there is a specific configuration for a biplane that results in minimum induced drag. This optimum condition can be achieved when the lift is equal on both wings and the distribution is elliptical on both. He further concluded that this result holds for designs with more wings. An optimum triplane exists with the induced drag lower than that of a biplane. This is achieved by having the top and bottom wing loaded elliptically and the center wing such that the lift decreases to zero in the symmetry plane. He further proves that this conclusion is valid for an infinite amount of wings. For a high number of wings, this means that each wing has a very low contribution of the total lift on the inboard sections, and hence can be approximated as a horseshoe vortex at the wingtip. Extrapolating this result to an infinite amount of wings means that the infinite number of intermediate wings that are approximated by a tip vortex only could then be replaced by a vertical vortex sheet connecting the top and bottom wing. Hence, this can be represented by a box where the side panels are equivalent to the tip vortices, and elliptically loaded top and bottom wings. This box design is what Prandtl describes as the 'best wing system'.

Prandtl's reasoning and the conclusions he draws from his analysis is shown in the following [4]. His starting point, the induced drag of a wing is a function of the circulation over the wing, the air density and the vertical velocity induced by the trailing vortex (Eq. 2.1). In the case of a monoplane with an elliptical lift distribution, this results in Eq. 2.2.

$$D_i = \rho \int_{-\frac{b}{2}}^{\frac{b}{2}} w(y)\Gamma(y)dy \quad (2.1)$$

$$D_i = \frac{L^2}{q_\infty \pi b^2} \quad (2.2)$$

For a biplane, the total induced drag is the sum of the induced drag of all lifting components and the interaction between them. This is given in Eq. 2.3. The first two terms denote the self-induced drag of the wings, the latter the drag induced by the wing and trailing vortices of the respective other wing. For this derivation it was assumed that both wings are loaded elliptically as well, same as the monoplane. The last term is a combination of both interaction effects. The subscripts 1,2 denote the respective wing, v_{12} and b_{avg} are defined in Eq. 2.4.

$$D_i = D_{11} + D_{22} + D_{12}^* + D_{21}^* = \frac{L_1^2}{q_\infty \pi b_1^2} + \frac{L_2^2}{q_\infty \pi b_2^2} + \rho \Gamma_1 \Gamma_2 \frac{4v_{12}}{\pi} \quad (2.3)$$

$$v_{12} = \frac{1}{4} \ln \left(\frac{\sqrt{b_{avg}^2 + G^2}}{\sqrt{(b_2 - b_1)^2 + G^2}} \right) \quad b_{avg} = \frac{b_1 + b_2}{2} \quad (2.4)$$

Assuming further that the circulations are invariant across the span, this can be simplified to Eq. 2.5.

$$D_i = D_{11} + D_{22} + D_{12}^* + D_{21}^* = \frac{1}{q_\infty \pi} \left(\frac{L_1^2}{b_1^2} + \frac{L_2^2}{b_2^2} + 2v_{12} \frac{L_1 L_2}{b_1 b_2} \right) \quad (2.5)$$

For an arbitrary split of the total lift between the two wings, $L_1 = L(1 - x_w)$, $L_2 = Lx_w$, and $r_w = \frac{b_2}{b_1}$, then Eq. 2.6 gives a function for the optimum total lift fraction factor x_w that results in minimum drag. Using this expression in the induced drag formula gives Eq. 2.7. This is now the full equation for minimum induced drag of the biplane.

$$x_w = \frac{r_w - v_{12}}{r_w + \frac{1}{r_w} - 2v_{12}} \quad (2.6)$$

$$D_i = \frac{L^2}{\pi q_\infty b_1^2} \frac{1 - v_{12}}{r_w \left(r_w + \frac{1}{r_w} - 2v_{12} \right)} \quad (2.7)$$

If the wing spans are equal, that is $b_1 = b_2 = b$, then this formula shows that the minimum induced drag is obtained when the lift distribution on the two wings is equal. It furthermore shows that the drag now solely depends on the vertical spacing $\frac{b}{G}$ on the structure; within the v in Eq. 2.8.

$$D_i = \frac{L^2}{q_\infty \pi b^2} \left(\frac{1}{2} + \frac{1}{2} v_{12} \right); \quad v_{12} = \frac{1}{4} \ln \left(\sqrt{\frac{b^2}{G^2} + 1} \right) \quad (2.8)$$

Eq. 2.8 shows further that the induced drag of the biplane is less than that of the monoplane while v_{12} is less than 1. This is true if $\frac{b^2}{G^2} \leq e^8$. Hence, the larger the vertical spacing, the more pronounced the benefits. For an infinite vertical distance, the biplane will have half the induced drag compared to a monoplane. Fig. 2.1 shows this relation. It shows the ratio of biplane induced drag over monoplane induced drag (κ) as function of span ratios (r) and vertical placement ($\frac{G}{b_1}$).

Prandtl furthermore details the benefits of a closed box system with side wings with a non-zero lift component. The optimum lift distribution is then the sum of a constant and an elliptic part on the horizontal wings, where the induced velocity is constant in the optimum case. The

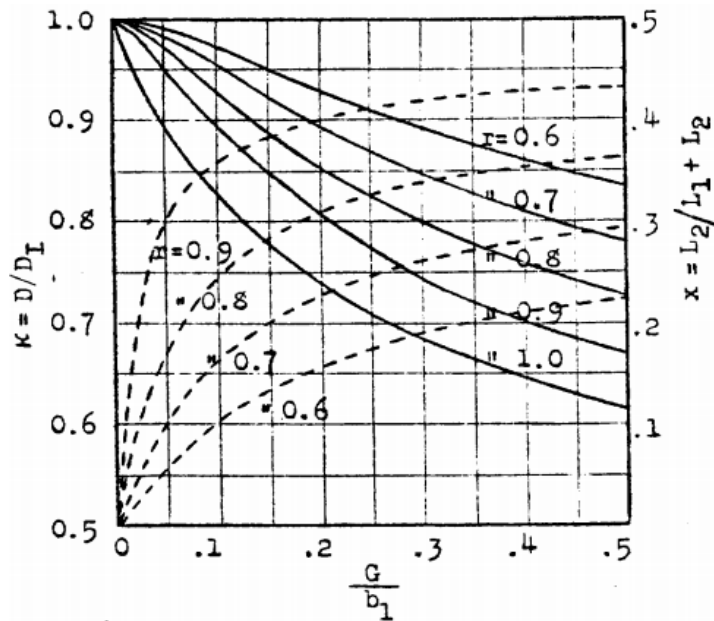


Figure 2.1: Drag efficiency for different span ratio and vertical spacing [4]

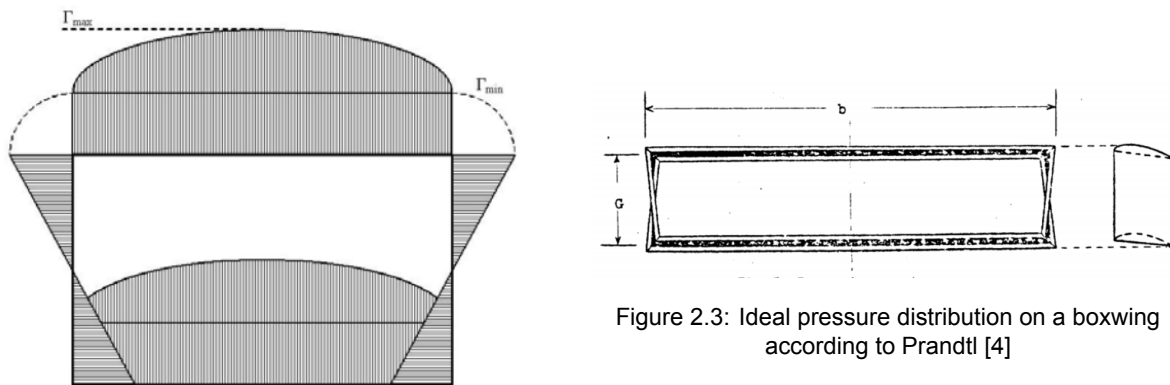


Figure 2.2: Lift distribution on ideal boxwing [3]

vertical wings have a butterfly force distribution. The upper portion has an outward facing force distribution, the lower portion inward facing, as shown in Fig. 2.2.

This is what he describes as the 'best wing system'. The ideal box-wing according to Prandtl is shown in Fig. 2.3. Following from this geometry, he made further analysis on the efficiency and compiled them in Fig. 2.4. This plot shows the benefit of the boxwing compared to ideal bi- and triplanes. It furthermore shows that the benefits increase for increasing vertical distance between the wings. For the range of practical interest of the h/b ratio of 0.1-0.2, the best wing system predicts induced drag reductions between 20-30% [3] with respect to a monoplane.

Prandtl used some simplifying assumptions and hence his results are only approximate. Frediani and Montanari [19] formalised the problem and used numerical optimisation to create an exact solution for the minimum induced drag. They showed that Prandtl's equation holds well for small values of the vertical ratio, but becomes overoptimistic for larger values as shown in figure 2.5.

Munk [20] also investigated multiplanes. His stagger theorem dictates that a displacement

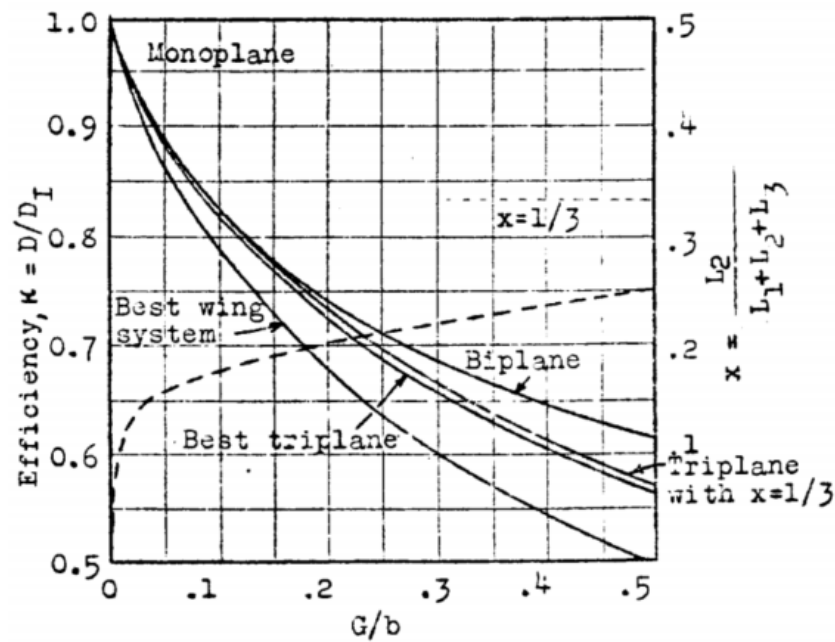


Figure 2.4: Drag reduction for boxwing compared to other multiplanes [4]

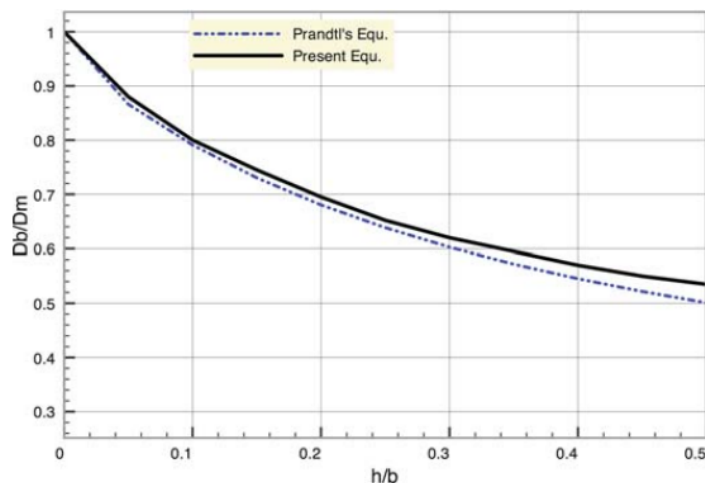


Figure 2.5: Comparison between Frediani's and Prandtl's results [19]

of the wings in a horizontal plane has no influence on the induced drag of the total system. This also holds for swept wings. Hence, the induced drag of a box and a staggered swept wing will always be equal provided that the wings are purely moved in a horizontal manner. This allows the use of box-wings also on high-subsonic and transonic transport aircraft where swept wings and stagger are necessary to reduce the wave drag of the system.

Further work on minimum drag for joined and closed wings done by Demasi et al. also found that the postulation of minimum induced drag for a closed wing also holds when the lift distribution between the two wings is not equal [5]. They have shown that the optimal circulation of a closed system is equal to the reference solution plus an additive arbitrary constant. This means that the load distribution between the wings can be changed to unequal amounts (e.g. to satisfy stability and controllability constraints) and still be an optimal solution [21]. His solution is shown in Fig. 2.6. The positive and negative values of the circulation on the initial

distribution are a result of the direction of the line integral used to compute the circulation. The physical meaning of adding the constant circulation results in a shift in total lift from an equal split to an unequal split. While the profile is not elliptic anymore, its derivative is analogous to the elliptic loading case, and hence this is still a condition that yields minimum induced drag. It should further be noted that the vertical wings now have to create a very different distribution than following Prandtl's results. This allows designers a much larger design space for a new concept, as it relaxes the restrictions to lift distribution and wing size and shape to still achieve an optimal solution.

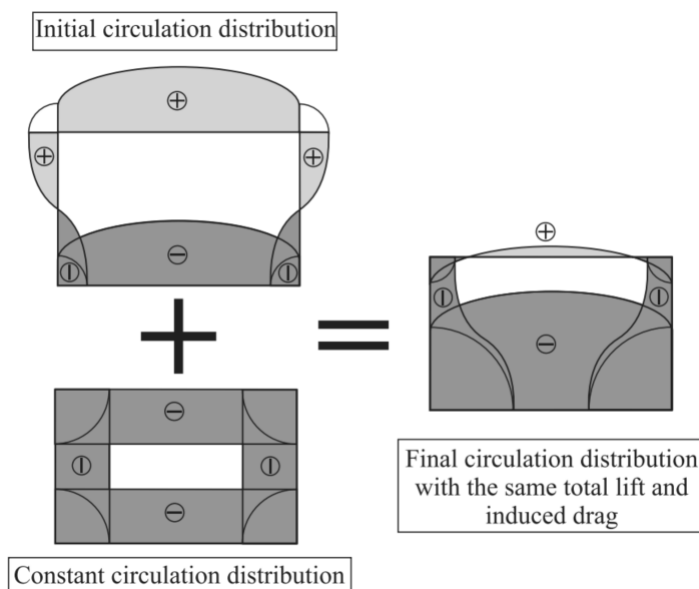


Figure 2.6: Demasi's solution to an unequal lift distribution [21]

2.2. The PrandtlPlane

The theory developed by Ludwig Prandtl has been applied in a number of conceptual design studies for transport category aircraft. A particular type of box-wing aircraft designed for transonic flight speeds are commonly referred to as PrandtlPlanes (PrP). The set-up is usually a positive stagger, that is the top wing is moved rearwards, and connected to either fuselage mounted engines or a vertical tailplane. Due to the speed regime in which these aircraft normally operate, the wings are swept to minimise wave drag. The front wing is swept backwards, the rear wing forwards. At the wing tips the wings are connected through winglets. Depending on the design, these are either straight (if the wingtips are at the same location), or swept back as well (if the rear wingtips lie behind the front wingtips).

Exploiting the concept of the lower induced drag should yield a higher lift to drag ratio. This will result in a lower fuel consumption compared to a conventional aircraft, as well as a decrease in operating cost. In a society where both a reduction of the climate impact and operational costs become increasingly relevant, these designs could be beneficial. Furthermore, noise can be reduced due to lower thrust requirements around the airfield. If the focus is shifted towards congestion of airports, then this concept can allow for more passenger or cargo capacity than a comparable aircraft, while respecting wing span limitations [3]. For the same span more lift can be created and hence the fuselage can be extended to fit more passengers. This extension is usually done through widening the fuselage rather than lengthening it to limit the potential CG excursion [6] [7].

Due to the novel concept of the wingbox, some interesting features have to receive special considerations, such as structural peculiarities or new options regarding control surface layouts.

2.2.1. Stability and control considerations

Due to the second large lifting surface, the boxwing has some peculiar features and challenges regarding its flight mechanics. These challenges relate to stability problems due to the rear aerodynamic center of a swept box-wing, but also some implications due to the special mass distribution.

A first challenge is a large moment of inertia around the pitch axis [3]. This requires larger and highly effective control surfaces for a sufficient pitching moment. A proposed way to improve the pitch response is to use the effectors on the front and back wing, moved in opposition. This way a pure pitching moment can be created.

Schiktanz and Scholz [7] report that replacing the conventional stabilizer with a lifting wing brings significant challenges to longitudinal stability. In general, the tail provides a downward force to balance the wing pitching moment. To adhere to the drag optimality, the allowable CG envelope is limited as illustrated by the following equations. Investigations by Schiktanz[22] using figure 2.7 found equation 2.9 as condition for stability and equation 2.10 as condition for control.

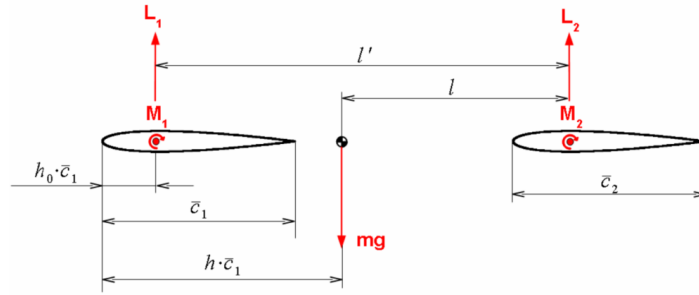


Figure 2.7: Forces and moments on a boxwing [22]

$$h < h_0 + \frac{dC_{L,2}}{dC_L} \frac{l' s_2}{\bar{c} c_1'}; \quad \frac{dC_{L,2}}{dC_L} = \frac{C_{L\alpha 2}}{C_{L\alpha}} \left(1 - \frac{d\epsilon}{d\alpha} \right) \quad (2.9)$$

$$h > h_0 + \frac{C_{L,2}}{C_L} \frac{l' s_2}{\bar{c} c_1'} + \frac{C_{M,1} s_1}{C_L} + \frac{C_{M,2} s_2}{C_L} \frac{\bar{c}_2}{\bar{c}_1} \quad (2.10)$$

The parameters in the control equation are all either defined through the aircraft geometry or flight condition, with s_x the reference area of the respective wing. For the stability condition, the fraction of $\frac{dC_{L,2}}{dC_L}$ was of special interest. The conclusions were that a high value for this fraction is the most beneficial for static longitudinal stability. The most influential parameter for this is the sweep of the wings. For the front wing, a high sweep is beneficial, for the aft wing a lower sweep is desired. Furthermore, the larger the stagger, the better for the stability margin. From the trim equation (Eq. 2.11) it shows that the rear wing lifting coefficient needs to be less than the front wing. This results in the left side of the equation being positive, even for negative wing pitching moments.

$$C_{M,1} c_1' s_1 + C_{M,2} c_2' s_2 - \left(C_{L,2} - \frac{dC_{L,2}}{dC_L} C_L \right) \frac{l' s_2}{\bar{c}} > 0 \quad (2.11)$$

This result is directly conflicting with the optimality discussed by Prandtl, that equal lift is necessary for minimum induced drag. While this condition was updated by Demasi [21], even current box-wing designs still try to approximate the equal lift condition [22]. It is also possible to manipulate the pitching moments of the wings by a tailored combination of sweep and wing twist to obtain a positive pitching moment. This, however, would cause the lift distribution over the wings to deviate significantly from the optimum again. The authors further give the idea to use reflexed airfoils to have a positive pitching moment. However, they do question the applicability of such airfoils in transonic aircraft. Also designing the fuselage with a reflexed rear section is discarded as infeasible [22].

Another proposed option is to include another horizontal stabilizer that is independent of the aft wing. This idea was also used by Frediani [3] in multiple box-wing designs through the addition of a V-tail. As the V-tail has both a horizontal and a vertical force contribution, it is possible to use the tail to help trim the aircraft by providing a stabilizing downward force without violating the optimality condition on the actual box system. A careful trade-off between the increase in induced drag due to unequal lift distribution and the increase in trim drag due to the V-tail deflection must be conducted to identify the ideal design.

2.3. Conceptual Design Studies

The idea of the boxwing configuration has been investigated in multiple studies. A selection of relevant or interesting studies is presented here, with a focus on the differences in outcomes and the conclusions drawn from these studies. The presented studies show that the box-wing concept is still in an exploratory phase, and that different studies solve common challenges differently.

In 1974 Lockheed Martin and NASA started an investigation into the feasibility of a transonic box-wing as new design concept [23]. The goal of the study was to design a 400 passenger aircraft with a range of 5500 NM. These objectives were directly taken from another study performed by Lockheed on a new 'modern' conventional aircraft design to allow direct comparison. The report is very detailed about each phase of the design process. Multiple design lay-outs were investigated, with the final design showing a four-engined box design with a slender fuselage and a single vertical tail. The aircraft has an equal lift distribution between the wings, and a higher sweep of the forward wing than the rear.

This study further researched aeroelastic effects in more detail. Flutter analyses showed symmetric and anti-symmetric instabilities well below the required flutter speed. A reduction in wing tip spacing remedied this issue but led to a large drag increase and was therefore considered infeasible. Further research showed that flutter instabilities can be improved by shaping the rear wing in a gull-like fashion, similar to a V-tail. Final comparison to the reference aircraft showed significant reductions in induced drag, yet no advantages in overall ramp weight. This and the unresolved aeroelastic issues led to the conclusion that a transonic box-wing is not feasible at the time. However, the remark is made that active or passive flight control systems could assist in the flutter problems and hence lead to improvements in the box-wing design.

A study performed by Andrews and Perez [8] has compared the performance of a box-wing regional-jet with a conventional jet of CRJ-200 size for a typical mission profile. For the analysed box-wing they find that the design has a lower structural weight than the reference conventional aircraft. Furthermore, they find that the range of stable CG locations limits the possible wing spacing, despite a higher spacing being advantageous for performance. For the overall design, the box-wing performed similar to the regional jet used as reference; the final box-wing system has a similar cruise lift-to-drag-ratio to the reference design. Hence, they concluded that the box-wing in cruise has no significant advantages over a conventional

regional jet. Despite having a lower structural mass, the fuel burn was very similar. Other studies have concluded that the shorter wing span of each individual wing will necessitate an overall increase in wing weight [7]. The paper does not detail reasons why the complete wing system is estimated to weigh less than the reference aircraft. Furthermore, the study shows a close match of the mission fuel required and a nearly identical cruise glide ratio, yet the cruise thrust for the box-wing is allegedly 25% higher for the box-wing. Lastly, this study concludes that box-wings will be more advantageous in flight phases where induced drag is more relevant.

This claim is further substantiated through a study by Jansen and Perez [9]. This study investigated the effect of mission requirements and size on non-planar aircraft configurations. This study also concluded that box-wing configurations are most beneficial for smaller aircraft and shorter missions, while long-range aircraft would benefit most from improved winglet design. A reason for this is that in cruise the induced drag is only a small part of the total drag, while for climb and ascend it is significant. Hence a reduction in induced drag is most beneficial for aircraft and missions where cruise is only a small part of the total mission duration. For long-range flights a boxwing is thus less desirable, also due to the increased profile drag resulting from the two lifting wings.

Between 2000-2003 a joint research project from 5 Italian universities has investigated the feasibility of a very large box-wing similar in size to the A380 and seating 600 passengers. This design also has a widened fuselage to seat all passengers on a single deck, a V-tail and an inflexed fuselage. The design has equal lift over both wings in cruise and through application of flaps on both wings can retain this condition even at low speed [24]. The same consortium has also developed a smaller version for 250 passengers, the PrP [6]. The Prantlplane has the same geometric and aerodynamic features, albeit only a single passenger deck.

Schiktanz and Scholz have also designed a box-wing which they use as basis of all their further research into the subsystems [7]. Their design is based on an A320 and its performance and mission profile. They also concluded that the box-wing system is most beneficial in short to medium missions. Although they have described methods to attain a stable aircraft with equal lift distribution over both wings, their design has 60% of the lift provided by the front wing [22]. They accept the resulting drag penalty to increase their stability margin for better handling qualities. The design still limits CG travel by using a widened and shortened fuselage section. Contrary to Andrews and Perez, this design finds that the structural weight of the boxwing is very similar to the reference aircraft. Their wing system is about 23% heavier than the reference wing, however this is mostly offset by a lighter fuselage. Furthermore, this design shows improvements in glide ratio and hence total mission fuel burn. This is more in agreement with other studies on box-wings and wing weight implications, and casts some doubt on the findings in the study by Andrews and Perez [8]. This study thus concludes that for short or medium range missions, an optimised boxwing can indeed be beneficial over the current generation of conventional aircraft. Lastly, some considerations regarding a family concept are given. While in conventional aircraft an extension of the fuselage is simple and commonly performed, for a box-wing this is more difficult. The stagger between the wings and the CG excursion will be affected. Hence, the vertical winglets need to be redesigned to accommodate the now different sweep. Furthermore, due to the change in wing stagger, the span efficiency factor for the family aircraft will decrease.

2.3.1. The PARSIFAL project

The promised benefits in fuel efficiency have also gained interest from the European Union in recent years. Under the Horizon 2020 research project, a large collaborative study was

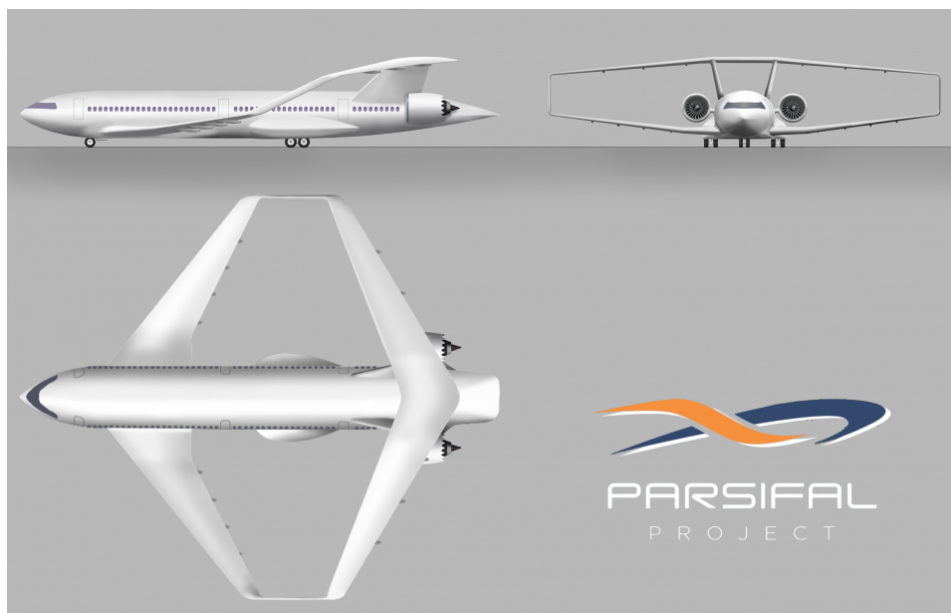


Figure 2.8: 3-side view of the PARSIFAL PrandtlPlane²

launched that involves multiple European universities and research institutes¹. The project focuses on establishing a scientific and engineering basis to introduce a box-wing aircraft into service, and to develop design tools that can be used in the process. This is developed on the basis of a medium size commercial aircraft with the dimensions and fuel consumption of A320/B737 size aircraft with the payload capacity of A330/B767 size aircraft [25]. The design mission was for high capacity at medium range (4000 nm). To fully cater to this mission, also quick turnaround times were specifically investigated. For this, the fuselage was widened to 8-seats abreast with two enlarged aisles, and the common circular shape was changed to tangent circular arcs, which give it a more oval shape. The widened aisles allow passengers to stow away their luggage while flow though the cabin can be maintained. In the same move, also the overhead bins were extended to fit more luggage and hence to reduce the amount of hold luggage that would be carried [25].

A comparative study to investigate the benefits of such a box-wing design found that the design is superior in efficiency to both A321 and A330 [26]. However, it is noted that both competitors are outside of their design point and hence less efficient. Comparing with a conventional design specifically designed for this mission still shows a slight benefit for the box-wing, but not much. It is further noted that a conventional design without wing span limitation would still be superior. This mostly results from differences in the structural mass. For larger wingspans, the conventional aircraft gains an advantage due to lower structural mass. In payload-range efficiency, the box-wing showed the best overall results. Comparing box-wings with low and high wing loading, the higher wing loading proved beneficial overall, and more competitive with the specifically optimised conventional design.

The study presented in this document is based on the PARSIFAL project. The used geometry and the aerodynamic properties of the aircraft stem from an early design of the PARSIFAL plane. The main differences to the final design in figure 2.8 are a trapezoidal wing, a larger wing area and higher maximum take off masses. The used geometry is described in further detail in chapter 4.

¹www.parsifalproject.eu

²[https://parsifalproject.eu/2018/03/28/parsifal-project-will-present-tra-2018-\](https://parsifalproject.eu/2018/03/28/parsifal-project-will-present-tra-2018-)

2.4. Control surface design in boxwings

The two wing layout of the boxwing allows for control surfaces to be mounted on both wings. This gives rise to some special features that only such a wing design can have. The most interesting of these capabilities would be the direct lift control. Having the ability to ascend or descend without having to change the aircraft attitude can be beneficial for multiple reasons, such as increased pilot visibility during take-off and landing, or improved comfort during altitude changes for the cabin service. Another strong advantage is that the controls do not need to be strictly determined anymore; ailerons can be placed on both wings to increase overall effectiveness and an application of elevators on both wings that are deflected in opposite ways.

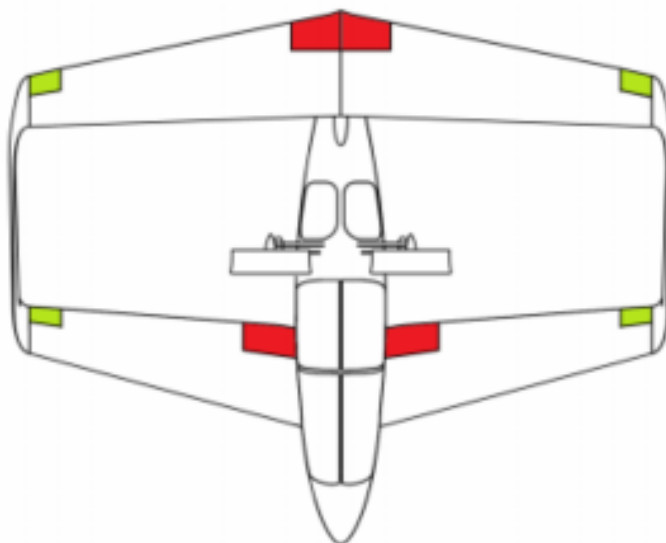


Figure 2.9: Classical control surface layout applied to PrP [15]

In the previous section it was described how the design of box-wing aircraft is currently mostly done on a conceptual basis. There are no transport category box-wings and also in general aviation this is a very exotic design choice. Hence, also most studies are focusing on the general aerodynamic shape of their box-wings, and the challenges that arise with the geometry itself. Most concepts merely describe a layout of their control surfaces without much detail to the exact sizing process. The only exception is the elevator, which is commonly analysed in stability and control questions. However, also here a design process is often lacking. An example of the classical control layout applied to a box-wing is shown in figure 2.9 [15]. All current studies use variation of this shape. Frediani [6] describes in his design that it will have two elevators to allow for pure pitching moments, but no further description of any other control surfaces is given. A planform view provided shows that this design features flaps and slats on both wings, and ailerons only on the rear wing. The design proposed by Schiktanz and Scholz features flaps on front and rear wing, but only the rear wing has elevators and ailerons [27]. No further description or investigation on the control surfaces of their design could be found. A similar lack of detail was found in the Lockheed study [23]. The high lift devices and their placement is described in much detail, however, the control surfaces are rarely mentioned. A roll rate criterion for aileron size is mentioned, but no further detail to the control system is given.

Van Ginneken et al. [12] have discussed control surface sizing on a 300 passenger box-

wing. In their analysis the planform was already fixed and hence the focus was purely on control surface design and sizing. In their analysis, a rough trade-off matrix comparing independent (classical) control surfaces and combined control surfaces was created, shown in figure 2.10.

	Scores		Weight	Weighted scores	
	separate roll/pitch	combined roll/pitch		separate roll/pitch	combined roll/pitch
control effectiveness per control function (large = good)	3	1	3	9	3
total control effectiveness per unit control surface (large = good)	1	3	2	2	6
complexity (low = good)	3	2	2	6	4
unintended control influence (small = good)	3	1	2	6	2
space for high-lift devices (large = good)	1	3	3	3	9
				26	24

Scores: 1 = bad
2 = fair
3 = good

Weights: 1 = less important
2 = moderately important
3 = very important

Figure 2.10: Trade-off independent versus combined controls from van Ginneken et al. [12]

It can be seen that, using the 3-point scale, both concepts score maximum and minimum points in three disciplines each. The result is solely dependent on the difference in 'complexity'. This simple matrix shows that good arguments can be made for both designs and that also a combined pitch/roll layout has very promising characteristics. The close outcome indicates that further research into the combination might prove beneficial. A second trade off investigated the benefits of using control surfaces on both wings over using only a single wing. Here, using both wings showed clear superiority over the other options. Hence, a similar choice to the other described designs was made; control surfaces on both wings, but with a classic layout of strictly independent ailerons and elevators.

As next step, an optimisation routine was devised using a simple mechanical gearing control allocation algorithm to optimise the given configuration for minimum elevator span. This was done as the elevators are located inboard on the wing. For high lift devices, it is better to position them close to the wing root as they are more effective. Hence, minimising the inboard elevator has a beneficial effect on the overall aircraft performance. The smaller elevator allows the flaps to begin further inboard and to have a larger total span width, hence increasing their high-lift performance. To analyse the effectiveness of the control surfaces, control maneuvers specified in the MIL-F-8785C [28] were used.

Varriale et al. [14] proposed an optimisation framework that optimises control surface sizes on a given aircraft design with respect to handling quality criteria using a mechanical gearing for the control surfaces. This analysis builds on the preliminary investigations by van Ginneken and improves on the aerodynamic analysis and the optimisation algorithm. Varriale created a multidisciplinary optimisation framework based on an aerodynamic database, a flight mechanics toolbox and a semi-empirical method to scale the aerodynamic database to match the current control surface sizes. The underlying aerodynamic model consists of a large reference data set of the aircraft in clean configuration and with deflected control surfaces. For this, the medium-fidelity 3D-panel solver VSAero is used.

This aerodynamic database is then used by a flight mechanics simulation toolbox to evaluate the behavior of the aircraft and whether the current control surface arrangement is sufficient for a selection of handling qualities. The results are then fed to an optimization algorithm which influences the control surface sizes. Changes therein are applied to the aerodynamic

database through a semi-empirical ESDU scaling method. Within this algorithm, the control surfaces are connected through mechanical gearing and the controls for aileron and elevator are disconnected. Hence, ailerons only react to a lateral stick command and elevators to a longitudinal. Contrary to van Ginneken, this optimisation thus actually kept roll and pitch surfaces completely separate. Furthermore, this framework optimised for overall minimum span of all control surfaces, not just for the elevator.

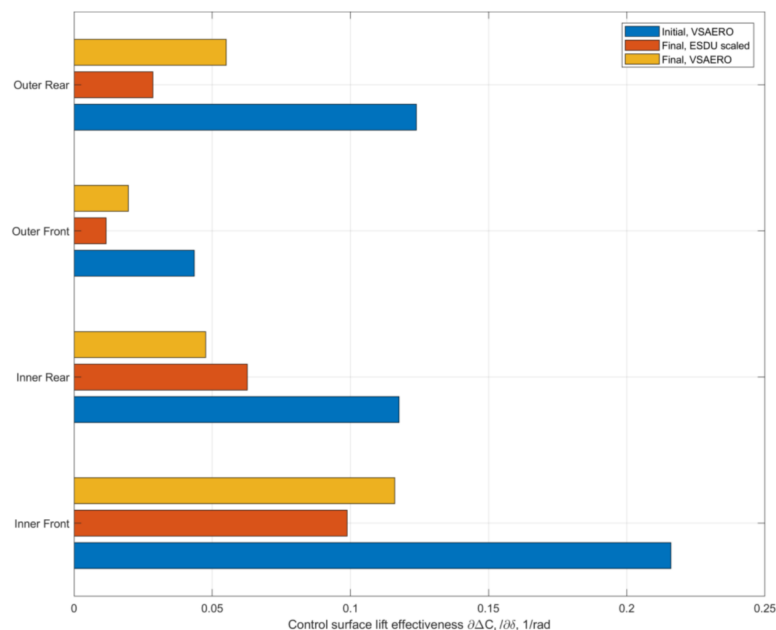


Figure 2.11: Control surface effectiveness results from Varriale [14]

Fig. 2.11 shows the final results of Varriale's optimisation. This is presented as lift effectiveness, yet directly translates to size of the surfaces. It can be seen that the optimal configuration is significantly smaller than the initial guess and shows the importance of proper investigation of control surface sizing already in a conceptual stage. Furthermore, it compares the output of the optimiser including the ESDU scaling with a full VSAero computation using the same sizes. It can be seen that the difference in effectiveness can be large. Hence, it shows that the simple scaling method introduces errors in the results that lead to an overestimation of the actual results. The high-fidelity aerodynamic analysis is completely disconnected from the actual optimisation and only provides a baseline. The ESDU method is based on existing aircraft wings in a conventional configuration and hence might not be completely suitable for such unconventional layouts. However, using VSAero within the optimisation loop is infeasible since the article states that a full database takes 1-3 CPU days. Hence for this set-up the ESDU method is necessary. Varriale also states in his conclusions that a new search strategy with a more general multi-fidelity model and a control allocation algorithm may produce very promising results.

Within the handling qualities analysis model developed by Oliviero et al. [15], control surface sizing is addressed as well; and applied to the IDINTOS aircraft. Contrary to van Ginneken and Varriale, this is not done on a final wing planform, but the estimation of the control surface parameters is taking place within the evaluation of the inherent handling qualities of the whole aircraft. The elevator is sized through two criteria, on trim ability and maximum normal force. The ailerons are sized on a roll rate requirement. This set-up is inherently different from the two previously discussed, and significantly simpler. Instead of an actual optimisation algo-

rithm, this assumes a small starting value and then increases the area for each iteration until the criteria were fulfilled.

Lastly, as part of a study Sousa et al. [16] investigated the effect of elevator placement (front only, aft only, both) on trim deflection, and compared the results with a reference aircraft having the same wing area and span. The results showed that the required elevator deflection is maximum for elevators at the forward wing only, and minimal if elevators are used on both wings. Comparing to the reference aircraft, it was found that the trim drag was lower for all box-wing designs for an equal static margin. Using both elevators for trim showed the lowest drag count. Also the resulting angle of attack for trimming is nearly unaffected if both elevators are used, showing how the pure pitching moment created by opposite deflections can help reduce trim drag and improve the maneuvering margin of the aircraft. For the maneuvering margin, it was found that using both elevators gives similar results to a conventional design while an elevator on one wing alone requires larger deflections.

2.5. Handling Qualities

The two primary considerations for a safe aircraft design are controllability and stability. Furthermore, good handling qualities are important for a successful aircraft design. Handling qualities are defined as a measure of the accuracy and ease that a pilot can perform tasks related to the aircraft's role[29]. The handling qualities that an aircraft exhibits are a direct result of the behaviour of the aerodynamic design and its stability features.

The basic aspect of stability is that the aircraft has an inherent tendency to oppose any input and return to the original condition. The physical basis was already covered in the previous chapter. Static stability is determined by difference between the wing aerodynamic center - and hence the wing placement - and the center of gravity of the full aircraft. For box-wings it is more challenging to have a similar stability margin to conventional designs due to the two fully lifting wings. Hence, box-wing fuselages must be designed to minimize the total CG shift during operations. Dynamic stability refers to the behavior in the time domain following a disturbance. An aircraft can be statically stable, but dynamically neutral or even unstable. This means that the initial aircraft response will counteract the disturbance, yet over time the oscillations will remain the same or diverge, that is increase in amplitude. For good handling qualities, it is important that an aircraft is both statically and dynamically stable, with good damping characteristics. The static margin in both longitudinal and lateral planes is relevant for a stable aircraft. Next to the usual investigation of the wings and the aerodynamic moments these create around the CG, for lateral/directional stability also drag forces of the fuselage and other protuberances are highly relevant in the analysis.

The second important part for good handling qualities is a well controllable aircraft. Controllability is mostly a result of good control surface design and placement, but also the overall shape of the aircraft plays a relevant part. The placement of the control surfaces is discussed in the next chapter. In this chapter, the focus is laid on the fundamentals of handling quality definition and evaluation; and presentation of inherent handling qualities of some box-wing aircraft design studies.

2.5.1. Handling qualities overview

While it is very important for a good aircraft design to have a well refined aerodynamic shape to achieve a high performance, it is also important that the aircraft has a good inherent behavior that allows the pilot to ensure a safe and smooth ride for its passengers under (nearly) all circumstances. For this, a set of handling qualities and a multitude of different criteria are defined that are designed to assure safe behavior for any pilot if properly adhered to.

Civilian certification authorities (e.g. EASA/FAA) have created a set of certification criteria that include specifications on handling qualities, however, these are often not very specific in their wording and hence difficult to use for a designer. An example of this is shown in the following quote from the Acceptable Means of Compliance for EASA CS-25.181 (Dynamic stability) [30]:

Any combined lateral-directional oscillations ('Dutch roll') occurring between 1.13 VSR and maximum allowable speed appropriate to the configuration of the aeroplane must be positively damped with controls free, and must be controllable with normal use of the primary controls without requiring exceptional pilot skill.

This statement only specifies that the aircraft must be stable and controllable by an average pilot. However, it does not give any further guidance to the actual definition of this. For this reason other, more descriptive specifications are used that were developed by other bodies. Nevertheless, these documents give valuable information about the cases that must be considered when analysing a configuration, as these must be proven for certification. An overview of all the relevant cases for civil aviation is shown in Fig. 2.12.

Control effector analysis	Applicable flight conditions	Critical CG location	Applicable requirement	Aircraft configuration
<i>Longitudinal</i>				
1-g trim	All	Fwd, aft	FAR/JAR 25.161C	Dependent on flight condition
Approach 1-g trim	Approach	Fwd	FAR/JAR 25.161C	Full flaps
Landing 1-g trim	Landing	Fwd	FAR/JAR 25.161C	Full flaps, landing gear down
Go-around 1-g trim	Climb	Aft	FAR/JAR 25.161C	Full flaps, landing gear down
Maneuver load	All	Fwd	FAR/JAR 25.255	Dependent on flight condition
Go-around maneuver	Approach	Fwd	FAR/JAR 25.255	Full flaps
Rotation on takeoff	Takeoff	Fwd	FAR/JAR 25.143	Takeoff flaps, landing gear down, in ground effect
Rotation on landing	Landing	Aft	FAR/JAR 25.143	Full flaps, landing gear down, in ground effect
Dynamic mode oscillation	All	Fwd, Aft	FAR/JAR 25.181A	Dependent on flight condition
<i>Lateral</i>				
Steady sideslip	All	—	FAR/JAR 25.177	Dependent of flight condition
One engine inoperative trim	All	—	FAR/JAR 25.161	Dependent of flight condition
Time to bank	All	—	FAR/JAR 25.147	Dependent of flight condition
Inertia coupling (pitch due to velocity axis roll)	Cruise	—	FAR/JAR 25.143	Dependent of flight condition
Yaw because of loaded roll pullout	Cruise	—	FAR/JAR 25.143	Dependent of flight condition
Coordinated velocity axis roll	Cruise	—	FAR/JAR 25.143	Dependent of flight condition
Dutch roll oscillation	All	—	FAR/JAR 25.181B	Dependent of flight condition
Roll subsidence	All	—	FAR/JAR 25.181B	Dependent of flight condition
Spiral divergence	All	—	FAR/JAR 25.181B	Dependent of flight condition
Closed-loop stability	All	—	FAR/JAR 25.177	Dependent of flight condition

Figure 2.12: Longitudinal and lateral sizing criteria overview for control surfaces [31]

The American military has developed and published their own specifications for different classes of aircraft. While technically only binding for American military aviation, these documents are very specific about requirements and hence are often used for civil designs as well. The most well known document is the MIL-F-8785C which details handling quality requirements for piloted aircraft [28]. While it has been superseded by MIL-STD-1797 [32] in 1980, it is still commonly used in conceptual aircraft design and analysis. These standards define acceptable behavior depending on the type of aircraft, the flight phase and potential maneuvers. For civil aviation, usually only the aircraft classes II & III (medium and large transport aircraft) are relevant (tab. 2.1).

The behavior of the aircraft is always rated in one of three levels (tab. 2.2). Level 1 handling means that everything is clearly adequate. Level 2 means that handling is adequate, but with an increase in pilot workload, and level 3 means that pilot workload is excessive. As shown in the table, it is not acceptable to have anything below level 1 qualities in normal flight.

Table 2.1: Mil-F-8785C Aircraft classes [28]

MIL-F Class	Aircraft characteristics
I	Small, light aircraft, low maneuver., MTOM < 6000 kg
II	Medium aircraft, low-to-medium maneuver., 6000 kg < MTOM < 30000 kg
III	Large, heavy aircraft, low-to-medium maneuver., MTOM > 30000 kg
IV	Highly maneuverable aircraft, no weight limit (e.g. aerobatic or fighter)

Degradation is only accepted if parts of the system have failed and only then with a very low probability.

Table 2.2: Mil-F-8785C Levels of acceptability [28]

MIL-F Level	Probability of encountering within normal flight envelope
1	Required under normal conditions
2	After failure < 10^{-4} per flight
3	After failure < 10^{-6} per flight
Unacceptable	Total loss of control < 10^{-9} per flight hour

Most requirements are given with constant limits and change with category and flight phase. Sometimes only lower or upper limits are specified, but mostly acceptable bands are defined that widen with higher level. For all maneuvers that are shown in Fig. 2.12, at least one criterion is given that allows direct analysis from a flight dynamic simulation. For the eigenmodes of the aircraft, usually damping ratios or time periods are specified. For other motions the criteria are then defined in a way relevant to the individual motion.

The MIL-F-8785C not only specifies requirements to the stability and controllability of the aircraft itself, but also many criteria directly related to the control system and the pilot interactions, such as maximum control forces or force gradients. For conventional reversible flight control systems such as pulleys, this is highly relevant for the overall control system design. For irreversible flight controls such as fly-by-wire systems that are currently standard in commercial aviation, these criteria have lost their relevance in the initial sizing process, as pilot forces are not directly related to control surface deflections anymore. However, for cockpit design and actuator sizing these are still relevant to this day.

2.5.2. Handling qualities in box-wings

For box-wing designs, the mentioned eigenmotions and associated handling quality requirements still hold true. Hence, it is important to investigate dynamic behavior of different box-wing designs to be able to draw conclusions on the specific challenges and differences that flying a box-wing aircraft might impose. Here, some results from flight dynamic studies are reported. As previously described, the MIL-F-8785C is predominantly used for these analyses. Hence, unless specified all handling levels described in this section derive from this specification.

The box-wing design by Schiktanz and Scholz [27] was fully analysed for its dynamic behaviour using both an aerodynamic solver and a hand method by Roskam [33]. The results from both methods were very alike, however, the hand method usually reported slightly higher characteristic values (damping or periods). The study investigated the behavior at different altitudes and velocities. In cruise, they reported short period and spiral to be at level one, aperiodic roll at level 3 and the rest at level 2. As altitude increased, these handling qualities would

decrease. For a velocity increase it was found that flight speeds beyond 140 m/s improved the handling at all altitudes. The study acknowledges that the inherent box-wing design has limited handling qualities, yet still within an acceptable range. They propose the implementation of a flight augmentation system to bring all criteria within level 1 range. A probability that the aircraft drops to level 2 or 3 following a failure of the automatic system was only found for altitudes above 10,000 ft for this design. In case of failure the pilot would have to descend below this for good handling qualities. Hence, the conclusion is that this design is suitable for certification by implementation of a necessary stability augmentation system.

The study performed by Sousa et al. [16] that was already described in the previous section also analysed the longitudinal handling qualities of the box-wing. It found that for the box-wing in short period the natural frequency is consistently higher than for a conventional aircraft, yet still well within level 1 range for a large variation in flight conditions and static margins. For the control anticipation parameter, it was level 2 for all box-wing results. Sousa notes that this shows that the box-wing is overall less stable than the conventional aircraft, yet that this is acceptable in a conceptual design phase. For the phugoid the box-wing shows very similar results to the conventional aircraft, and well within level 1 criteria. Similar to Scholz, he concludes that the box-wing shows overall good qualities that would be certifiable with the implementation of a stability augmentation system. Oliviero's analysis of the IDINTOS design [15] shows the same results. He also concludes that the box-wing performs well at short period motions, yet phugoid damping in cruise is only a level 2. He notes that his results show high values for pitch stiffness and pitch damping, which degrade longitudinal maneuverability. Yet, the stability margin becomes only a factor for these criteria if it is reduced to very small values.

Lastly, the PrandtlPlane designed by the Italian research consortium also performed an analysis of their 250 passenger version of the PrP. The inherent flying qualities were analysed at sea level conditions and medium speed [34]. Results show that the longitudinal motions are all level 2, the spiral, while slightly unstable, level 1. The aperiodic roll only shows level 3, and the Dutch roll is unstable. They concluded that this design has deficiencies that would need to be further investigated and addressed.

These cases show that the current state of research and development regarding box-wing flight control systems is limited. The studies either utilise a classical layout with some adaptation to the different geometry of a box-wing aircraft, or completely restrict themselves to an analysis of the inherent flying qualities. Detailed investigations in optimal control surface sizing or placement have not been performed yet. Also, while the potential benefits of using combined control surfaces were mentioned, no systematic studies have investigated these implications for a box-wing design yet.

3

Control Allocation

Classically, aircraft controls are designed such that every distinct type of control effector primarily influences a single degree of freedom by creating a moment. Increased availability of computational resources and novel aircraft configuration allow a deviation from this approach and to utilise every control surface as an individual effector to generate moments around multiple axes. These over-actuated systems require algorithms that are used that adopt a given effector layout and then deflect different surfaces to appropriate amounts to give the desired moment generation. These algorithms can vary in complexity and range from simple ganging of control surfaces at fixed proportions to highly sophisticated nonlinear models that can reconfigure themselves in flight to compensate for a malfunction in a control effector.

Over-actuated designs are commonly found in industrial applications and aircraft for a variety of reasons, such as [18]

- Control effector redundancy may be required to meet fault tolerance and control reconfiguration requirements (e.g. twin tails in combat aircraft)
- It may be desirable to choose between sets of effectors to perform the same task under different circumstances (e.g. different ailerons for low- and high-speed flight)
- Certain effectors can be shared among other control systems with different objectives and therefore be redundant (e.g. an aircraft roll can be initiated through one sided spoiler deflection even though their primary objective is lift dumping after touchdown)

The design of such over-actuated systems is divided into several levels. A general representation of this is given in Fig. 3.1. The first stage is the design of a high level motion control algorithm that creates a vector of virtual inputs (τ_c) to the system. On aircraft level, this can be an autopilot or the pilot itself in manual flight. Next, the actual control allocation algorithm is used to map the set of virtual input moments into individual effector deflections in an effort to achieve the virtual command such that the total equals the virtual command. Here, also control constraints such as saturation or rate limitations are taken into account. The actuator cannot physically move beyond a certain limit or exceed certain movement speeds. Third, there may be additional actuator controllers at a lower level whose dynamics must be accounted as well. Lastly, the final command is given to the control surfaces to induce the motion. The structure shown in Fig. 3.1 also shows that a control system is a modular structure. Hence, it is usually possible to design high-level control systems without detailed knowledge of the effector and actuator systems [18].

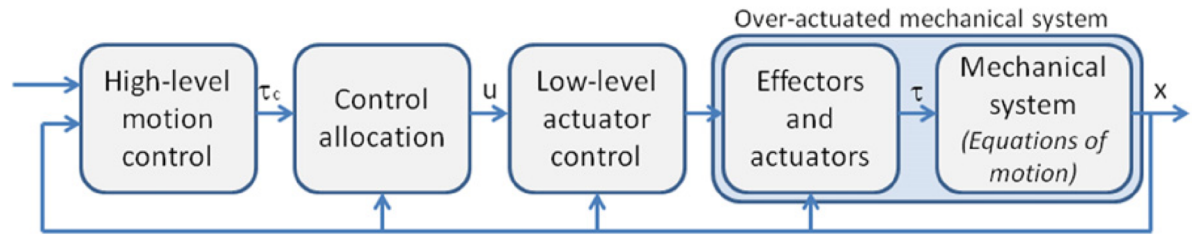


Figure 3.1: Control system structure including control allocation [18]

The primary goal of any control allocation algorithm is to compute a control output that ensures that the virtual command input is produced by the joint operation of all control surfaces at all time. It is possible to fail to achieve this goal if the commanded input is beyond the capabilities of the effectors. If this happens, the algorithm usually degrades its performance to find a solution that is able to minimise the deviation from the commanded input. Often priorities are defined for certain objectives and hence the allocation becomes a constrained optimisation problem with some form of weight matrix. For over-actuated systems it is common to include secondary objectives to drive the non-unique control allocation to optimise for other constraints as well. These additional objectives are often chosen from an operational perspective, such as minimizing control power or total deflection [35].

In aviation, mostly linear allocation methods are used [18]. In flight dynamics, the behavior of the aircraft is commonly linearised around a certain flight condition, and this linear model is then used for behavior analysis. This holds under the assumption that the aircraft's environment is varying slowly, and that the aircraft is in a condition that does not create large nonlinear effects. Large transport aircraft commonly operate within these limitations, and hence good results are obtained from this linearisation method. The basic state-space model used in aviation application is shown in equation 3.1. The A_s matrix collects the inherent flight dynamics of the aircraft, B_s the effects of the control effectors; x , d , u and y are all vectors. The x -vector includes parameters regarding the flight condition, the y -vector the outputs such as angular rates. The control vector u contains the control surface deflections. For a classical system, the dimension of u can be as low as three, for over-actuated systems this dimension can be much higher.

$$\dot{x} = A_s x + B_s u + d, \quad y = C_s x \quad (3.1)$$

This equation gives the dynamic response of the aircraft as a combination of the inherent aircraft dynamics in matrix A_s and the control surface effects in the input matrix B_s . For control allocation, it is convenient to separate the two effects. This allows the control allocation and the distribution of control effector deflections to become a separate problem from determining the dynamic response of the aircraft [35]. For this, a dynamic inversion algorithm is used. The goal is to express the aircraft dynamics in the form of equation 3.2. This function assumes that f describes the (non-)linear aircraft dynamics, but the control effectiveness $Bu(t)$ has a linear relationship.

$$\dot{x} = f(x(t)) + Bu(t) \rightarrow Bu(t) = (\dot{x} - f(x(t))) \quad (3.2)$$

If the dynamics of the process are known and the states can be measured accurately, then this process allows to solve for the required moments due to the control inputs by subtracting the natural dynamics from the desired behaviour. This process requires a known mathematical model for the inherent behaviour of the aircraft as well as good sensing equipment for the

aircraft states. In a simulation, these are obtained as outputs of the flight mechanic simulation computations. The dynamic inversion then provides a transformation between the aerodynamic states and the allocated moments.

The control allocation problem can be simplified to equation 3.3, where the input matrix B describes the relationship between the control inputs \mathbf{u} and the desired aerodynamic moment \mathbf{m}_{des} . It is thus a collection of control effectivenesses for all effectors (equation 3.4). It is important to note that this matrix B differs from the matrix B_s in equation 3.1 in the derivatives. In flight mechanics, the states of the system are commonly aerodynamic parameters such as flight path angle or angle of attack. In control allocation, the states are the moments around the three principal axes of the aircraft.

This matrix B is not constant, but depends on the state of the system (e.g. velocity, air density). In a linear model, it is assumed that the variation in system states do not alter the matrix for the duration of the control. To create a unique solution, it is necessary to create a system where every effector in B is linearly independent from the others, hence B must always have full rank as a matrix.

$$\mathbf{m}_{des} = B\mathbf{u} \quad (3.3)$$

$$B = \frac{\partial C_F}{\partial \mathbf{u}} = \begin{bmatrix} \frac{\partial C_{F_1}}{\partial u_1} & \dots & \frac{\partial C_{F_1}}{\partial u_n} \\ \vdots & \ddots & \vdots \\ \frac{\partial C_{F_n}}{\partial u_1} & \dots & \frac{\partial C_{F_n}}{\partial u_n} \end{bmatrix} \quad (3.4)$$

The control effectors on an aircraft are typically hinged surfaces at the trailing edges of the wings and at the tail. The limits in travel of the control effectors are given in two vectors, \mathbf{u}_{min} and \mathbf{u}_{max} . Hence, the control vector u must always satisfy eq. 3.5.

$$\mathbf{u}_{min} \leq \mathbf{u} \leq \mathbf{u}_{max} \quad (3.5)$$

This set of equations 3.3 and 3.5 form the basis for every control allocation problem. The set of achievable moments is determined by the control effectiveness matrix B and the limits on the control vector. The deflection limits bound the set of admissible controls, the matrix B maps this to the greatest attainable moment set (GAMS) as shown in figure 3.2.

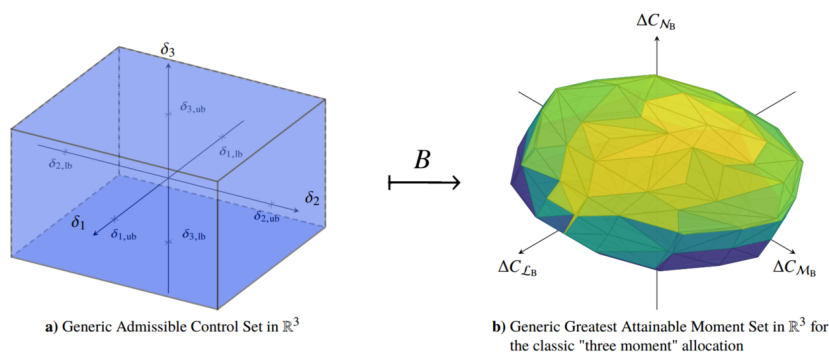


Figure 3.2: Mapping of the admissible control set to the attainable moment set through control effectiveness matrix B [36]

To solve Eq.3.3 for the individual control inputs u , matrix B must be inverted. This is the main challenge of linear control allocation, as B is not a square matrix due to the over-actuated system, and hence there is an infinite amount of potential solutions to the problem.

3.1. Pseudo Inverse

A popular algorithm for control allocation is the generalised inverse. This inverse is a matrix P that satisfies equation 3.6.

$$\mathbf{u}_P = P\mathbf{m}_{des} \rightarrow B\mathbf{u}_P = \mathbf{m}_{des} \quad (3.6)$$

In this equation, B is a $n \times m$ matrix, where $n = 3$ is the number of aerodynamic moments and m is the number of control effectors in the problem. Respectively, the inverse, matrix P , must have the shape $m \times n$. All such generalised inverses can be represented as equation 3.7. The elements in N may be arbitrary, as long as the product BN is not singular.

$$P = N[BN]^{-1} \quad (3.7)$$

While N may have arbitrary elements, the matrix P has to satisfy equation 3.7, and hence the elements are interdependent. Furthermore, the attainable moments using the matrix P are only a subset of the total attainable moment space. For a given matrix P , the deflections required to create a desired moment \mathbf{m}_{des} are thus the vector \mathbf{u}_P . Also, the moment can be created by multiplying the control vector with the matrix B , hence equation 3.8 holds. P has n columns, and thus it has a rank of n , due to the robust rank requirement on B .

$$\mathbf{u}_P = P\mathbf{m}_{des} \rightarrow \mathbf{u}_P = PB\mathbf{u}_P \quad (3.8)$$

However, as $n < m$ due to the underdetermined nature of the allocation problem, the solutions \mathbf{u}_P do not form a basis in m -space. Thus, the control space spanned by the matrix P is only a subset of the total admissible control set and hence the total attainable moment set will be smaller than the greatest attainable moment set. This limitation is also shown in figure 3.3. The attainable moment set using a pseudo-inverse is clearly visible as a subset of the greatest attainable moment set with the given control effectors.

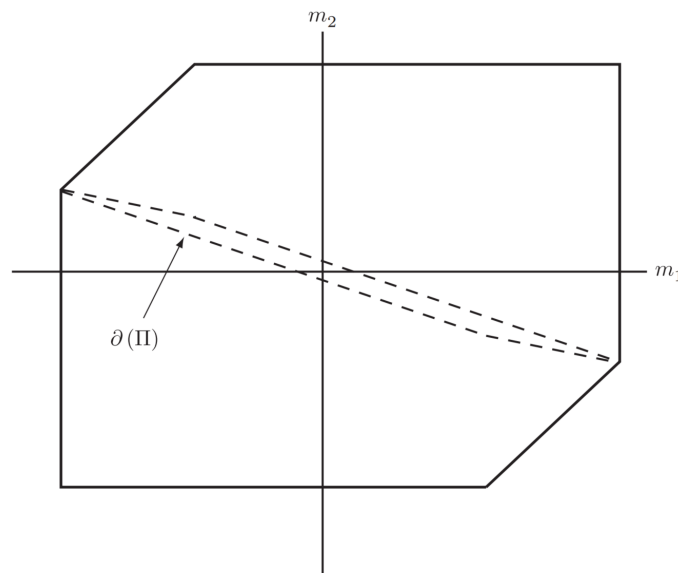


Figure 3.3: Comparison of a 2-dimensional moment set with pseudo-inverse (dashed lines) as subset of the AMS (solid lines) [35]

Depending on the application, this approach for a generalised inverse can be tailored to a specific problem, to include other limitations as well. A particular common generalised inverse

is the Moore-Penrose pseudo-inverse. This particular formulation minimises the l_2 -norm of the control vector. The l_2 -norm describes the positive square-root of the sum of the squares of the individual controls in the vector. Hence, this norm minimises the total deflection of the control surfaces.

The matrix P is determined through an optimisation problem that minimizes $\mathbf{u}^T \mathbf{u}$, the sum of squares, subject to equation 3.3. Using LaGrange multipliers, the optimisation problem is set up as shown in equation 3.9.

$$H(\mathbf{u}, \lambda) = \frac{1}{2} \mathbf{u}^T \mathbf{u} + \lambda^T (\mathbf{m}_{des} - B\mathbf{u}) \quad (3.9)$$

The function H will be at an extreme point if either partial derivative is equal to zero (equation 3.10).

$$\frac{\partial H}{\partial \mathbf{u}} = 0, \quad \frac{\partial H}{\partial \lambda} = 0 \quad (3.10)$$

$$\frac{\partial H}{\partial \lambda} = \mathbf{u}^T - \lambda^T B = 0 \quad (3.11)$$

$$\frac{\partial H}{\partial \mathbf{u}} = \mathbf{m} - B\mathbf{u} = 0 \quad (3.12)$$

Performing these operations in equations 3.11 and 3.12 and combining the terms results in equation 3.13.

$$\mathbf{m}_{des} = B\mathbf{u} = BB^T \lambda \Rightarrow \mathbf{m}_{des} = B\mathbf{u} = BB^T \lambda \quad (3.13)$$

From the definition that B is full rank, it follows that BB^T is too and hence invertible, leading to the final result for the matrix P in equation 3.14. Comparing this result to the form of the generalised inverse, $N = B^T$ in this case.

$$\lambda = [BB^T]^{-1} \mathbf{m}_{des} \Rightarrow P = B^T [BB^T]^{-1} \quad (3.14)$$

This allocation method so far was only described for the unconstrained case. However, for an engineering application, it is natural that limits on the control vector must be imposed. For the pseudo inverse, many different methods exist. An example of such a method is the cascaded generalised inverse. This method uses the Moore-Penrose pseudo inverse as a basis to find an initial allocation. If the required deflections exceed the imposed limits, these effectors are assumed at their maximum position and the respective entries of the saturated effectors are removed from the B-matrix. The moment achieved by the saturated effectors is subtracted from the initial commanded moment.

Now, this process is repeated to allocate the remaining moment. The process continues until either the desired moment is reached, or no control effector is left to be allocated.

3.2. Direct allocation

The direct allocation is a very popular method in modern control allocation. It is a more complex algorithm and requires more computational power than the pseudo-inverse, but it has some advantages that warrant these expenses. A main limitation on the pseudo-inverse is that the matrix P does not span a basis of the control space, hence the available moments are a subset of the total AMS, and dependent on the method used to determine the entries in P.

Direct allocation is able to access the full attainable moment set and hence is able to allocate moments where the previous algorithm would fail. The algorithm works with four main steps:

1. Creating a vector from the origin of the moment space to the desired moment \mathbf{m}_{des}
2. Constructing the AMS and testing each edge and facet of it to determine whether the vector intersects them
3. Once the correct edge of facet is found, the geometry of this intersection is used to calculate the respective control vector that generates the moment at this point
4. If \mathbf{m}_{des} is less or equal in length to the moment at the intersection, then \mathbf{m}_{des} is attainable. If the moment lies on the boundary of the AMS, the resulting control vector is unique, else it requires scaling to create a solution. If \mathbf{m}_{des} is larger than the intersection, then the moment is unattainable with the current control effector set.

This description shows how the algorithm makes use of the greatest attainable moment set as a requirement for the basic functioning, in contrast to the pseudo-inverse. The difference in attainable moments between the two algorithms is visualised in figure 3.4. The AMS of the direct allocation is equal to the GAMS. The differences in the figure are due to different methods for the computation.

For three-dimensional problems, the creation of the AMS and the facet testing is a laborious task and not used within this research problem. The actual implementation of the direct allocation algorithm utilises a numerical optimisation routine as shown in the next section.

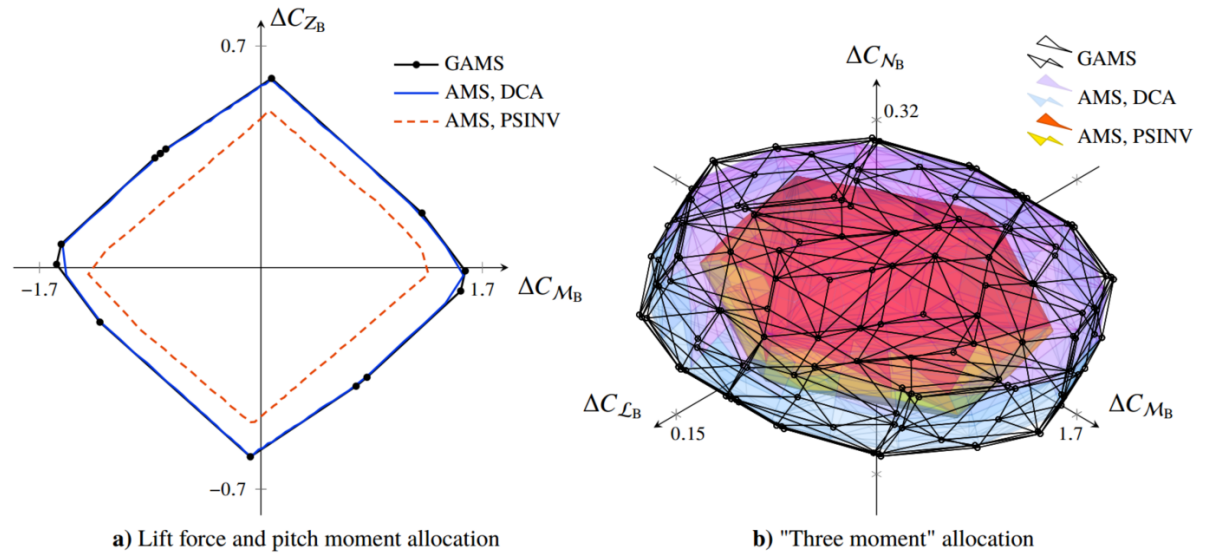


Figure 3.4: Comparison of greatest attainable moment set (GAMS) with attainable moment sets from pseudo-inverse (PSINV) and direct allocation (DCA). Note that the GAMS and DCA are not distinguishable graphically as they are equal. [36]

The direct allocation algorithm implementation requires an internal optimisation algorithm to determine the attainable moment set and hence the required control surface deflections. For this, a linear programming approach is used as the basic equations for control allocation (3.15) is already in a linear form.

$$B\mathbf{u} = \mathbf{m}_{des} \{ \mathbf{u}_{min} \leq \mathbf{u} \leq \mathbf{u}_{max} \} \quad (3.15)$$

The direct allocation formulation is direction preserving. This means that for an unattainable moment, the control vector will point from the origin towards the unattainable moment, while the result will lie on the boundary of the AMS (Φ) as shown in figure 3.5. For an attainable moment, this vector will point towards the moment within Φ .

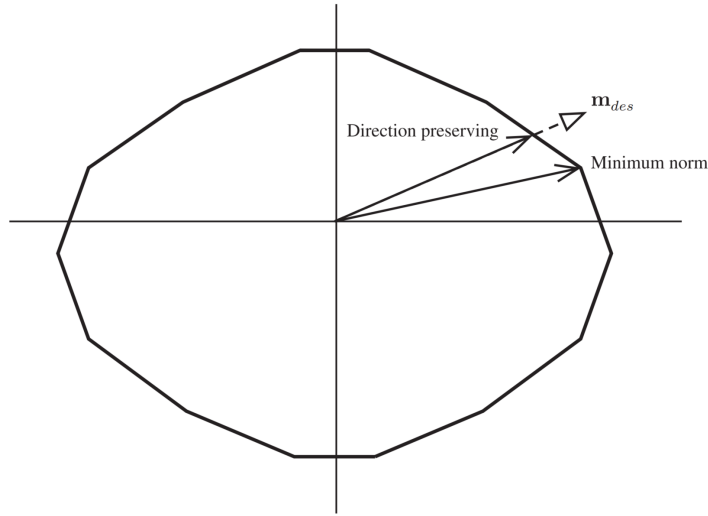


Figure 3.5: Direction preserving solution for an unattainable moment command [35]

This direction preserving formulation requires the inclusion of a scaling factor λ in the problem formulation (equation 3.16). This scaling factor is always positive and thus ensures the resulting moment is always in the direction of the original moment \mathbf{m}_{des} . For commands within Φ , this factor must always be $\lambda = 1$. Outside Φ , $\lambda < 1$ to scale the moment to its boundary.

$$B\mathbf{u} = \lambda\mathbf{m}_{des} \{1 \geq \lambda \geq 0, \mathbf{u}_{\min} \leq \mathbf{u} \leq \mathbf{u}_{\max}\} \quad (3.16)$$

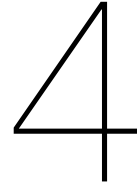
The aim of the linear program is now to maximise the scaling factor of λ to ensure that the moment is attained. Optimisation problems are commonly set-up to minimise the objective, hence the objective function will be $\min -\lambda$. Adding the scale factor to the control vector and rearranging equation 3.16 leads to the following set of equations that define the basic optimisation problem.

$$\begin{aligned} \min \quad & -\lambda \\ \text{s.t.} \quad & [B - \mathbf{m}_{des}] \begin{pmatrix} \mathbf{u} \\ \lambda \end{pmatrix} = 0 \\ & 0 \leq \lambda \leq 1 \\ & \mathbf{u}_{\min} \leq \mathbf{u} \leq \mathbf{u}_{\max} \end{aligned} \quad (3.17)$$

As both objective function and all constraints are purely in a linear form, a linear programming optimisation algorithm can now be used for the optimisation. For this, the Matlab function of *linprog* is used. This program solves the linear optimisation problem using a simplex method to determine the control deflections. The nature of this allocation algorithm using an internal optimisation routine will result in longer computational time compared to the other algorithms using only linear algebra.

Bodson [37] used algorithms from linear programming to efficiently solve direct allocation problems on different over-actuated aircraft layouts. His results show that the implementation

of a direct allocation method can be computed in less than a millisecond on modern computers for a set of eight control actuators. This shows that the increased complexity of direct allocation does not limit its use for real time applications on aircraft. Modern computational power is well sufficient to make use of these algorithms in realistic designs. Comparisons of results between eight and 16 actuators with an interpreted language show slower computation times, in the range of milliseconds, but do not show significant differences in execution time between the amount of actuators. Hence, it can be assumed that also for larger actuator numbers this algorithm is still feasible in a real-time environment. Bodson used a simplex method for his optimisation problem. He notes that the required code is relatively complex, and that other optimisation algorithms should be considered as well. He proposes that interior point algorithms could be beneficial for very large problems as they would then require less iterations than a simplex method [37].



The optimisation framework

The optimisation system is the main body of this research project. It is used to assess and compare the performance of different control allocation (CA) algorithms used in control surface (CS) sizing on various objective functions. It optimises the size of the CS under the constraints of good handling- and flying quality (HFQ) criteria. The general layout is shown in figure 4.1.

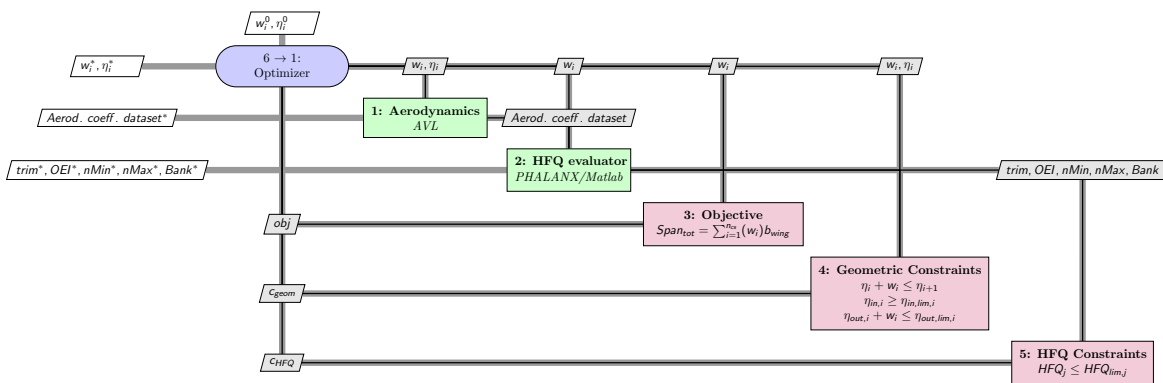


Figure 4.1: XDSM diagram of developed framework

The optimisation system consists of three main parts:

1. The optimiser, that evaluates the objective function to determine the feasibility and optimality of the current design point and to find the subsequent point for the next iteration.
2. The aerodynamic analysis module, that uses the control surface layout at each step in the optimisation to create an aerodynamic database with the static and dynamic coefficients of the current design.
3. The flight mechanics module, that simulates the different HFQ maneuvers of the PrP. Within this simulation, the CS deflections are determined by the CA algorithms. The results of the HFQ evaluations are passed as nonlinear inequality constraints to the optimiser.

4.1. The optimiser

The optimisation framework is created to size a set of CS on the wing. Hence, the CS span widths (w_i) are the design variables. These parameters are non-dimensionalised over the total

wingspan. For optimisations that also investigate the placement of the CSs along the wing, additionally, the inboard span locations (η_i) are added as design variables.

4.1.1. Objective functions

The current framework has two objective functions implemented for the studies. The optimisation is performed for either minimum total CS span or minimum total CS area.

The minimum span function computes the sum of the non-dimensional span of all CS (w_i) on the wings multiplied by the wing span (b_{wing}) (equation 4.1). Optimising for minimum span is a common objective function in CS sizing [12, 14]. Having a small total span width allows more space on the trailing edge for other subsystems such as larger high lift devices. This could be beneficial for improved airfield performance.

$$\min Span_{tot} = \sum_{i=1}^{n_{cs}} (w_i) b_{wing} \quad (4.1)$$

The second objective function optimises for minimum total CS area. This may lead to a more balanced distribution of the CS, as now not only the span width, but also the position on the wing have a direct influence on the objective. Hence, CS at smaller wing chord sections may be preferential in this case.

The minimum area function finds the chord lengths (c_{in}, c_{out}) of the beginning and end sections of each CS and then find the area based on chord length, width and hinge location ($\frac{x}{c}$) of the control surfaces as shown in equation 4.2. For this investigation, the hinge location was kept constant at 30% wing chord.

$$Area_{tot} = \sum_{i=1}^{n_{cs}} \frac{1}{2} \left(\frac{x}{c} \right)_{hinge} (\eta_{out,i} - \eta_{in,i}) (c_{out,i} + c_{in,i}) b_{wing} \quad (4.2)$$

4.1.2. Constraints

For cases that only optimise for the size, the η_i s are formulated as bounds with minimum and maximum values such that the CSs cannot intersect each other, or move out of the wing limits. If the η_i s are included in the optimisation formulation, additional geometric constraints are added to the system to assure a feasible design and prevent intersecting surfaces.

- Compenetration constraints ensure that control surfaces do not intersect each other. If the optimiser creates such a design, the inboard surface is cut off at the beginning of the next surface to assure a well posed aerodynamics case for the AVL solver. A geometric constraint violation is then used for the optimiser.

$$\eta_i + w_i \leq \eta_{i+1} \quad \forall i = 1, 2, \dots, n_{cs} - 1 \quad (4.3)$$

- Hard constraints limit the position and size along the wing to prevent CS to grow beyond the wing span or into obstacles like the fuselage or the V-tail.

$$\begin{aligned} \eta_{in,i} &\geq \eta_{in,lim,i} & \forall i = 1, 2, \dots, n_{cs} \\ \eta_{out,i} + w_i &\leq \eta_{out,lim,i} & \forall i = 1, 2, \dots, n_{cs} \end{aligned} \quad (4.4)$$

Summarizing, the optimisation problem for a minimum span objective is formulated as:

$$\begin{aligned}
 \min Span_{tot} &= \sum_{i=1}^{n_{cs}} (w_i) b_{wing} \\
 \text{s.t.} \quad \eta_i + w_i &\leq \eta_{i+1} \quad \forall i = 1, 2, \dots, n_{cs} - 1 \\
 \eta_{in,i} &\geq \eta_{in,lim,i} \quad \forall i = 1, 2, \dots, n_{cs} \\
 \eta_{out,i} + w_i &\leq \eta_{out,lim,i} \quad \forall i = 1, 2, \dots, n_{cs} \\
 HFQ_j &\leq HFQ_{lim,j} \quad \forall j = 1, 2, \dots, n_{HFQcriterion}
 \end{aligned} \tag{4.5}$$

The optimisation problem for minimum area objective is formulated as:

$$\begin{aligned}
 \min Area_{tot} &= \sum_{i=1}^{n_{cs}} \frac{1}{2} \left(\frac{x}{c} \right)_{hinge} (\eta_{out,i} - \eta_{in,i}) (c_{out,i} + c_{in,i}) b_{wing} \\
 \text{s.t.} \quad \eta_i + w_i &\leq \eta_{i+1} \quad \forall i = 1, 2, \dots, n_{cs} - 1 \\
 \eta_{in,i} &\geq \eta_{in,lim,i} \quad \forall i = 1, 2, \dots, n_{cs} \\
 \eta_{out,i} + w_i &\leq \eta_{out,lim,i} \quad \forall i = 1, 2, \dots, n_{cs} \\
 HFQ_j &\leq HFQ_{lim,j} \quad \forall j = 1, 2, \dots, n_{HFQcriterion}
 \end{aligned} \tag{4.6}$$

4.1.3. Optimiser settings

This optimisation problem is implemented in the *fmincon* function in Matlab using the sequential quadratic programming algorithm. This is a robust medium-scale algorithm and thus well suitable for the posed optimisation formulation. It satisfies the bounds at all iterations, which is particularly important for the aerodynamics discipline. This prevents impossible surface placement that would cause AVL to crash. Furthermore, it is able to recover from *NaN* and *Inf* results, which could happen in case the flight condition is not trimmable. The optimiser settings are reported in table 4.1.

Table 4.1: Options for *fmincon*

Option	Description	Value
DiffMinChange	Minimum change in variables for gradient	$2 \cdot 10^{-2}$
DiffMaxChange	Minimum change in variables for gradient	∞
ConstraintTolerance	Tolerance on constraint violations	$1 \cdot 10^{-6}$
OptimalityTolerance	First-order optimality termination tolerance	$1 \cdot 10^{-6}$

4.1.4. Implementation overview

The implementation of the framework is presented in figure 4.2. The whole process from initial geometry definition to the optimisation structure is shown.

The optimisation process starts with the input geometry and an initial set of CS sizes. From this, the aerodynamic discipline creates the aerodynamic data set which is then fed to the flight mechanics discipline. This function uses the respective control allocation algorithm to analyse a set of flight maneuvers. The results are fed to the optimisation algorithm, which uses the results to compute a gradient to find a new design point. This updated point is then used as the next step in the optimisation process.

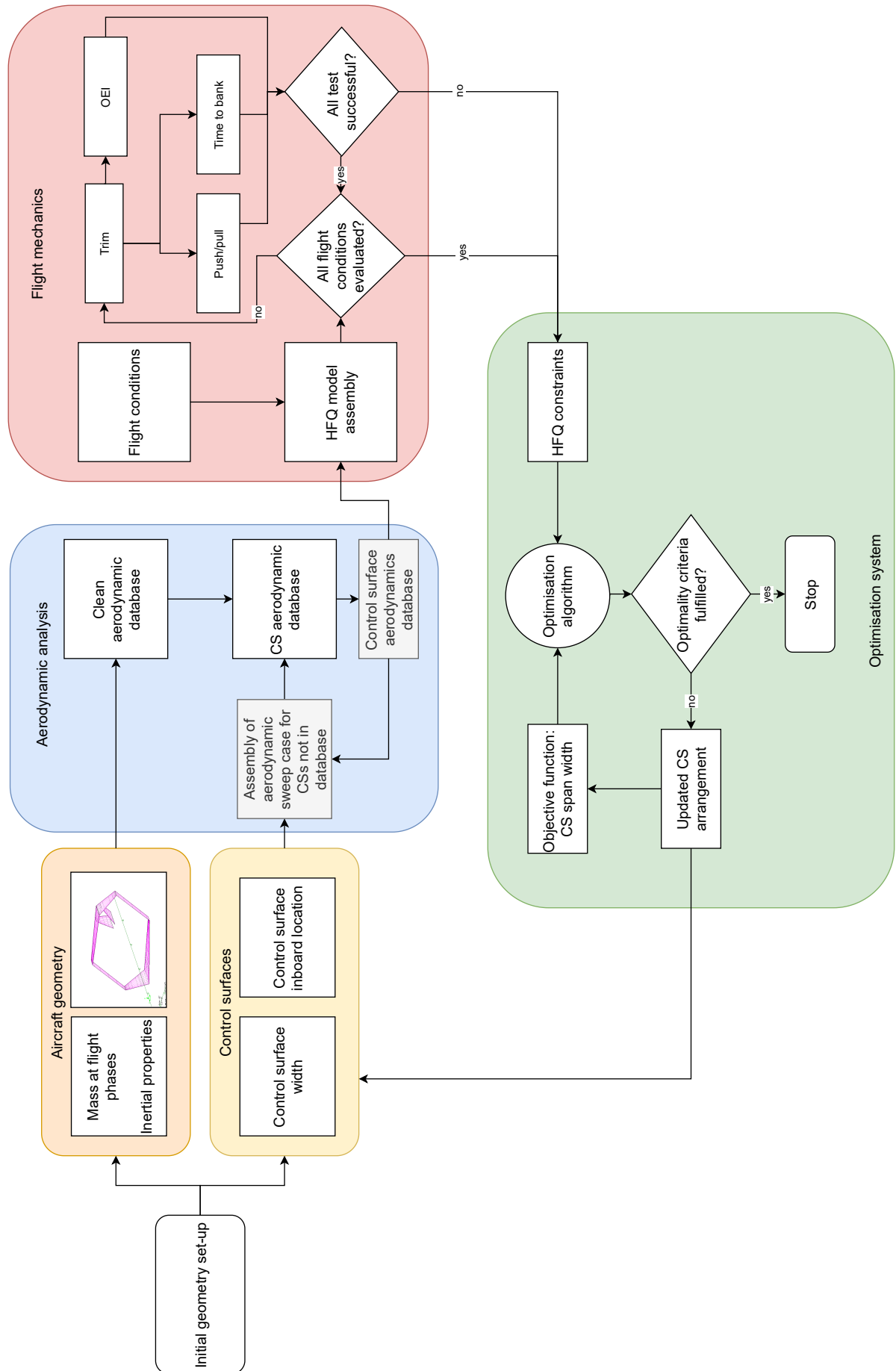


Figure 4.2: Overview scheme of control surface sizing optimisation system

4.2. PrandtlPlane geometry

The aircraft geometry used in this study is based on an early geometry layout of the PARSIFAL study. The continuous trailing edge on front and rear wing are beneficial for this investigation as it allows the CS to move along the wing in a continuous manner, without requiring additional geometric constraints such as kinks. The implemented geometry is shown in fig. 4.3. The exact input parameters are shown in tables 4.2 and 4.3.

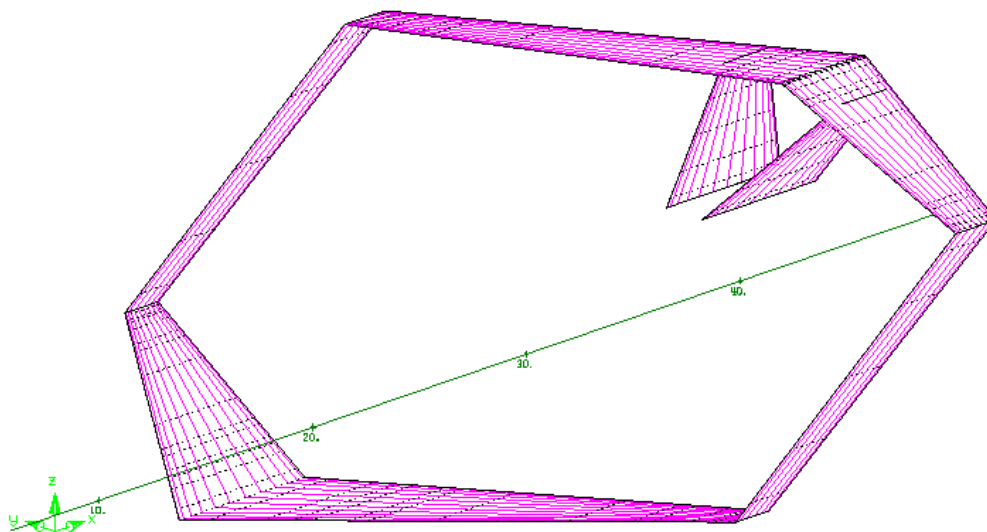


Figure 4.3: Parsifal Milestone 1 geometry shape used for this study

The tailplanes have ruddervators that are assumed a fixed size, and hence not included in the CS sizing process. For the mechanical gearing, these surfaces are constrained to move together to act as yawing moment generators. For the control allocation algorithms, the two surfaces are included as individual control effectors and hence are included in the allocation problems for all aerodynamic moments.

The position of the center of gravity (CG) is set to achieve a 10% static margin for all flight cases [14]. As described in chapter 2, PrandtlPlane configurations have design-imposed low allowable ranges for the CG location [7, 38], this study assumes that the CG stays at the same location during the flight, which could e.g. be achieved through internal pumps redistributing the fuel during the mission. This design choice was also used in other studies investigating control surfaces and stability effects on PrP configurations [14].

4.3. Aerodynamics

The aerodynamic solver is an essential part of the optimisation system. At every objective function evaluation it creates an updated set of aerodynamic coefficients. This implementation necessitates that the chosen solver is able to provide a full set of aerodynamic data very fast in order to keep the total run time of the optimiser at an acceptable level. At the same time,

Table 4.2: Geometric input parameters defining the main wings of the aircraft

Geometric parameter	Front wing	Rear wing
Span	28.598 m	28.598 m
Aspect ratio	7.69	9.85
Taper	0.267	0.485
Leading edge sweep angle	39.4°	-23.33°
Dihedral	2.3295°	0°
Incidence	3°	2.3°
Root chord	5.869 m	3.911 m
Airfoil	NACA 2710	NACA 2710
Chordwise elements/section	12	12
Chord spacing	Cosine	Cosine
Spanwise elements/section	5	5
Span spacing	Cosine	Cosine
CS number	variable	variable
CS begin spanwise position	variable	variable
CS span width fraction	variable	variable
CS chord fraction	0.3	0.3

Table 4.3: Geometric input parameters defining the tailplanes of the aircraft

Geometric parameter	Right vertical tail	Left vertical tail
Span	3.917 m	3.917 m
Aspect ratio	2.1	2.1
Taper	0.4	0.4
Leading edge sweep angle	49.4°	49.4°
Dihedral	60°	120°
Incidence	0°	0°
Root chord	5.329 m	5.329 m
Airfoil	NACA 0010	NACA 0010
Chordwise elements/section	12	12
Chord spacing	Cosine	Cosine
Spanwise elements/section	6	6
Span spacing	Cosine	Cosine
CS number	1	1
CS begin spanwise position	0	0
CS span width fraction	1	1
CS chord fraction	0.4	0.4

the solver needs to be robust and reliable in the results. Under these considerations, the Athena Vortex Lattice (AVL) solver was chosen [39]. This linear solver approximates the wing planform using 2-dimensional quadrilateral panels. The 2-D assumption restricts the analysis of the aircraft shape to thin structures, hence only the lifting surfaces are included in this model. The shape and influence of the fuselage is neglected.

4.3.1. Vortex lattice method

The vortex lattice method discretises the analysed surface in quadrilateral panels, shown in figure 4.4. Due to this 2-dimensional discretisation, only thin airfoils or structures can be anal-

ysed. Correction factors can be applied to correct for this limitation, and also give good results for thick or cambered airfoils, however, generally this method is limited to thin structures [39]. This also means that usually only the lifting system of the aircraft can be analysed accurately.

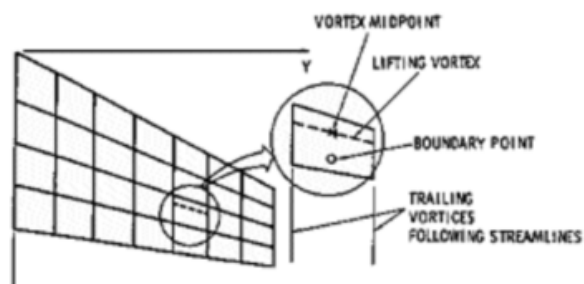


Figure 4.4: Vortex distribution on a flat surface in VLM solver [40]

For each panel, a horseshoe vortex of unknown strength is placed on the quarter-chord line of the panel. The downstream components of the vortex follow the sides of the panel. This discretisation is shown in Fig. 4.5. Furthermore, each element has a control point placed on the three-quarter-chord line at which the flow is assumed tangential to the surface to satisfy the Kutta condition. Hence, the normal flow velocity at these points is zero.

With this discretisation, the Biot-Savart law is used to compute the induction of each vortex on each panel, equation 4.7. This law describes the relationship between the induced velocity V the panel creates due to the circulation Γ of the vortex and distance r to the control point of the element.

$$V = \frac{\Gamma}{4\pi} \int \frac{dl_v \times r}{|r|^3} \quad (4.7)$$

Using the equation and the known geometric parameters of the panels, a system of equations is assembled that has the circulations for every element as the only remaining unknowns. The imposed boundary condition of zero normal velocity at each control point determines the values for the left-hand side of the Biot-Savart equation. These can be rewritten as a matrix that defines the influence coefficients from every vortex point to every control point over the total geometry. This matrix equation can then be solved for the unknown circulations of the panels. Lastly, using the Kutta-Joukowski theorem in equation 4.8, the total lifting force L_{tot} of the wing can be computed by summation of the individual panel results.

$$L_{tot} = \sum_{j=1}^n \rho V_{\infty} \Gamma_j \quad (4.8)$$

The Athena Vortex Lattice (AVL) is a solver originally developed by Mark Drela and Harold Youngren at the MIT [39]. AVL is designed to analyse low Reynolds number flows and assumes quasi-steady flow. The core has been enhanced with additional features to also allow modelling of simple slender fuselages as well as compressibility corrections for higher Mach numbers. A strength of AVL is the support of an arbitrary amount of control surfaces and deflections, including the option to have multiple control functions for a surface, e.g. a flaperon. Flexible control surfaces can be implemented as well, with a linearly interpolated deflection between two specified points.

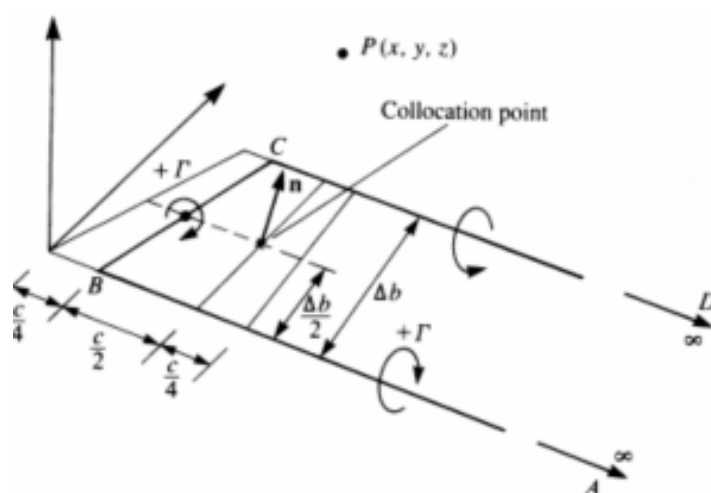


Figure 4.5: Detailed view on horseshoe vortex [41]

4.3.2. Implementation

AVL is a standalone program, hence a wrapper is needed to translate the input geometry and the desired aerodynamic sweep data points in a form accepted by AVL. For this, the AVL wrapper from R. Elmendorp¹ was used. The optimisation framework and the flight mechanics simulation require the use of Matlab as main programming interface. The wrapper is written in Python, hence interfacing with the Matlab environment is necessary at this point. Matlab allows the use of Python objects and has built-in capabilities to run a python engine and execute python scripts. The Python wrapper writes the geometry definition in AVL format in a text file. Then, AVL is launched to read this text file and execute a parameter sweep cases. The results are again written to a text file which is read by the Python wrapper and then converted to a Matlab structure. The resulting Matlab structure is then used for the subsequent steps in the optimisation process. The MATLAB wrapper is coded fully configuration agnostic to allow flexibility and also to allow the wrapper be used by other researchers for different investigations

The aerodynamics discipline is initialised by a file with key parameters of the studied airframe. These are constant parameters that define the aerodynamic surfaces for the geometry. By default, the code creates trapezoidal shapes for all surfaces. It is also possible to pass custom arrays to define every individual wing section and hence model more complex geometry such as kinks, if necessary in a future study.

The basic input parameters are:

- wing span
- aspect ratio
- taper ratio
- leading edge sweep angle
- dihedral angle
- incidence angle
- position of the wing root leading edge
- root chord
- airfoil
- number of panels in chord/span wise direction
- chord/spanwise section spacing
- position/number of control surfaces
- chord ratio of control surfaces
- inner/outer limits for the control surfaces

¹<https://pypi.org/project/avlwrapper>

Based on this input a trapezoidal wing shape is generated. Furthermore, to create the boxwing geometry, side panels are defined that connect the wings.

The CSs on each wing are defined by three parameters: the inboard location of the CS (η_i), the CS span width (w_i) and the fraction of the wing chord that is used for the CS. w_i and η_i are used as dimensionless fractions of the wing span. The CS input files are defined for the right-hand wings and starting at the inboard section. For the full simulation model, the left wing CS are mirrored by calculation.

From this definition, the wing geometry input file for AVL is created. The wing is partitioned in sections, depending on the number of CS defined. Every CS creates an inboard and outboard section. Additional sections are placed at the root and the inner CS position limit and at the outer CS position limit and the wing tip.

With the given geometry, a sweep over a range of data points at different aerodynamic conditions is specified to create an aerodynamic data set consisting of all steady and unsteady aerodynamic force and moment coefficients at each data point. The data points are defined in function of the angle of attack (α), angle of sideslip (β), Mach number (M) and control surface deflections (δ_i). The list of aerodynamic coefficients extracted from the AVL analysis is shown in table 4.4. Due to the potential flow assumptions of AVL, it does not compute any dynamic derivatives for the forces in X-direction.

Table 4.4: Coefficients obtained from AVL analysis

Steady coefficients	Unsteady coefficients
CFX	-
CFY	CFYp
	CFYq
	CFYr
CFZ	CFZp
	CFZq
	CFZr
CMX	CMXp
	CMXq
	CMXr
CMY	CMYp
	CMYq
	CMYr
CMZ	CMZp
	CMZq
	CMZr

The differential actions due to control surface deflection are determined by subtracting the clean steady coefficients from the results of the data point at the same flight condition with a control deflection. Hence, the saved entries for the control surface coefficients show the difference in aerodynamic forces and moments compared to the undeflected case. This decoupling of the clean aerodynamics and the differences due to a control surface deflection allow a simple superposition of different control surface deflection effects to recreate the aerodynamic performance of a wing with multiple deflected control surfaces. Each aerodynamic action (F) is then gathered from look-up tables through the summation of coefficients of this data set, as shown in equation 4.9. This approach assumes linear independence of the aerodynamic

actions with respect to the angular rates. Furthermore, interaction effects between deflected control surfaces are neglected.

$$\begin{aligned}
 F(\alpha, \beta, M, p, q, r, \delta_i) = & F(\alpha, \beta, M, p = 0, q = 0, r = 0, \delta_i = 0) + \\
 & + \sum_{\omega=p,q,r} \frac{\partial F}{\partial \omega}(\alpha, \beta, M, \delta_i = 0) \omega + \\
 & + \Delta F(\alpha, \beta, M, p = 0, q = 0, r = 0, \delta_i)
 \end{aligned} \tag{4.9}$$

To increase efficiency and reduce computational time, a database feature is implemented in the aerodynamic discipline. This database stores the results per control surface based on the name of the wing, its span wise location and its span width. If a control surface is already in the database, the respective aerodynamic analysis is not performed again. All new control surfaces are added to the database. Another function then searches the updated database for the required elements and assembles the aerodynamic data set for the following steps. Unless the underlying aircraft geometry is altered, this database is constantly growing the more analyses are done with the optimiser, hence the aerodynamic computations will require less time as the optimisation progresses. The database is stored in a *.mat* object and can easily be extracted for other uses if required.

4.4. Flight mechanics

The flight mechanics discipline is evaluated using the in-house developed Performance, Handling Qualities and Load Analysis toolbox (PHALANX), which is programmed in Matlab and Simulink. PHALANX is a modular toolbox for non-linear, six degrees of freedom flight simulation and analysis [14]. The flight mechanics simulation consists of multiple modules, such as the aerodynamics, engine, mass and inertia, flight control system and the pilot input. The model is created in the Simulink environment to implement the control system.

The propulsion data is obtained from the in-house developed GTpy tool. This tool uses thrust, the design flight condition and specific engine design parameters as input and is able to generate thrust and fuel flow maps in off-design conditions depending on altitude, Mach number and corrected fan speed. Using this, a data set for engine performance and thrust settings at different flight conditions is created and used within the flight mechanics simulations. The engine specifications are based on an early design from the Parsifal project.

The implementation of PHALANX used in this framework is based on pilot stick input. Every control command is given by deflecting the simulated pilot stick, pedals and throttle. This deflection is then translated to a commanded force or moment and fed to the control allocation. The resulting deflections are passed through an actuator simulation and used in combination with the state of the aircraft model to analyse the dynamic response to the inputs. This top level scheme is shown in figure 4.6.

Regarding the control system, three options are implemented for this study to determine the required control surface deflections: mechanical gearing (MG), constrained pseudo inverse (CPI) and direct allocation (DA).

The mechanical gearing (MG) option uses a predetermined gearing matrix to determine the deflections. The inner control surfaces react purely to a longitudinal stick input, the outer control surfaces purely to a lateral stick input. Control surfaces of the same function are ganged to act together to achieve a maximum moment. The inner front and rear surfaces are constrained to move in opposite directions, working as an effective pitching moment generator and thus act like a classical elevator. The outer left and outer right surfaces are also ganged to deflect

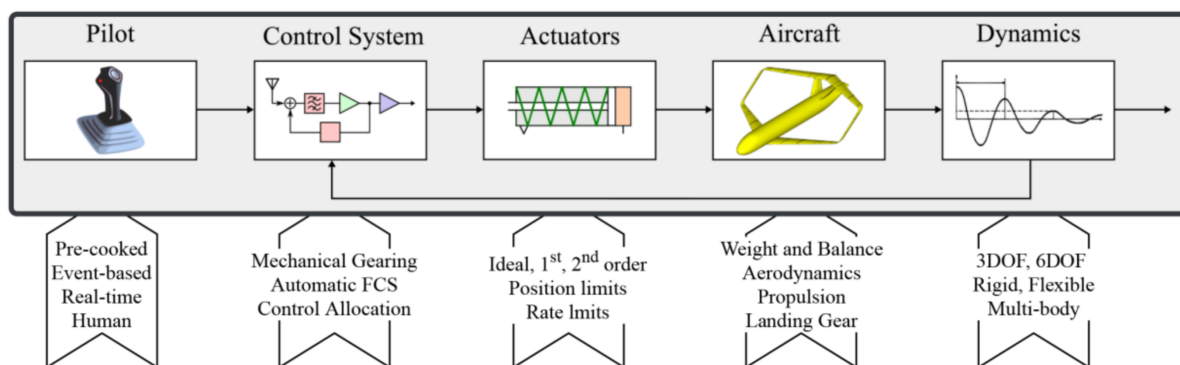


Figure 4.6: Top level overview of PHALANX workflow [14]

in opposing directions, to act as rolling moment generators. These surfaces are acting as classical ailerons. The rudders on the V-tail of the aircraft are ganged to deflect at the same direction and angle and react only to a pedal command, thus acting as classical rudders.

The constrained pseudo inverse algorithm (CPI) option is based on the *lsqin* Matlab function and uses a linear least squares approach to finding a solution to the underdetermined system under deflection constraints. It is a simple control allocation method, but it has a limited attainable moment set. Hence, the algorithm might not find a solution even though the moment is actually attainable with the given set of CS.

The direct allocation (DA) is a more complex algorithm. It uses a linear programming optimisation routine to find a control vector in the direction of the required moment. This control allocation algorithm has by definition the largest attainable moment set, hence as long as the CS are able to generate the desired moment, this algorithm will be able to find the required CS deflections for it.

Both CPI and DA make use of an optimisation routine within their allocation. The capacities of Simulink to natively support Matlab functions is limited such that neither routine can run within Simulink. Hence, both have to be executed extrinsically, increasing the total runtime.

The B matrix that forms the basis of both allocation algorithms consists of the control effectiveness derivatives for every surface at the given flight condition. The matrix entries are created within PHALANX through interpolation of the data tables from the aerodynamic database for the respective flight condition. The control derivatives are then found by numerical differentiation.

4.5. Handling and flying qualities

The model created by PHALANX is used to investigate a selection of different handling and flying quality criteria (HFQ), that are typically required for the certification of a full aircraft design. The selected tests and their target values are extracted from the MIL-F-8785C standards for the American military [28] for transport category aircraft. All tests conducted within this study are deemed successful if the result is within the level 1 category. The following cases are described in this specification and performed by PHALANX using the numerical requirements for category III aircraft:

- Trim in straight and level flight. The aircraft must be trimmable at a given flight condition. This includes counteracting moments from a side wind. This test forms the basis for all subsequent tests. If trim is not achieved, all further tests are skipped and the optimiser moves on to the next function evaluation.

- Push/pull. Full longitudinal stick deflections must create normal load factors of at least 2.0g for an aft deflection and -0.5g for a forward deflection.
- Time to bank. A full lateral deflection of the stick must result in a bank angle of 30 degrees within 2.3 seconds.
- One engine inoperative (OEI). The aircraft must be trimmable to fly in steady flight at the given conditions with the critical engine being inoperative.

These tests are run at two design points of the aircraft, in the cruise and the approach phase, as well as two different wind conditions. The matrix detailing this is shown in table 4.5. The cruise phase parameters are taken from the PARSIFAL mission requirements, the approach speed is chosen as a typical value on comparable commercial transport aircraft. The side wind magnitude is set as $V_w=25$ kts as prescribed in current certification regulations for commercial aircraft [30].

Table 4.5: Handling and flying quality test matrix used as constraints in the optimisation

	Cruise <i>h = 11km, M = 0.79</i>	Approach <i>h = 0km, V = 120kts</i>
No side wind $(\beta = 0)$	Straight and level trim Push/pull Time to bank	Straight and level trim Push/pull Time to bank OEI
Side wind $(\beta \neq 0)$	Straight and level trim Push/pull	Straight and level trim Push/pull OEI

The results from each test are recorded and scaled according to equation 4.10. This scaling is still resulting in a violation if the level 1 criterion is not met, but violations are normalized to the limit values. Hence, all constraints are weighted more equally to the optimiser.

$$x_{scaled} = \frac{x - x_{level1limit}}{x_{level1limit}} \quad (4.10)$$

The adherence or violation of each test to the given constraint value is used to define the total constraint violation of the current design point. The limit values are all set to the level 1 handling quality limits. Hence, a feasible final control surface arrangement will fulfill level 1 handling qualities.

The handling qualities are evaluated using the PHALANX simulations. The trimming routine is formulated as an optimisation problem to find CS deflections that minimise the residual accelerations around all axes. The algorithm's objective function is an array of the linear and angular accelerations in the body axes, and the error in prescribed sideslip angle. The algorithm then perturbs every control (stick, pedal and throttle) that prescribe a desired moment that the control allocation transforms into an effector deflection, and records the effect of the perturbation on the objective values. Based on this, a gradient is computed to find a new point in the direction of the steepest gradient. The routine finishes if either all objective values are below a threshold, or any of the simulated controls have reached their maximum position. The OEI test uses the same trim optimisation algorithm, with a modified thrust vector.

The push/pull and time-to-bank tests build upon the control deflections from the trim case. For these, a maximum moment around the pitch and roll axis is commanded respectively and the time response is recorded. For the push/pull, maximum and minimum values are recorded, the bank criterion records the duration to achieve a given bank angle.

4.6. Hardware and Software

The optimisation system is programmed in Matlab R2019b and Simulink 10.0. The aerodynamic module utilises Python 3.8 with AVL 3.36. The post processing of the results and all figures are done in Matlab. The programs are run on Windows 10 with an Intel I7-6700HQ processor.

The flight mechanics simulations are time intensive. The main core of the PHALANX program is a Simulink routine that performs the actual dynamic simulations. For the mechanical gearing, this system can run efficiently as the Simulink file is compiled once and then can be reused for every simulation step and for each point in the trim optimisation routines. The two control allocation algorithms use functions that Simulink cannot execute natively. Hence, these must be run extrinsically by Matlab which significantly increases the execution time of the program. Furthermore, these two functions are optimisation algorithms, compared to a simple matrix multiplication for the mechanical gearing. Thus, each function evaluation has a significant cost in computational power and thus in time.

An exemplary time breakdown of one function evaluation is shown in table 4.6 for a complete aerodynamic data set, and a flight mechanics simulation of the approach phase. These values are using the initial layout as presented in the results chapter and using the direct allocation algorithm. As four of the sections involve the trim optimisation routine, the actual time requirements fluctuate depending on the number of iterations of the optimiser. As the optimiser progresses and the aerodynamic database grows, the time for the aerodynamics diminishes and becomes an insignificant contribution to the total. Depending on the number and quality of the design points of the optimiser, one full design optimisation requires on average 2.5 days, with an average of 80 ± 25 function evaluations. Hence, available computational time and resources pose a limitation to the amount of optimisations that can be performed for this study.

Table 4.6: Sample computational time breakdown for one function evaluation

Program section	Time (min)
Aerodynamic data set	7
Trim approach/side wind	8
Push/pull criterion	12
One engine inoperative trim	15
Trim approach/ no wind	5
Push/pull criterion	12
Time to bank criterion	7
One engine inoperative trim	9
Total time for one objective function evaluation	75

5

Verification

An important part in the creation of the framework is the verification process of all subsystems and the interlinking of the whole system. For this, every function implemented in the system was unit tested for correct processing of the inputs as well as robustness. The main modules of the framework were compared to external data to assure a correct working.

5.1. Aerodynamics

AVL as aerodynamic solver is widely used and verified in scientific literature, and hence verification is not strictly necessary. Here, the most important parts of the verification process is the correct parsing of the input geometry and processing of the output file. For this verification, a Cessna Citation II aircraft was modeled using the aerodynamics module and a full aerodynamic sweep case was created. These results were then compared to an existing database of this aircraft from an analysis performed with the 3D-panel solver VSAero. A comparison of the two results is shown in figure 5.1. The figure shows the steady aerodynamic coefficients at a Mach number of 0.3 and three different side slip angles. The results are similar, with small differences which are expected because the AVL implementation does not model the aircraft fuselage as AVL cannot properly analyse these shapes. This and the linearity and potential flow assumptions lead to small differences in the coefficients, especially the normal force (CFX) as AVL can only simulate induced drag. It furthermore shows that AVL over-predicts the rolling moment but has a lower side force coefficient. This again could be a result of the missing fuselage modelling. Under a side slip, the fuselage will create a side force, and the altered flow field has an impact on the rolling moment. Th

5.2. Control allocation

The implementations of the control allocation algorithms are based on the book 'Aircraft Control Allocation' by Durham [35]. The book contains multiple examples including results to verify the correct working of the programmed code. The allocations were verified against an example of a 5-surface canard aircraft in chapter 6.11. A comparison of the results showed that the results were equal to the reference values, hence the correct implementation is confirmed.

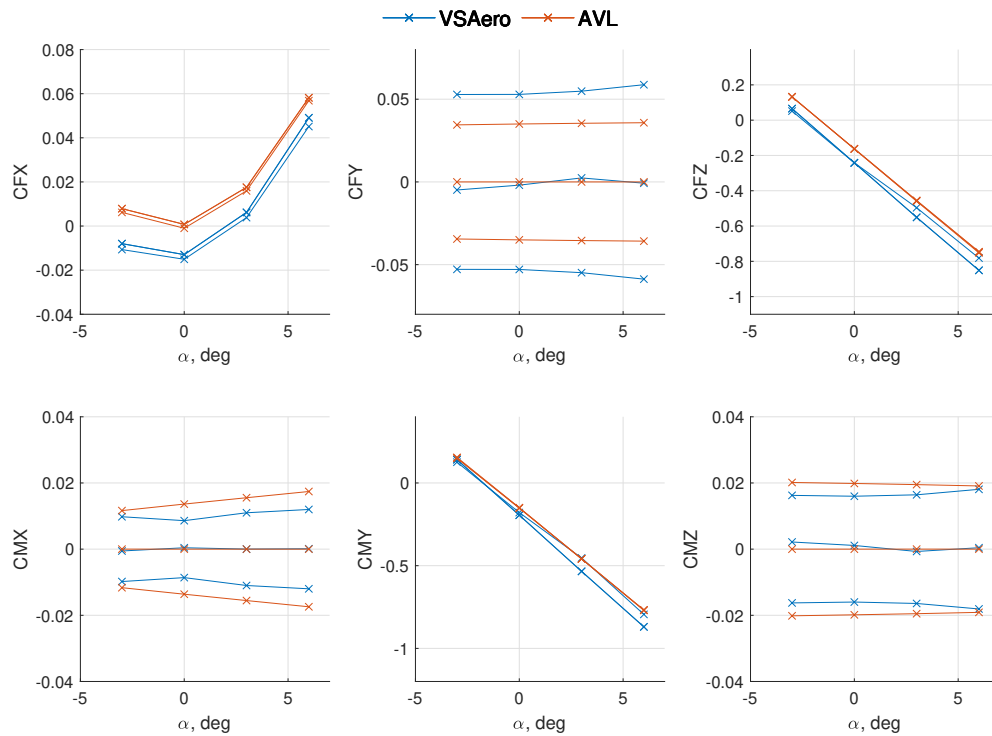


Figure 5.1: Steady aerodynamic coefficient comparison between VSAero and AVL for a Cessna Citation II

5.3. System test

The verification of the full simulation model and the optimisation system is difficult, as no commercial PrandtlPlanes currently exist. Hence, it was decided to verify the full system by qualitative comparison to a similar case from scientific literature. Varriale [14] has created a similar simulation framework and applied it to a PrandtlPlane configuration. His framework used only mechanical gearing for the sizing of the control surfaces, hence the new optimisation system is verified with this method. The comparison study uses a similar design. The aircraft has slightly smaller wings and a lower maximum take-off mass. Furthermore, the optimiser used for that study is discrete and designs for a balanced distribution between front and rear control surfaces for each effector function. Hence, it aims to have pitch, and roll effectors of similar width respectively. The optimisation framework described in this thesis does not have this restriction. The verification was made with the study results for the mechanical gearing. Varriale used a CS layout with inboard surfaces on both wings to act as pitch effectors and outboard surfaces for the rolling moments. The geometry and CS layout is shown in figure 5.2.

The CS layout used in the present study to optimise with the MG algorithm is equal to the layout of Varriale. The inboard surfaces begin at the same relative span location; the outboard surface end at the same relative span position. The initial and final values of the CS span widths differ. Further details on the CS layout and the design variables are given in chapter 6. The shape of the resulting CS layout is compared to the mean value of all minimum span optimisations performed using the MG algorithm.

The comparison between the two results is shown in figure 5.3. The results show larger CS for the present study, as the geometry is larger and heavier. However, the relative size of the individual CS is very similar to Varriale's results. The inboard CS are larger than the outboard CS, and the front wing has a slightly larger CS on the inboard side. The outboard

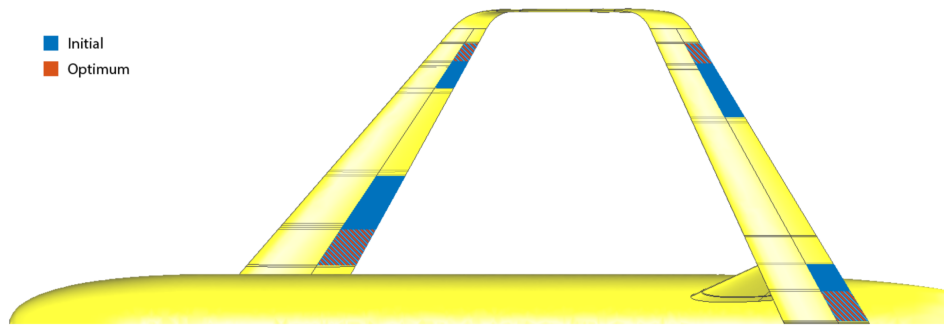


Figure 5.2: Geometry and CS layout of Varriale [14]

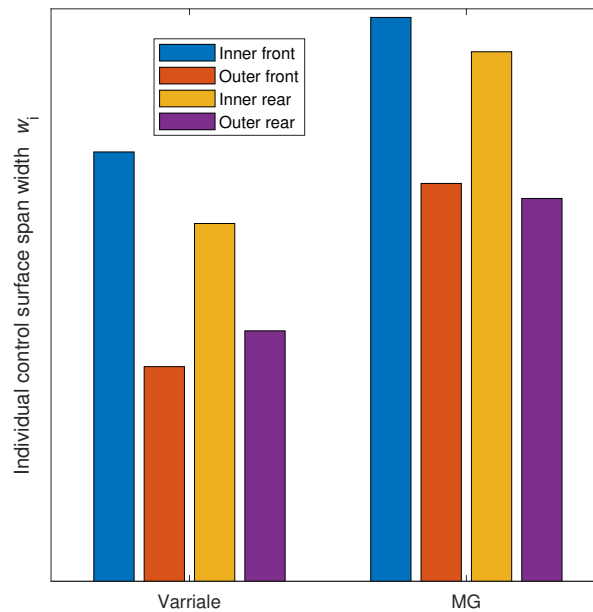


Figure 5.3: Verification comparison of mean MG layout to results from Varriale [14]

CS are very similar in size. While Varriale's layout has a slightly larger outboard surface at the rear wing, the MG created two nearly equal surfaces. The overall layout and the relative sizes of the CS are very similar for the MG and Varriale. This gives further confidence in the correct working of the optimisation system and its suitability for the goal of comparing different control methods.

6

Results and Discussion

The main application of the optimisation system is to compare the MG, CPI and DA algorithms by means of optimising the CS layout. For the comparison, two different objective functions were applied: total span width of the control surfaces, and total area of the control surfaces. The layout is chosen to have an inboard control surface at each wing, placed at the inboard limit and an outboard control surface placed at the outer limit. Within the optimisation, these surfaces can grow towards the center of the wing. Thus, for the inboard surfaces, the inner limit is fixed and for the outboard surface, the outer limit is fixed.

On the front wing, the space in between the two CS is treated as an additional movable surface, representing a plain flap. The span wise position and size of this flap is not a design variable. It is calculated from the CS arrangement and sizes, and set to a deflection of 30 degrees for the approach condition and zero degrees for the cruise. The flaps are not included in the sizing process as they are secondary flight controls and as such only indirectly related to aircraft controllability. For this study, it is assumed that there are no requirements on the airfield performance that would pre-set a certain flap size or type. Instead, the set-up of the optimisation system will create the largest possible flap span. The initial configuration is shown in figure 6.1. The CS span widths are non-dimensionalised with the aircraft's wing span. The CS design variables, the initial point and bounds are shown in table 3.

Table 6.1: Initial values for the design variables and bounds

Control surface	Symbol	Initial value	Lower bound	Upper bound
Inner front	w_1	0.08	0.01	0.1
Outer front	w_2	0.08	0.01	0.1
Inner rear	w_3	0.08	0.01	0.1
Outer rear	w_4	0.08	0.01	0.1

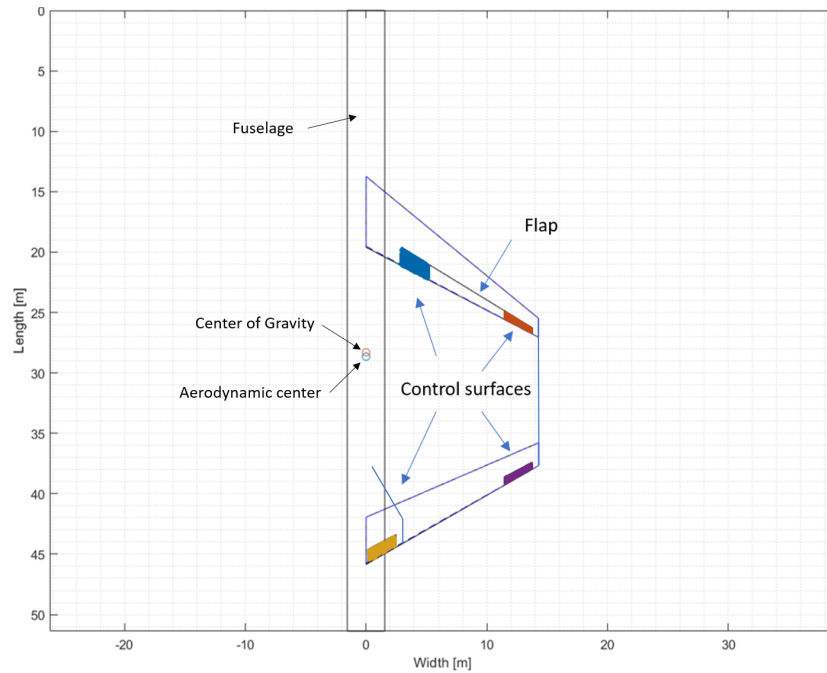


Figure 6.1: Initial layout of the study case showing the non-dimensional CS span widths and bounds

6.1. Minimum span objective function

For the minimum CS span objective, the optimiser is used with the initial values for all three control allocation methods. The results of the optimisations are shown in tables 6.2 and 6.3. Regarding the objective function value, differences between the three allocation methods can be seen. MG requires the largest overall CS widths. This can be explained, as roll and pitch are only commanded by the respective control surfaces. CPI reduces the total required span width by about 9.5%. DA reduces the required span width even further, achieving a reduction of about 17% compared to MG. This results from the properties of the DA. It can access a larger maximum attainable moment set with a given set of effectors. Hence, it is expected that the DA method will yield the smallest total control surface size, it is able to utilise every effector in the most efficient way.

Table 6.2: Resulting objective function values for minimum span objective function

Algorithm	Objective result [m]	Difference to MG [%]
Initial	9.15	+23.7
MG	7.40	[-]
CPI	6.70	-9.45
DA	6.13	-17.21

The resulting CS layouts in table 6.3 and their graphical representations in figure 6.2 show large differences between the three different methods. For MG, all four surfaces reduce in width compared to the initial values, but are still rather large. The inboard surfaces are larger than the outer surfaces. The respective front and rear surfaces are very similar in size. The CPI shows a preference for the rear surfaces. Both remain large and of very similar size. The front surfaces reduce in size, especially the outer front. The DA algorithm shows large values for the inner front and outer rear, and small values for the outer front and inner rear surfaces. While it also utilises the outer rear surface as an effective rolling moment generator,

this algorithm shows a clear preference to the inner front surface as primary pitch effector. The outer front surface is reduced for both CPI and DA to a similar size. This shows that for the rolling moment, both algorithms prefer the rear wing CS.

Table 6.3: Resulting CS sizes as fraction of wing span for the minimum span optimisation

Algorithm	Inner front	Outer front	Inner rear	Outer rear
Initial	0.08	0.08	0.08	0.08
MG	0.076	0.057	0.081	0.051
CPI	0.06	0.025	0.073	0.075
DA	0.097	0.027	0.016	0.074

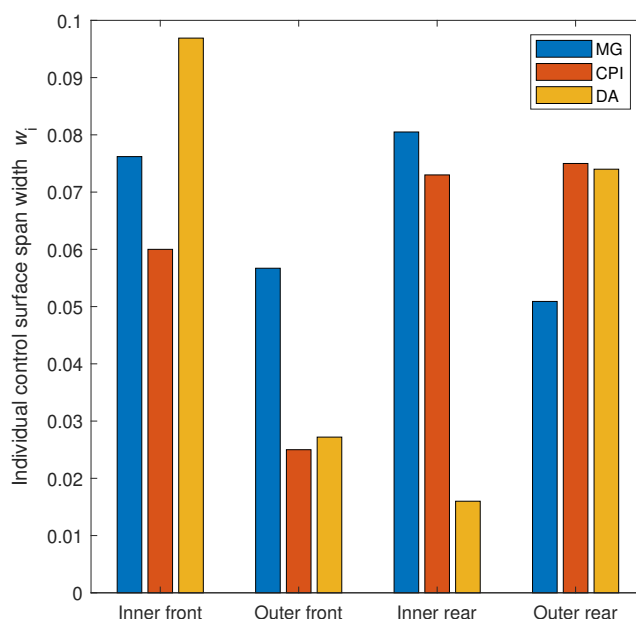


Figure 6.2: CS size comparison for minimum span objective

6.1.1. Optimiser behaviour

This section shows the behaviour of the optimisation system and the histories of the design variables and constraints over the iterations. Figure 6.3 shows the development of the objective functions for the three optimisations. It is interesting to note the difference in shapes. The MG had significantly more iterations than the two other algorithms. However, the changes in objective function were much smaller per iteration. This shows that the optimiser was not able to find a large gradient in the beginning, hence the changes were only incremental. The largest leap was only at iteration 13, after which it was not able to find a better design point. The CPI had its largest change at the first iteration. The subsequent design points did not change much with respect to the overall objective function value. The DA shows an intermediary behaviour. In the beginning the improvements are clearly visible, yet the largest change only happens at iteration 6. After this, the improvement of the objective function was only in small increments.

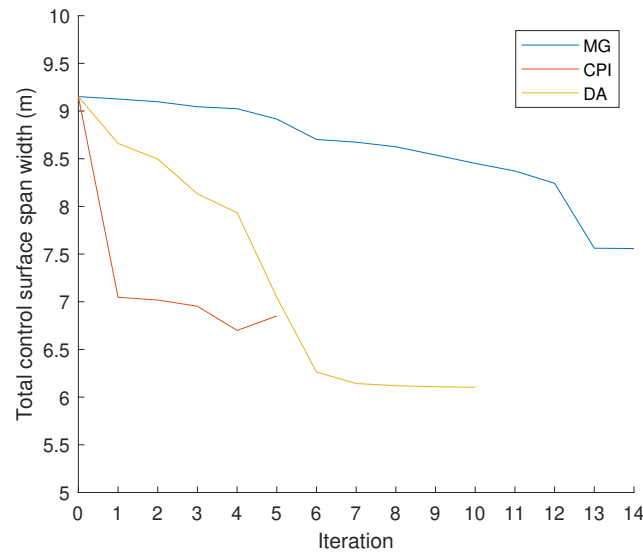


Figure 6.3: Objective function development for minimum span for mechanical gearing (MG), constrained pseudo inverse (CPI) and direct allocation (DA)

Details on the performance and the constraints of the optimisation are shown in the subsequent figures. For MG, figure 6.4 shows the development of the control surface sizes and figures 6.7 and 6.10 the development of the constraints. Figure 6.4 shows the development of the CS span widths for the MG case. These curves show that the inner CS were largely unchanged by the optimiser. The improvements in the CS width was mainly due to reductions in the rear CSs. The CPI optimisation in figure 6.5 shows that all design variables were varied for every iteration. The main changes happened for the CS on the front wing, whereas the rear wing CS did not change much for the later iterations. Lastly, the DA results in figure 6.6 show the largest changes. The sizes of all surfaces was changed significantly over the course of the optimisation. The larger the changes in the design variables, the smaller the final objective result.

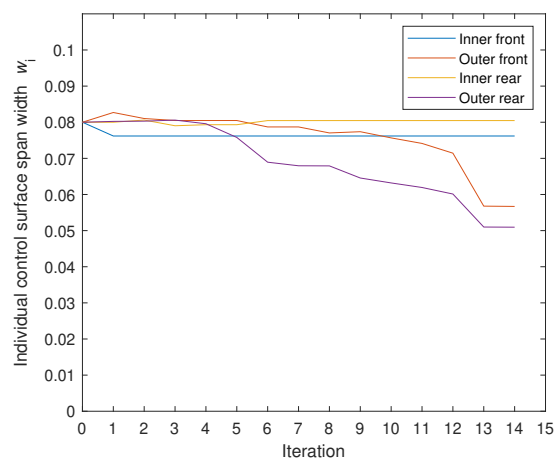


Figure 6.4: Non-dimensional span width design variables behaviour for MG

The trim routine uses an internal optimisation process to find the trim point. For this internal optimisation, the residual accelerations of the aircraft are the objective function. Within the

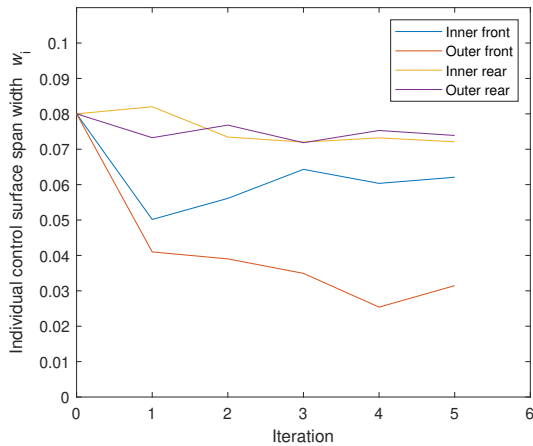


Figure 6.5: Non-dimensional span width design variables behaviour for CPI

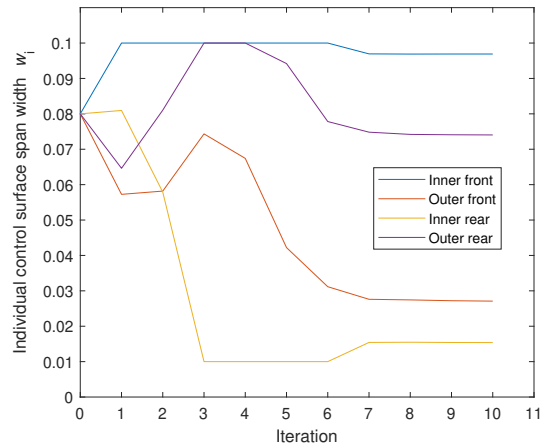


Figure 6.6: Non-dimensional span width design variables behaviour for DA

large optimisation system for the CS sizing, these accelerations are now used as constraints. As constraints, they are scaled with the limit value. Hence, as long as all acceleration values in figure 6.7 are below zero, trim is achieved. The closer the results are to the value of -1, the better the performance of the internal trim optimisation. Lines exceeding the upper limit indicate that for this point, trim was not achieved in one or more of the four trim cases.

Every trim case uses seven constraints. For clarity of the plot, only the largest absolute acceleration value is shown for each analysed case. The figure shows the largest residual acceleration values at values of about -0.3, hence for every design point, the aircraft was trimmable, both in normal flight and with OEI. Inspections of the results have shown that the approach phase is always more limiting than the cruise phase for this aircraft configuration and flight conditions. To save computational time, some runs presented in the results chapter have been set to only optimise for the approach condition with only a check of the final result at cruise to assure the limits are met as well. This does not impose any limitations on the validity for the research question. For better comparison of all results, only the constraints at the approach condition are shown in the figures.

All three methods show that for every design point, trim was always achieved for all four test cases, as shown in figures A.26 to 6.9. Due to the origin of these constraint values as results from the internal trim routine, no further information can be derived from these figures.

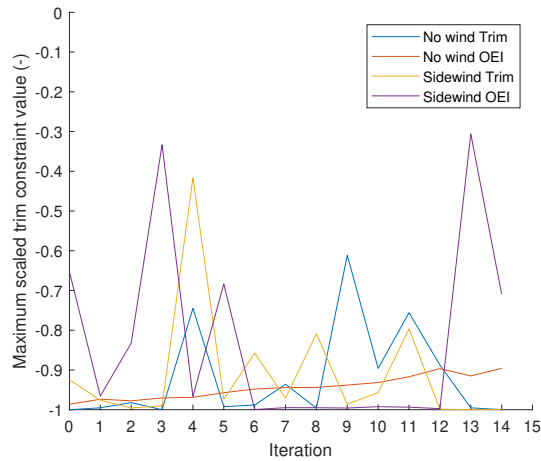


Figure 6.7: Scaled trim and OEI constraints for MG

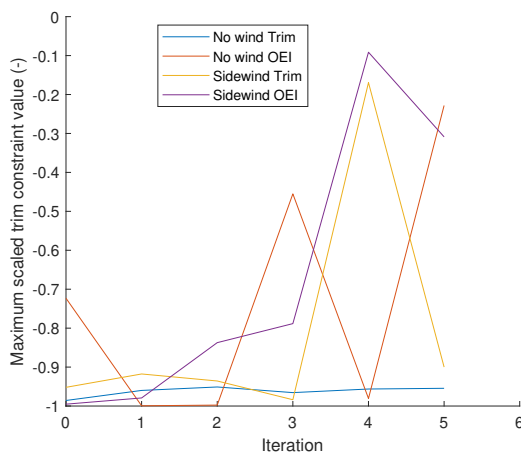


Figure 6.8: Scaled trim and OEI constraints for CPI

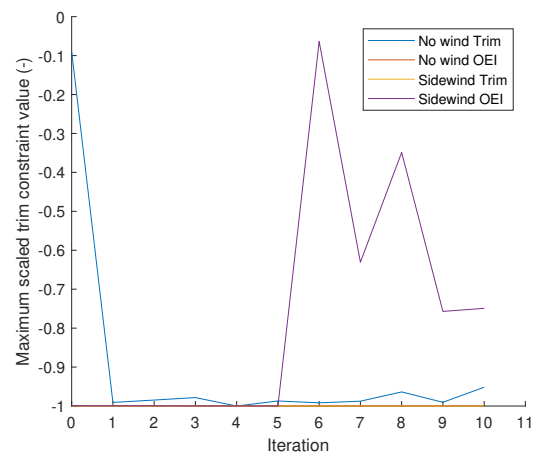


Figure 6.9: Scaled trim and OEI constraints for DA

Lastly, the results for the HFQ tests defined by MIL-8785C [28] are shown. For the handling qualities, figures 6.10 to 6.12 show the results for the three cases. Analogous to the trim constraints, the figures show scaled values. Hence, a constraint value below zero shows that the constraint is met, above zero shows a violation. For a better illustration, the violation zone is hatched in these plots.

The HFQ results for the three optimisations allow some interesting observations. Generally, the time to bank is the most limiting criterion. All three optimisations show how this constraint is moving towards the limit. However, only the DA algorithm actually has the time to bank as limiting constraint. For the other two, it approaches the limit, but does not reach it. The CPI design variable behavior shows how the outer rear surface decreases for every iteration, while the outer front CS stays the same. Still, the time to bank criterion barely changes. This shows how the algorithm uses both the inboard and outboard surfaces in a trade-off situation. While one CS reduces in span, the other increases; but the constraint remains virtually constant.

The maximum pull-up load factor $nMax$ is always well below the critical limit. The reason for the pull-up being nearly constant is the definition of the flap. For maximum pitch up moment, the front wing surfaces are fully deflected downwards, while the rear surfaces are deflected

upwards. With the flap always filling the gap between the front CS, this implementation means that the full trailing edge on the front wing is deflected downwards. The differences in the constraint visible in the figures is thus solely due to the changing rear wing CS. This is especially well visible for the DA run in figure 6.12. Figure 6.6 showed that the inner rear surface greatly reduced in width. Hence, the achievable pull-up acceleration decreases and the constraint value moves closer to the limit value. The MG and CPI optimisations had less reduction in the rear wing surfaces and thus the changes in this constraint are small. The behaviour of the minimum load factor $nMin$ in the push-over maneuver is influenced by all CS, and is thus more affected by the optimisation and the overall reduction in CS width.

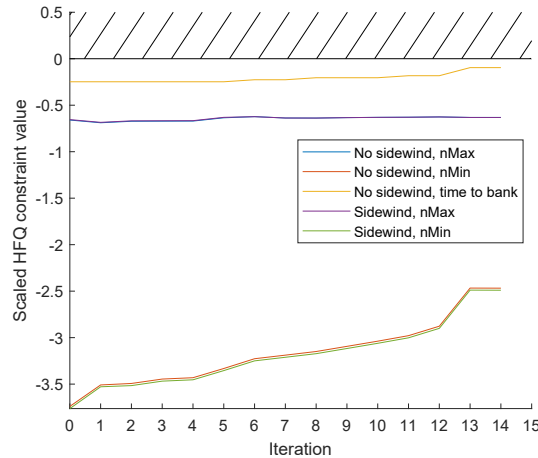


Figure 6.10: Scaled HFQ constraints for MG

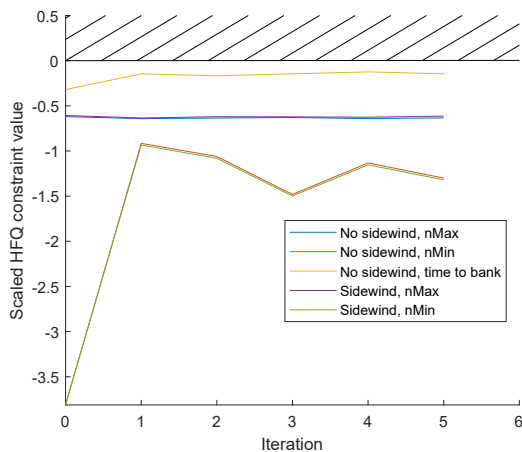


Figure 6.11: HFQ constraints behaviour for CPI

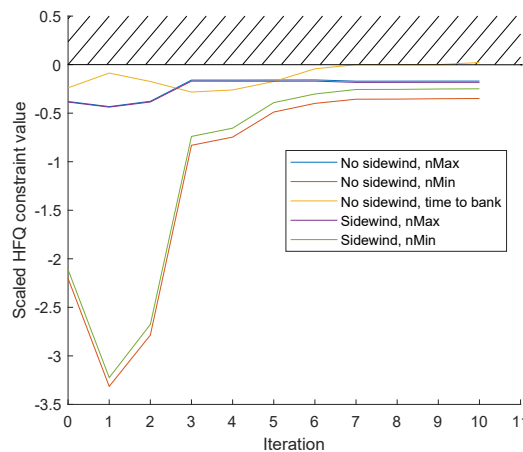


Figure 6.12: HFQ constraints behaviour for DA

All three optimisations show that not all constraints are at their limits at the final design points. The optimiser always ended as the step size fell below the default tolerance. This means that the optimisation algorithm tries to use very small steps in the perturbations in an attempt to find a new design point. However, the smaller the change in CS width, the smaller the difference in the aerodynamic coefficients of the surface. Very small changes have only a negligible influence on the overall HFQ and hence the optimiser has trouble finding a new design point. Hence, while the results have converged to a final point, a global minimum would thus probably give smaller total CS sizes.

6.2. Sensitivity analysis

In order to assess the effect of the initial point on the results of the optimisations, and attempting to find a lower value for the converged result, a sensitivity analysis is performed by initialising the optimiser with different initial points and comparing the results. For this, each allocation is used two more times with different starting points, and using the minimum CS span objective function. The results are shown in table 6.4. The first row for each algorithm shows the results described in section 6.1, the other two rows show the results for different initial points. The results are graphically shown in figures 6.13, 6.14 and 6.15.

Table 6.4: Sensitivity analysis for minimum span objective function. The initial layout described the initial point with the distribution: inner front/outer front/inner rear/outer rear

Alg.	Run	Initial layout	Objective	Inner front	Outer front	Inner rear	Outer rear
MG	1	0.08/0.08/0.08/0.08	7.399 m	0.0762	0.0567	0.0805	0.0509
MG	2	0.08/0.06/0.08/0.06	7.553 m	0.080	0.055	0.075	0.055
MG	3	0.06/0.08/0.06/0.08	7.330 m	0.081	0.055	0.0664	0.0545
CPI	1	0.08/0.08/0.08/0.08	6.700 m	0.060	0.025	0.073	0.075
CPI	2	0.08/0.06/0.08/0.06	6.855 m	0.047	0.053	0.098	0.043
CPI	3	0.06/0.08/0.06/0.08	6.675 m	0.1	0.01	0.033	0.099
DA	1	0.08/0.08/0.08/0.08	6.125 m	0.0969	0.0272	0.016	0.074
DA	2	0.08/0.06/0.08/0.06	6.088 m	0.0905	0.0532	0.0134	0.0557
DA	3	0.06/0.08/0.06/0.08	6.124 m	0.047	0.036	0.089	0.043

These additional points again show the clear distinction between the three algorithms. MG results in the largest required CS span width, and the DA in the lowers. It can be seen that the choice of initial point only has a minor influence on the final value of the objective function. For each of the three algorithms, the spread of the three objective function results is less than 3%. Thus, these results give confidence in the validity of the optimiser set-up.

The resulting control surface arrangements are very similar for the three MG optimisations as shown in figure 6.13. The main differences lie in the distribution between the front and rear inner surfaces. The CPI results in figure 6.14 show that the three optimisations resulted in relevant differences between the CS layouts. However, the final objective function values are similar. This shows that there is no clear preference for a certain layout to achieve similar HFQs and objectives. It has to be assumed that the topography of the optimisation problem is complex and has different local minima. The results for the DA in figure 6.15 show a similar behaviour, albeit less pronounced. The runs DA 1 & DA 2 show a similar behaviour, with the notable difference that the outer front surface is smaller in DA1 to offset larger values of the inner front and outer rear CS. DA 3 shows a radically different layout. Again, the HFQ and the objective results are very similar. Hence, this investigation concludes that for these modern control allocation algorithms using combined surfaces, there exists no single optimum distribution. The layouts show a trade-off between the span widths of the individual effectors while being equally optimal globally.

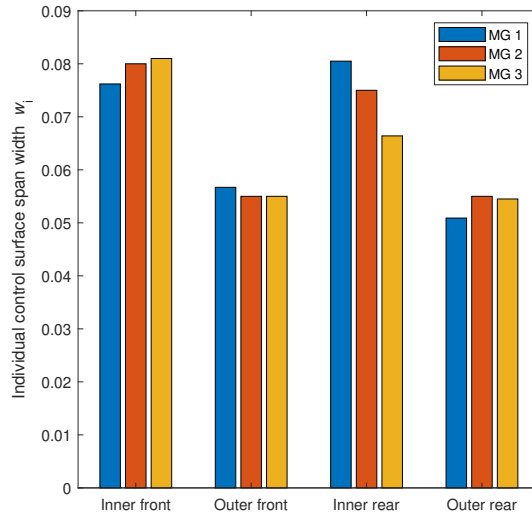


Figure 6.13: CS size comparison using MG for minimum span objective

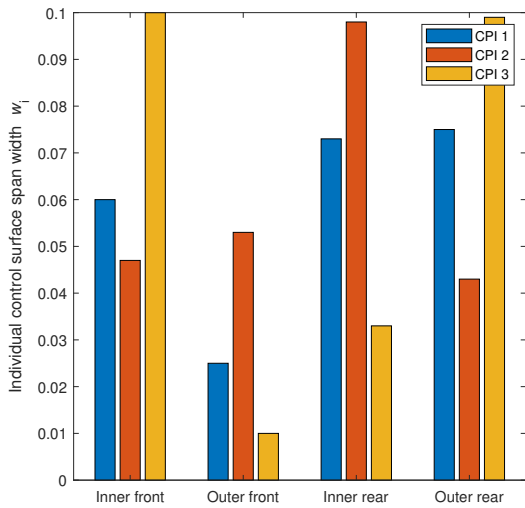


Figure 6.14: CS size comparison using CPI for minimum span objective

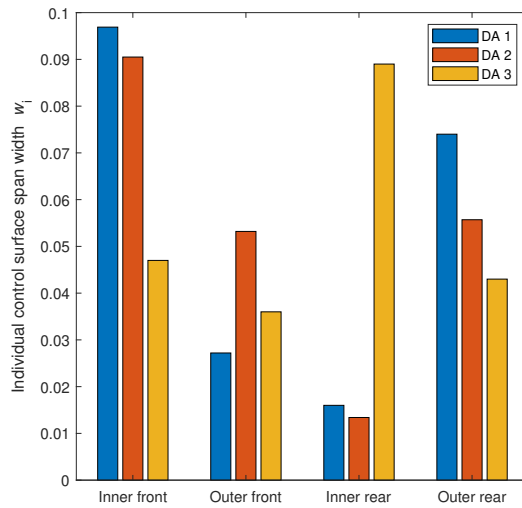


Figure 6.15: CS size comparison using DA for minimum span objective

The development of the objective functions for the three CA methods is shown in figures 6.16, 6.17 and 6.18. For each CA method the development is similar. As the span width objective is not influenced by the CS position, subsequent optimisations share the same starting point in objective function despite the actual initial CS layout being different. All three curves show a monotonous decrease of the objective functions to their final values. Interesting to note is the first MG run, as it shows a different optimisation behavior than the other two despite giving the same result. It seems, that the generated gradient has been always very small and hence changes happened only incrementally, while the other two optimisations generated larger gradients and hence lower objectives for their iteration steps, yet the final result is very similar. Furthermore, the starting point can have an influence on the iterations before convergence as shown in figure 6.18. Despite converging to very similar values, DA 2 only requires

half as many iterations as DA 1. The further optimisation outputs for the remaining six optimisation runs are placed in the appendix A.1. The curves show a similar behaviour and features to the optimisation curves shown and discussed in section 6.1.1.

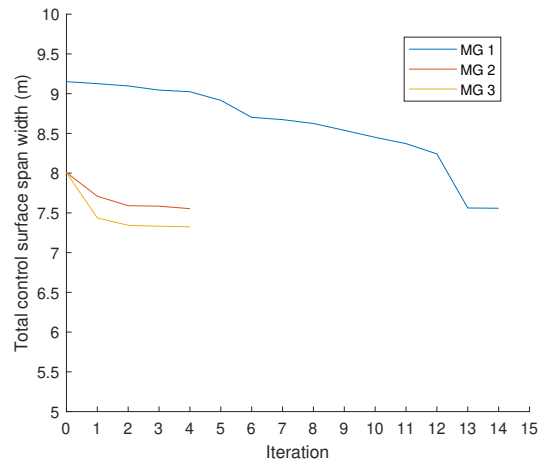


Figure 6.16: CS total span width objective development using MG for minimum span objective

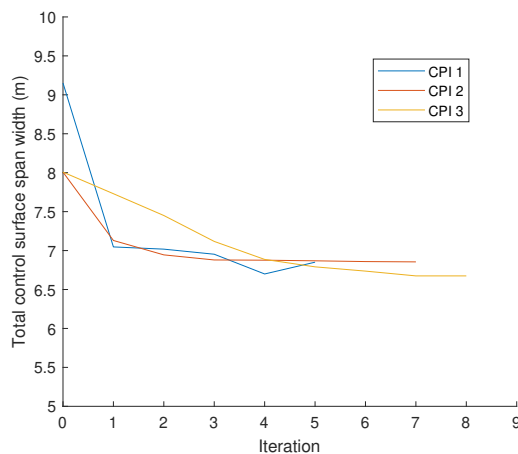


Figure 6.17: CS total span width objective development using CPI for minimum span objective

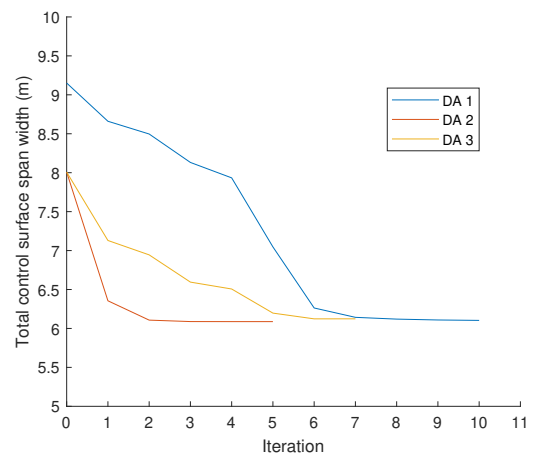


Figure 6.18: CS total span width objective development using DA for minimum span objective

6.3. Minimum area objective function

A comparison was performed using a minimum area objective function. The intention of using this function is to create a more balanced design. The span objective function would prefer surfaces at a larger wing chord as the larger area would create larger control moments for a given span width. Optimising for minimum area intends to investigate how the CS layout changes when the CS area is optimised for directly. The results are shown in tables 6.5 and 6.6. Similar to the minimum span optimisations, MG again results in the largest CSs. CPI reduces this area by about 8%. DA is able to reduce the required size further, achieving a reduction of about 26% compared to MG.

analysing the values in table 6.6 and figure 6.19, it shows that MG and CPI have resulted in a similar layout. Both show a strong preference for the outer front CS. Both results also

Table 6.5: Resulting objective function values for minimum area objective function

Algorithm	Objective result [m^2]	Difference to MG [%]
Initial	8.5781	+15.0
MG	7.46	[-]
CPI	6.85	-8.16
DA	5.49	-26.31

favour the inner rear surface over the inner front CS. The smaller chord of the rear wing allows a larger CS span for the same area compared to the front wing. Hence, for a minimum area it is expected that rear wing surfaces are preferred. While the DA also prefers the outer rear surface, the optimiser has resulted in a large inner front CS. On the front wing, the DA has thus the opposing trend compared to the CPI and MG.

Table 6.6: Resulting CS sizes as fraction of wing span for minimum area objective function

Algorithm	Inner front	Outer front	Inner rear	Outer rear
Initial	0.08	0.08	0.08	0.08
MG	0.033	0.099	0.088	0.075
CPI	0.039	0.098	0.061	0.081
DA	0.077	0.019	0.048	0.080

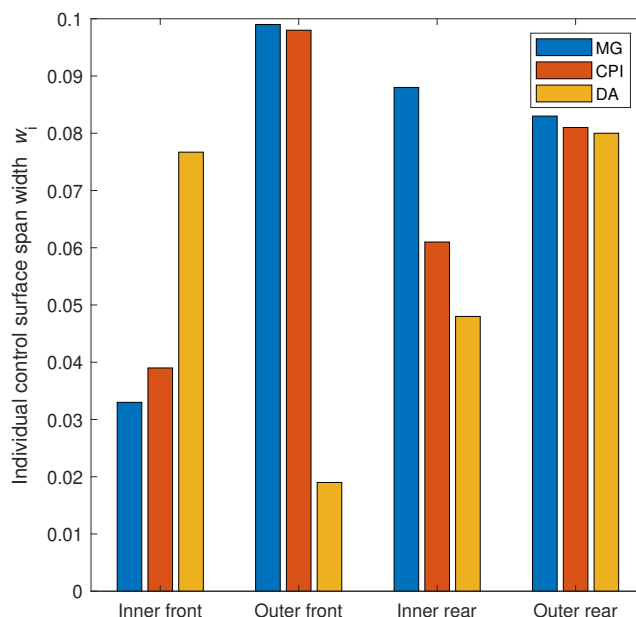


Figure 6.19: CS results for minimum area objective

Comparing the resulting CS layout from the minimum area optimisation with the results from the minimum span optimisation show that the differences in resulting layouts are small. The minimum span study showed that radically different layouts can be similarly optimal with respect to the objective function, hence there is no visible trend towards preferred CS locations for an optimal layout. This also shows with respect to the area objective. While the MG and CPI

show a similar shape, the DA shows a different trend, more in line with the results obtained with the span objective. A contributing factor is that the average CS chord length is approximately one meter, hence the results for minimum span and minimum area are similar in value. For the minimum area objective the same conclusion as for the span holds, that there is no single optimum CS layout along the wing.

The development of the three objective functions is shown in figure 6.20. Contrary to the objective function developments in section 6.1, now the MG has the lowest number of iterations. All three optimisations show good improvements in the objectives for each iteration. While the DA has the highest number of iterations, it shows that the actual objective value did not change much for the last 5 iterations. Hence, effectively both DA and CPI had a similar number of iterations. More detail on the behaviour of the optimisers for the area objective functions are placed in appendix A.

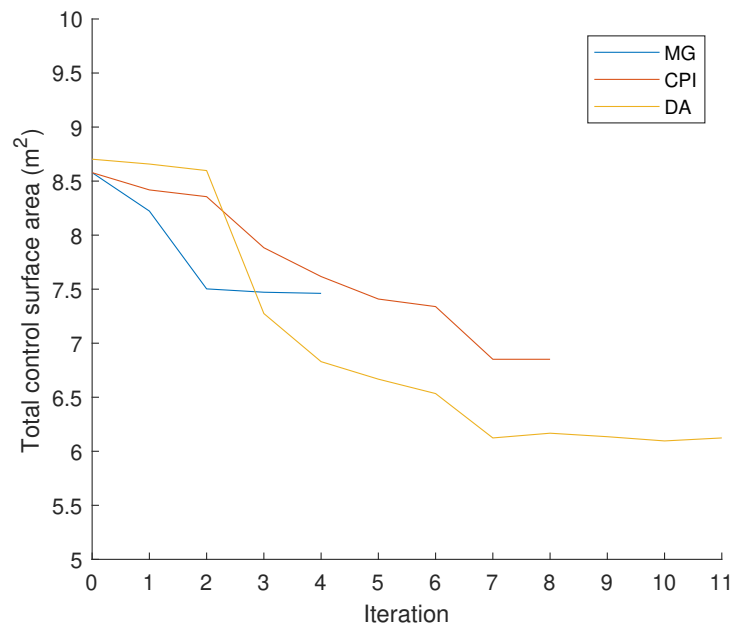


Figure 6.20: CS total wing area objective development for minimum area objective

6.4. Proposed improved CS placement on the rear wing

The control surface layout applied in the study has its roots in the current state of the art aircraft design approaches. Individual mechanically geared effectors for each moment result in typical positions at the wing root for elevator function and the outer wing for aileron function. Control allocation in combination with the two wings of the unique geometry of the PrP may allow for considerably more flexible CS placements.

Initial exploratory investigations were performed into a flexible number and free positioning of the CS along the wings (appendix B). However, the set-up had limitations due to its higher complexity that limited the comparability to the main research. A main observation was that the inner CS on the rear wing benefit from a location further mid-wing. So, as example application of the developed control allocation optimization system, it seemed interesting to evaluate the effect of one additional, mid-wing CS on the rear wing.

Within the development of a PrP in the PARSIFAL project, the design highlighted shock problems in the channel underneath the rear wing and between the rudders. The close proximity of the surfaces create a complex aerodynamic flow field that lead to shock interactions at high speeds. From an aerodynamic efficiency point of view it might thus be beneficial to remove the CS from this area. If the surface is placed outside of this area, the shock problems do not interfere with the CS deflection anymore and hence the aerodynamic efficiency of the CS would improve. These conclusions from the PARSIFAL project give further motivation to investigate the effects of CS that are placed further outboard in the rear wing. Hence, the additional CS was placed at a mid-wing position outboard of the V-tail intersection with the rear wing.

The comparison is made between three different placements. From the previous investigations, it has shown that the DA algorithm is performing the best, hence this algorithm is used. The first case, A, represents the layout used throughout this chapter. The initial and final values of case A are directly taken from section 6.1. The second case, B, uses both an inboard CS at the symmetry axis, as well as a mid-wing CS on the rear wing. The third case, C, only uses a CS at the mid wing position on the rear wing. For all three cases, the CS on the front wing and the outboard CS on the rear wing are unchanged. This new shape is shown in figure 6.21. The input values for the optimiser are given in table 6.7.

Table 6.7: Initial values for the design variables and bounds for the three cases A,B and C

CS	Symb.	Case A	Case B	Case C	Lower bound	Upper bound
Inner front	w_1	0.08	0.06	0.08	0.01	0.1
Outer front	w_2	0.08	0.06	0.06	0.01	0.1
Inner rear	w_3	0.08	0.06	-	0.01	0.1
Mid rear	w_4	-	0.06	0.08	0.01	0.1
Outer rear	w_5	0.08	0.06	0.06	0.01	0.1

The results are shown in tables 6.8 and 6.9. Comparing case B to case A shows a reduction in the required total span, albeit the overall change is small. Thus, while it shows an improvement, it also shows that this set-up of three control surfaces is not optimal yet. The changed position of the CS in case C results in a decrease of about 10% in required span compared to case B. When comparing it to case A, it shows an improvement of nearly 14%.

By comparing the CS sizes in table 6.9 and the graphical representation in figure 6.22, it can be seen that the inboard front surface is similar in size for all three cases. For case C, the other surfaces are now concentrated on the rear wing and show a balanced distribution between them. The front outer surface is reduced to its minimum size. This shows how

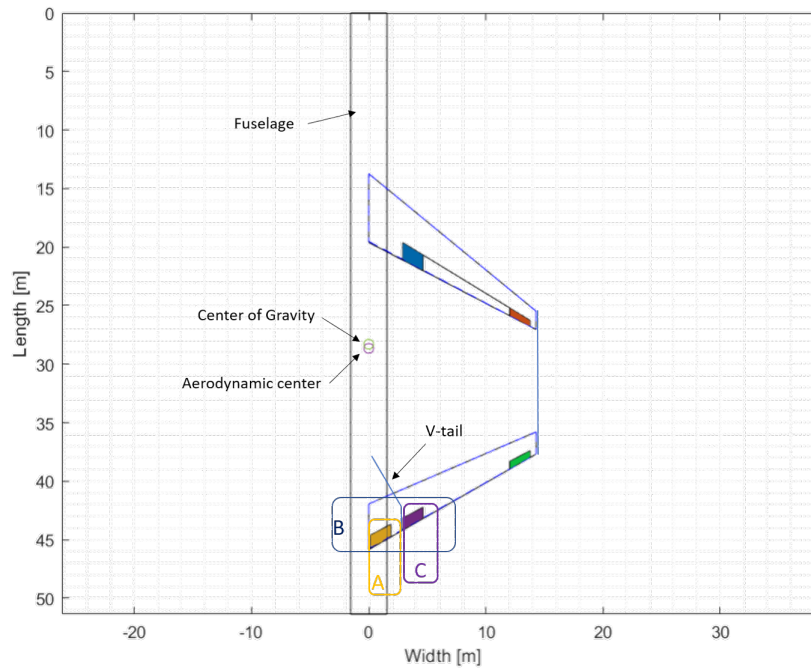


Figure 6.21: CS layout for the cases A, B and C. Both inner and the outer rear CS are equal for all cases

Table 6.8: Span objective result comparison between cases A, B and C

Case	Objective result (m)	Difference to case A (%)
A	6.13	-
B	5.93	-3.3
C	5.297	-13.6

the center rear surface is very effective in both pitch and roll and hence allows smaller CSs overall. It furthermore shows that the rear wing outboard surface is preferred over the front wing surface for rolling moments. Case B's results are in between cases A and C. On the front wing, it resembles case A. On the rear wing it resembles case C. Hence, it shows both in CS distribution and objective function that it is a combination of the two layouts and hence in between regarding its shape and size. Plots of the detailed optimisation results are given in appendix A.

Table 6.9: CS size comparison between the cases A,B and C

Case	Inner front	Outer front	Inner rear	Center rear	Outer rear
A	0.097	0.027	0.016	[-]	0.074
B	0.078	0.028	0.016	0.04	0.047
C	0.1	0.01	[-]	0.038	0.038

Figure 6.23 shows the behaviour of the objective function for the three cases. For case A, the optimiser is able to find new and improved design points for every iteration, until it converges to the final value at iteration 7. For case B, the optimiser finds its minimum by iteration 4, but tries to further optimise the point. However, it is not able to find an improved design point, hence it converges to this final value. The same behaviour is seen for case C. Again, the optimiser manages to find a highly optimised design point very quickly, but is then not able to improve this point further. Both are due to the trim routine. Any reduction in CS

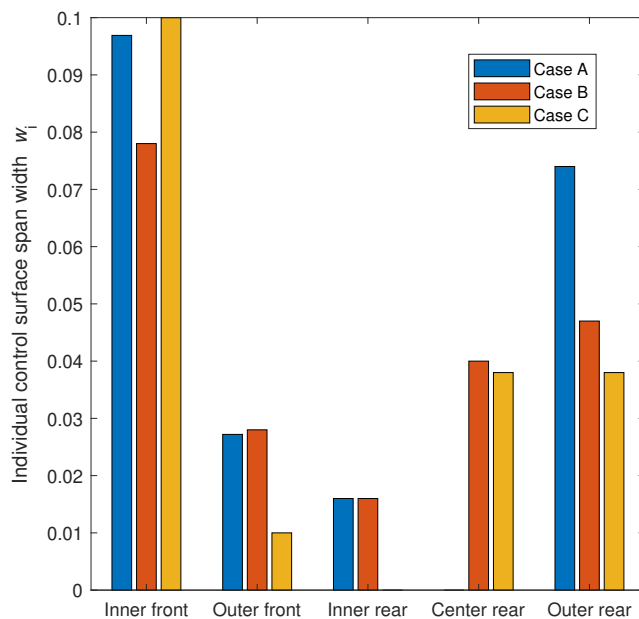


Figure 6.22: Final CS layout comparison of cases A, B and C using DA for minimum span

width leads to the trim routine not being able to trim the aircraft anymore. Hence, the optimiser is not able to find a usable gradient to improve the point. However, this shows that the trim constraint is a limiting constraint at the design points. This gives confidence that the attained result is close to a local minima.

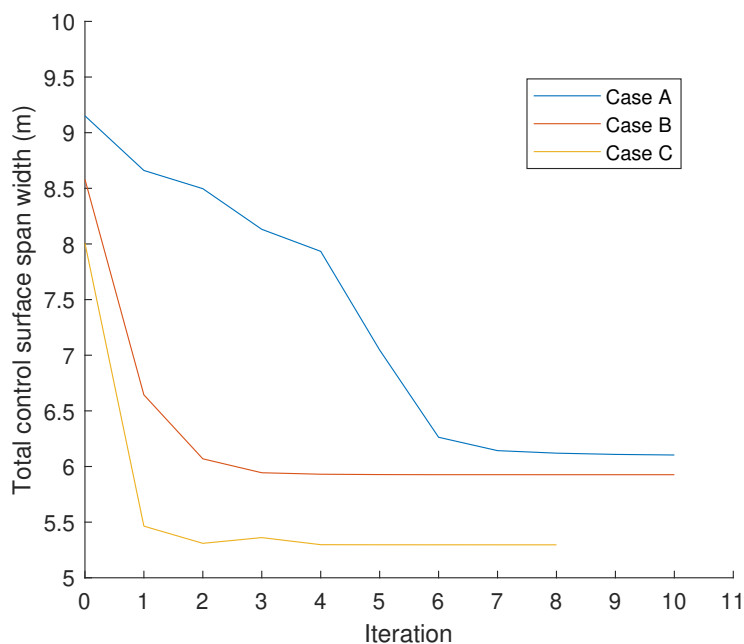


Figure 6.23: CS total span width objective development using DA for minimum span objective with improved layout

These results support the conclusion that the PrP configuration can very well benefit from the use of control allocation algorithms. The second full size wing give flexibility to the positioning of the control surfaces. Hence, the effectors can be placed in such a way that they are very efficient in providing both a pitching and rolling moment. The improved capabilities are only harnessable because of the control allocation, classical mechanical gearing would be unable to operate these surfaces in the most efficient way.

6.5. Attainable moment set

A way of visualising the reductions in the control surface span is by analysing the changes in the Attainable Moment Set (AMS) for each algorithm. The plots show isometric views of the AMS from the initial and optimised results for the minimum span objective shown in section 6.1. The bodies shown in the figures represent the outer facets and vertices of the AMS for the respective algorithm for moments in X, Y, and Z direction.

Figure 6.24 shows the AMS for the MG case. It can be seen that the initial layout has a larger AMS, especially in the longitudinal moment M_X and the lateral moment M_Y . The reduction is largest for M_X as the roll control CS were mostly affected by the optimisation. The changes in directional moment capability are small. This is due to the fixed size of the rudders on the V-tail. Hence, the optimiser has limited ability to change the directional moment capabilities.

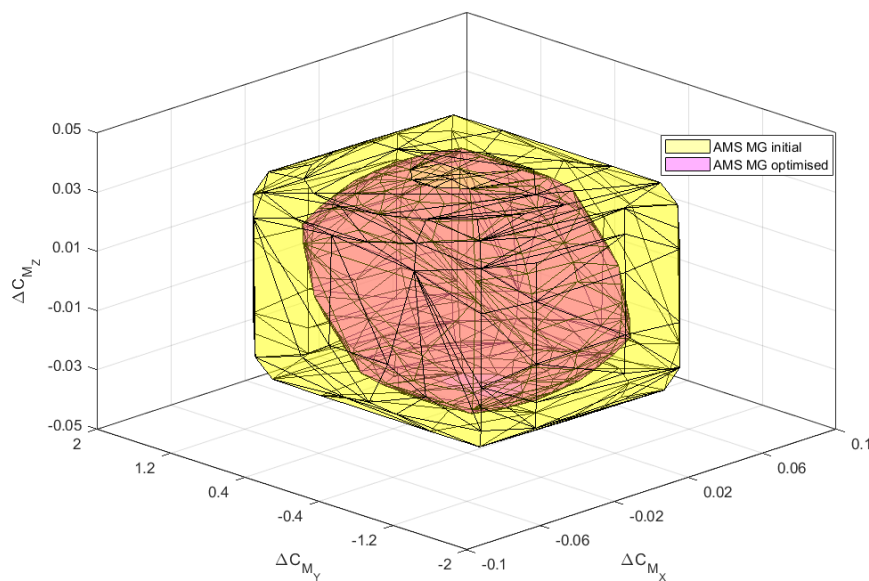


Figure 6.24: Comparison of AMS for initial and optimised CS span for the MG algorithm

The AMS of the CPI algorithm is shown in figure 6.25. Again, the overall reduction is well visible. For the CPI, the reductions in M_X and M_Y are similar compared to the MG results. A direct comparison of the initial AMS for the CPI and the MG case shows that they are similar in overall size. However, the MG set is larger at some corners. Hence, if large combined moments are required, the MG would actually outperform the CPI algorithm. If individual moments are required, then the CPI has the larger AMS around the principal axes.

The AMS of the DA algorithm is shown in figure 6.26. It is clearly visible that this algorithm gives the largest AMS for the initial condition. This is expected as the AMS of the DA is equal to the GAMS of this CS layout. Also, the reduction in the AMS due to the reduction in CS size

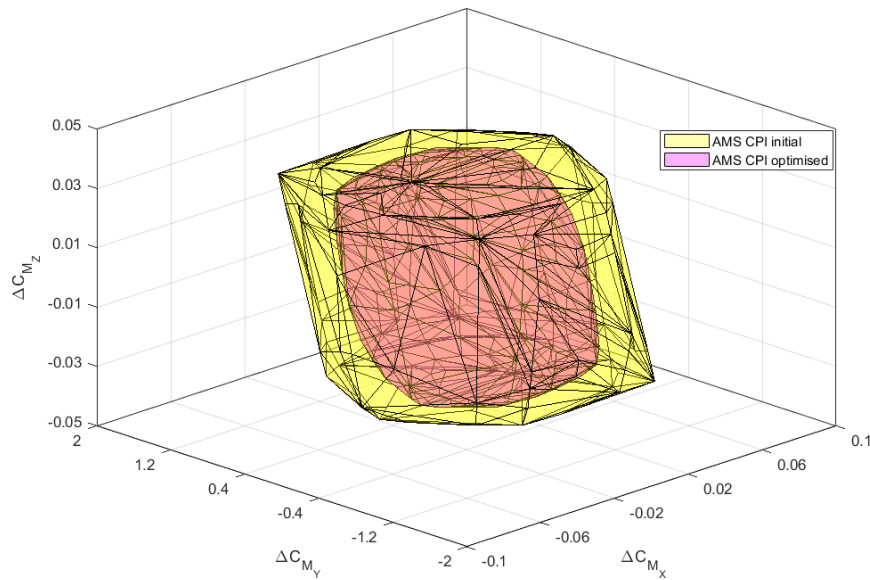


Figure 6.25: Comparison of AMS for initial and optimised CS span for the CPI algorithm

is largest for this case. In contrast to the other two algorithms which reduced primarily the attainable M_x and M_y , the DA also shows a visible reduction in directional moment capability M_z . However, the comparison of the three figures also shows that all three algorithms have resulted in an AMS of similar shape and size.

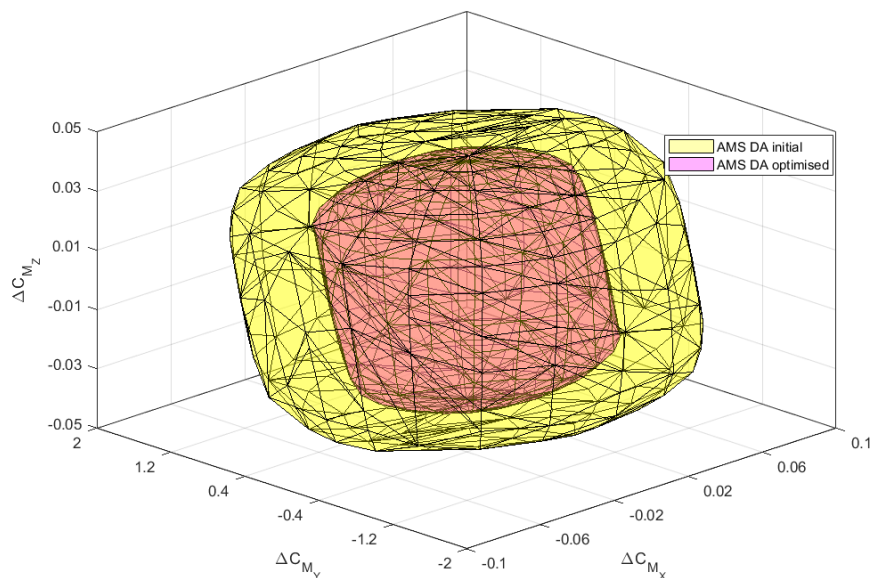


Figure 6.26: Comparison of AMS for initial and optimised CS span for the DA algorithm

The figure 6.27 plots the volume of the AMS against the required total CS span width for all optimisations performed with the minimum span objective, and shows the achieved reductions compared to the initial layout. The volume of the AMS is a common measure to quantify the

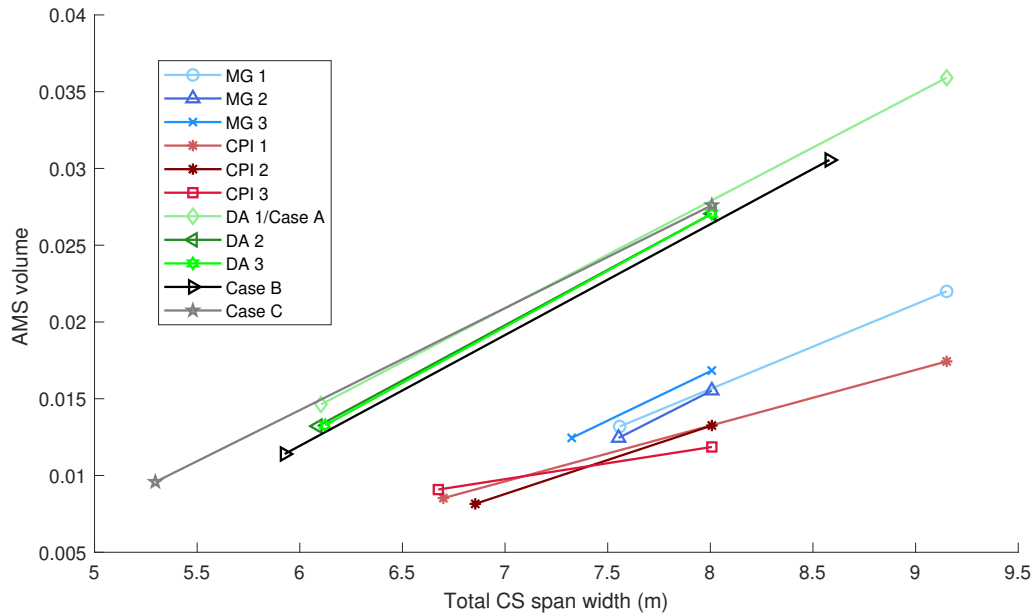


Figure 6.27: Volume of the AMS for initial and end points of all minimum span optimisations as function of CS span width: MG (blue), CPI (red), DA (green) and improved cases (grey)

total control power that a control allocation method can provide. The figure shows that the different CA method results are forming clearly distinguishable clusters. For the MG, the figure shows a large CS span and medium AMS volume. The CPI have both smaller CS widths and a smaller AMS volume. As described in chapter 3, the CPI can only access a certain subset of the GAMS. Along the principal axes, it is large, but it does not have access to the corners like the AMS for the MG. Hence, it can be more efficient while also having a smaller AMS volume. The DA has both the lowest required CS area and the largest AMS volume. As the DA accesses the GAMS of the layout, it will result in large moment generation capabilities in directions that are not specifically required in the HFQ tests. This comparison shows again that the DA method has the highest control power at the smallest CS. Comparing CPI and MG, it shows that the AMS of the CPI is more tailored to the requirements of the control problem and thus utilises the CS more effectively. The AMS volume is lower than the MG, hence it can generate less control power overall, but it also uses smaller CS.

Comparing the results of the improved placement cases, it shows that the CS widths and the AMS are correlated. The smaller the CS, the smaller the AMS. This also shows how the improved placement allows a reduction in CS span and AMS, while still adhering to the HFQ limits. Hence, the improved placement allows a more efficient use of the CS for the given set of HFQ tests. It also highlights the benefits of the mid-wing surface. Compared to the case A, case C allows a large reduction in required CS width. In order to achieve the same AMS volume as the CPI or MG algorithms, the CS can be 20-40% smaller.



Conclusions and Recommendations

Control allocation, the combination of control effector functions, is especially interesting for a PrandtlPlane. The unique geometry having two full wings, and a large longitudinal moment arm to the center of gravity, allows more flexibility in control surface placement while retaining control effectiveness. While a conventional aircraft is restricted in position for effective ailerons and elevators, the PrPs wings allow the placement of extra control surfaces.

A new optimization system for automatic control surface sizing under the constraints of adequate handling qualities has been developed and programmed. The correct functioning of the system has been shown by comparison with the results of a publication using a similar framework and higher fidelity aerodynamics data, but limited to the mechanical gearing mechanism. With application to a box-wing aircraft configuration, different control allocation methods have been assessed on their effect on control surface design. As primary objective function the span minimization was chosen, as this is a popular and well quantifiable parameter of the control surface layout. Another optimisation was performed using a minimum area objective function.

Results show that advanced control allocation methods achieve smaller control surface layouts with respect to classic mechanical gearing, in terms of total control surface span or area. For a given set of control surfaces, a simple allocation algorithm such as the constrained pseudo inverse shows reductions in required span and area of the control surfaces. For the direct allocation, the improvements increase. Hence, the use of control allocation is superior to the classical control methods when optimizing for control surface span. Given sufficient computational resources, the use of direct allocation is the most beneficial. Regarding an optimization for minimum area, the conclusions are similar. The pseudo inverse provides an improvement over the mechanical gearing. The direct allocation again shows a further improvement over the pseudo inverse.

For the task of utilizing these redundant control surfaces at maximum efficiency, control allocation is the best option, as illustrated by the main research findings. However, the use of control allocation can also have an impact on the positioning of the surfaces. The combination of the functions allows a mid-wing placement of the surface where it can function as both an effective pitch and rolling moment generator. This conclusion is illustrated in a last study. The results show a further benefit if the inner rear surface is positioned further mid-wing compared to the initial case. Hence, for a PrandtlPlane, the classic control surface layout may not be an optimal solution. It should be considered to place the surfaces more centrally on the wings.

Comparisons of the attainable moment sets for the algorithms further highlighted the benefits of direct allocation. In order to have a comparable volume of the attainable moment set,

direct allocation requires significantly less control surface span width compared to the other algorithms.

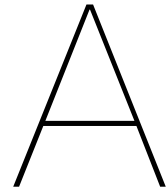
The improvement seen in the results of the study implies that for future studies the use of the direct allocation algorithm is recommended. The pseudo inverse has consistently performed lower and is hence not recommended. An extension of this study would be the option to allow free placement of the control surface on the wing. For this, special emphasis must be laid on the integration of flaps when allowing the surfaces to vary the position along the wing. Furthermore, for investigations using higher numbers of control effectors, it is advised to change the aerodynamic solver or include correction factors for non-linear effects on small surfaces to achieve credible results. For a more complete analysis of the control surface requirements, future investigations should include all potentially critical flight phases, including modelling of take-off and landing performance. Another possible extension of this framework could include the aerodynamic forces in the allocation problem. With such a framework, other test cases or performance criteria can be created that make use of direct lift or direct side-force control. With this, the effects of these features on the handling qualities of the PrandtlPlane and the required control surface sizes could be analysed further. Lastly, it is advised to use the framework with an objective function that includes aerodynamic parameters such as the maneuver drag. This requires the integration of a drag model in the framework. The drag results can be extracted from the flight mechanics analysis and fed to the objective function. Another possible implementation is the addition of a secondary objective function to the control allocation algorithm that takes drag into account.

Bibliography

- [1] W Schneider. "The importance of Aerodynamics in the development of commercially successful transport aircraft". In: *Aerodynamic Drag Reduction Technologies*. Potsdam, Germany: Springer, 2001, pp. 9–16.
- [2] SV Gudmundsson, M Cattaneo, and R Redondi. "Forecasting temporal world recovery in air transport markets in the presence of large economic shocks: The case of COVID-19". In: *Journal of Air Transport Management* (2020), p. 102007.
- [3] A Frediani. "The prandtl wing". In: *VON KÁRMAN INSTITUTE FOR FLUID DYNAMICS: VKI Lecture Series: Innovative Configurations and Advanced Concepts for Future Civil Transport Aircraft*. Rhode St-Genèse: Von Kármán Institute for Fluid Dynamics (2005).
- [4] L Prandtl. *Induced Drag of Multiplanes*. Tech. rep. 182. National Advisory Committee for Aeronautics, 1924.
- [5] L Demasi et al. "Minimum Induced Drag Theorems for Joined Wings, Closed systems, and Generic Biwings: Theory". In: *56th AIAA/ASCE/AHS/ASC Structures, Structural Dynamics, and Materials Conference*. Kissimmee, Florida: American Institute of Aeronautics and Astronautics, Jan. 2015. ISBN: 978-1-62410-342-1. DOI: 10.2514/6.2015-0697. URL: <http://arc.aiaa.org/doi/10.2514/6.2015-0697> (visited on 01/27/2020).
- [6] A Frediani, E Rizzo, and C Bottoni. "A 250 Passenger PrandtlPlane transport aircraft preliminary design". In: *Aerotecnica Missili & Spazio* 84.4 (2016), pp. 152–163.
- [7] D Schiktanz and D Scholz. "Box Wing Fundamentals - an Aircraft Design Perspective". In: *Deutscher Luft- und Raumfahrtkongress 2011*. 2011.
- [8] S A Andrews and R E Perez. "Stability and Control Effects on the Design Optimization of a Box-Wing Aircraft". In: *14th AIAA Aviation Technology, Integration, and Operations Conference*. Atlanta, GA: American Institute of Aeronautics and Astronautics, June 2014. ISBN: 978-1-62410-282-0. DOI: 10.2514/6.2014-2592. URL: <http://arc.aiaa.org/doi/10.2514/6.2014-2592> (visited on 01/21/2020).
- [9] P Jansen and R Perez. "Effect of Size and Mission Requirements on the Design Optimization of Non-Planar Aircraft Configurations". en. In: *13th AIAA/ISSMO Multidisciplinary Analysis Optimization Conference*. Fort Worth, Texas: American Institute of Aeronautics and Astronautics, Sept. 2010. ISBN: 978-1-60086-954-9. DOI: 10.2514/6.2010-9188. URL: <http://arc.aiaa.org/doi/10.2514/6.2010-9188> (visited on 04/10/2020).
- [10] C N Zohlandt. *Conceptual Design of High Subsonic Prandtl Planes*. Delft, Netherlands, Feb. 2016.
- [11] E Torenbeek. *Advanced aircraft design: conceptual design, analysis, and optimization of subsonic civil airplanes*. Chichester, West Sussex, United Kingdom: John Wiley & Sons Inc, 2013. ISBN: 978-1-118-56809-5.
- [12] D van Ginneken et al. "Automated Control Surface Design and Sizing for the Prandtl Plane". In: *51st AIAA/ASME/ASCE/AHS/ASC Structures, Structural Dynamics, and Materials Conference & 18th AIAA/ASME/AHS Adaptive Structures Conference & 12th Orlando, Florida: American Institute of Aeronautics and Astronautics, Apr. 2010. ISBN: 978-1-60086-961-7. DOI: 10.2514/6.2010-3060. URL: <http://arc.aiaa.org/doi/abs/10.2514/6.2010-3060> (visited on 01/21/2020).*
- [13] "Design of Control Surfaces". In: *Aircraft Design*. Chichester, UK: John Wiley & Sons, Ltd, Sept. 2012, pp. 631–753. ISBN: 978-1-118-35270-0. DOI: 10.1002/9781118352700.ch12. URL: <http://doi.wiley.com/10.1002/9781118352700.ch12> (visited on 04/14/2020).

- [14] C Varriale et al. "A HYBRID, CONFIGURATION-AGNOSTIC APPROACH TO AIRCRAFT CONTROL SURFACE SIZING". In: *Italian Association of Aeronautics and Astronautics XXV International Congress*. Rome, Italy, 2019.
- [15] F Oliviero, D Zanetti, and V Cipolla. "Flight dynamics model for preliminary design of PrandtlPlane wing configuration with sizing of the control surfaces". In: *Aerotecnica Missili & Spazio* 95.4 (Oct. 2016), pp. 201–210. ISSN: 0365-7442, 2524-6968. DOI: 10.1007/BF03404728. URL: <http://link.springer.com/10.1007/BF03404728> (visited on 01/27/2020).
- [16] A N Sousa et al. "Box wing longitudinal flight quality evaluation". In: *AIAA Aviation 2019 Forum*. Dallas, Texas: American Institute of Aeronautics and Astronautics, June 2019. ISBN: 978-1-62410-589-0. DOI: 10.2514/6.2019-3490. URL: <https://arc.aiaa.org/doi/10.2514/6.2019-3490> (visited on 03/09/2020).
- [17] W C Durham. "Constrained control allocation". In: *Journal of Guidance, Control, and Dynamics* 16.4 (1993), pp. 717–725.
- [18] T A Johansen and T I Fossen. "Control allocation—A survey". In: *Automatica* 49.5 (May 2013), pp. 1087–1103. ISSN: 00051098. DOI: 10.1016/j.automatica.2013.01.035. URL: <https://linkinghub.elsevier.com/retrieve/pii/S0005109813000368> (visited on 03/09/2020).
- [19] A Frediani and G Montanari. "Best wing system: an exact solution of the Prandtl's problem". In: *Variational Analysis and Aerospace Engineering*. Vol. 33. Series Title: Springer Optimization and Its Applications. New York, NY: Springer New York, 2009, pp. 183–211. ISBN: 978-0-387-95856-9. DOI: 10.1007/978-0-387-95857-6_11. URL: http://link.springer.com/10.1007/978-0-387-95857-6_11 (visited on 03/11/2020).
- [20] M Munk. *Elements of the wing section theory and of the wing theory*. Tech. rep. 191. National Advisory Committee for Aeronautics, 1924.
- [21] L Demasi. "Investigation on the conditions of minimum induced drag of closed wing systems and C-wings". In: *Journal of Aircraft* 44.1 (2007), pp. 81–99.
- [22] D Schiktanz and D Scholz. "The Conflict of Aerodynamic Efficiency and Static Longitudinal Stability of Box Wing Aircraft". In: *21st AIDAA Congress*. Oct. 2011.
- [23] R H Lange et al. *Feasibility study of the transonic biplane concept for transport aircraft application*. Tech. rep. National Air and Space Agency, 1974.
- [24] A Frediani et al. "DEVELOPMENT OF AN INNOVATIVE CONFIGURATION FOR TRANSPORT AIRCRAFT; A PROJECT OF FIVE ITALIAN UNIVERSITIES." en. In: *XVII Congresso Nazionale AIDAA*. 2003.
- [25] V Cipolla et al. "Conceptual design of a box-wing aircraft for the air transport of the future". In: *2018 Aviation Technology, Integration, and Operations Conference*. Atlanta, Georgia: American Institute of Aeronautics and Astronautics, June 2018. ISBN: 978-1-62410-556-2. DOI: 10.2514/6.2018-3660. URL: <https://arc.aiaa.org/doi/10.2514/6.2018-3660> (visited on 04/22/2020).
- [26] R J M Elmendorp and G LaRocca. "COMPARATIVE DESIGN & SENSITIVITY STUDIES ON BOX-WING AIRPLANES". In: *Italian Association of Aeronautics and Astronautics XXV International Congress*. Rome, Italy, Sept. 2019.
- [27] R Caja and D Scholz. "Box Wing Flight Dynamics in the Stage of Conceptual Aircraft Design". In: *Deutscher Luft- und Raumfahrtkongress*. 2012.
- [28] US Military Specification. *MIL-F-8785C Flying qualities of piloted aircraft*. Tech. rep. US Air Force, 1980.
- [29] R P Harper Jr and G E Cooper. "Handling qualities and pilot evaluation". In: *Journal of Guidance, Control, and Dynamics* 9.5 (1986), pp. 515–529.
- [30] EASA Tech. Rep. Amendment 13. *Acceptable means of compliance for large aeroplanes CS-25*. Tech. rep. Cologne, Germany: European Aviation Safety Agency, 2013.

- [31] R E Perez, H HT Liu, and K Behdinan. "Multidisciplinary Optimization Framework for Control-Configuration Integration in Aircraft Conceptual Design". In: *Journal of Aircraft* 43.6 (Nov. 2006), pp. 1937–1948. ISSN: 0021-8669, 1533-3868. DOI: 10.2514/1.22263. URL: <https://arc.aiaa.org/doi/10.2514/1.22263> (visited on 01/21/2020).
- [32] Military Specifications Office. *Flying qualities of piloting vehicles MIL-STD-1797 (USAF)*. United States Air Force. 1997.
- [33] J Roskam. *Airplane flight dynamics and automatic flight controls*. Analysis and Research Corporation, Lawrence, KS, 2001.
- [34] G Buttazzo and A Frediani, eds. *Variational analysis and aerospace engineering: contributions from a workshop held at the school of mathematics in Erice, Italy*. Springer optimization and its applications v. 66. New York, New York: Springer, 2012. ISBN: 978-1-4614-2434-5.
- [35] W Durham, K A Bordignon, and R Beck. *Aircraft Control Allocation*. en. Chichester, UK: John Wiley & Sons, Ltd, Dec. 2016. ISBN: 978-1-118-82778-9 978-1-118-82779-6. DOI: 10.1002/9781118827789. URL: <http://doi.wiley.com/10.1002/9781118827789> (visited on 01/21/2020).
- [36] C Varriale, M Voskuijl, and L L Veldhuis. "Trim for Maximum Control Authority using the Attainable Moment Set". In: *AIAA Scitech 2020 Forum*. 2020, p. 1265.
- [37] M Bodson. "Evaluation of Optimization Methods for Control Allocation". In: *Journal of Guidance, Control, and Dynamics* 25.4 (July 2002), pp. 703–711. ISSN: 0731-5090, 1533-3884. DOI: 10.2514/2.4937. URL: <https://arc.aiaa.org/doi/10.2514/2.4937> (visited on 03/09/2020).
- [38] P O Jemitola and J P Fielding. "BOX WING AIRCRAFT CONCEPTUAL DESIGN". In: *28th International Congress of the Aeronautical Sciences*. 2012.
- [39] M Drela and H Youngren. *AVL 3.36 User Primer*. MIT Aero & Astro. Feb. 2007.
- [40] J Nathman and A McComas. "Comparison of Stability and Control Calculations from Vortex Lattice and Panel Methods". In: *46th AIAA Aerospace Sciences Meeting and Exhibit*. Reno, Nevada: American Institute of Aeronautics and Astronautics, Jan. 2008. ISBN: 978-1-62410-128-1. DOI: 10.2514/6.2008-314. URL: <http://arc.aiaa.org/doi/10.2514/6.2008-314> (visited on 01/22/2020).
- [41] J Katz and A Plotkin. *Low-speed aerodynamics*. Vol. 13. Cambridge university press, 2001.



Detailed optimisation results

This appendix contains the detailed behaviour of all optimisations mentioned in the results chapter. The main text showed these plots for the initial minimum span optimisations for all three control algorithms. This appendix now shows all plots from the remaining optimisation runs that are not specifically shown before.

A.1. Detailed optimisation results for minimum span objective function

This section shows the optimisation plots for the additional optimisations using the minimum span objective function from the sensitivity study. It contains the iteration histories of the CS spans, and the constraint behaviours at every iteration of the optimiser for the six optimisation runs.

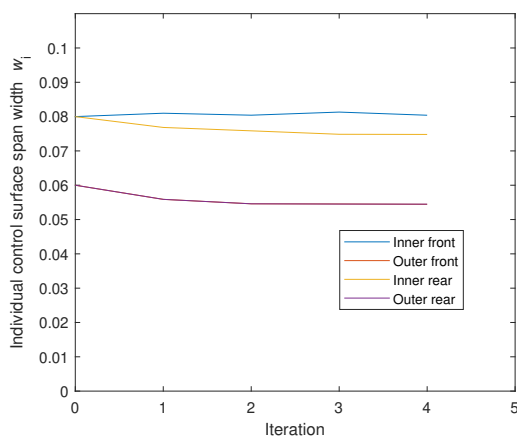


Figure A.1: CS span development for MG 2

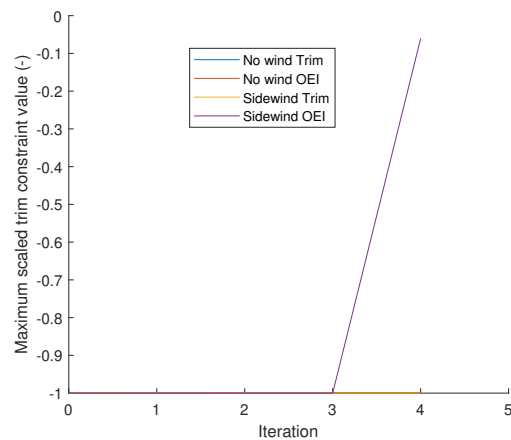


Figure A.2: Trim and OEI constraints for MG 2

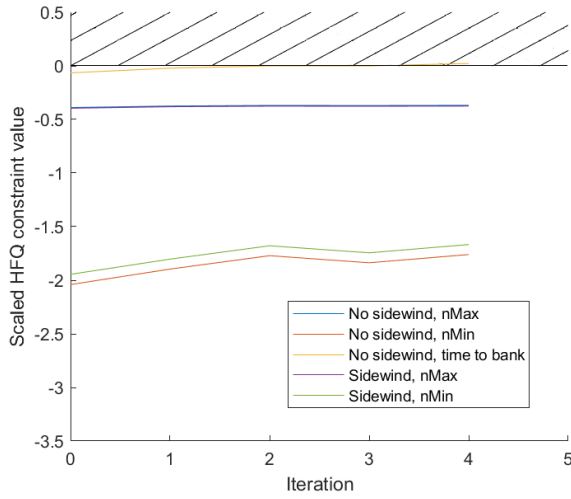


Figure A.3: HFQ constraints for MG 2

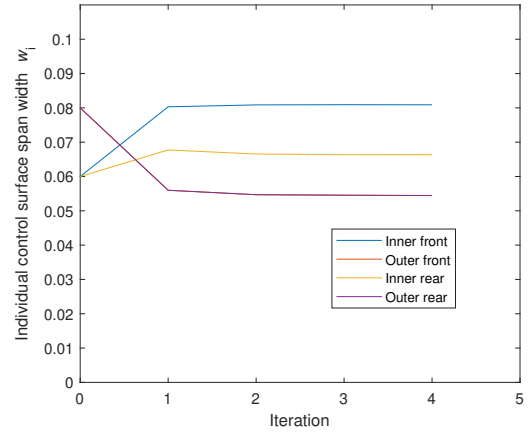


Figure A.4: CS span development for MG 3

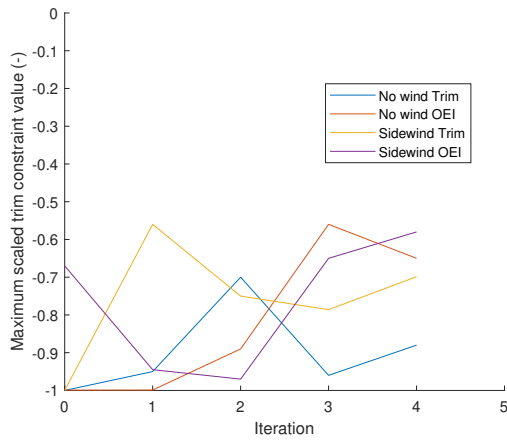


Figure A.5: Trim and OEI constraints for MG 3

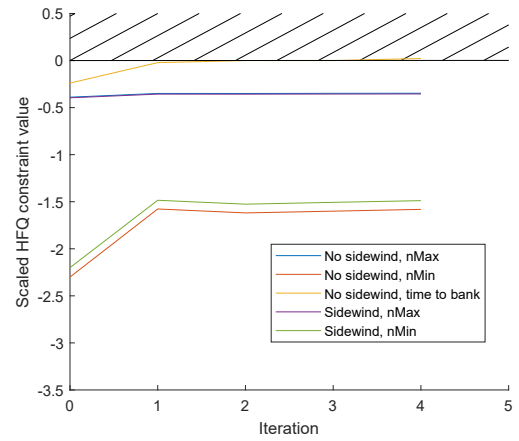


Figure A.6: HFQ constraints for MG 3

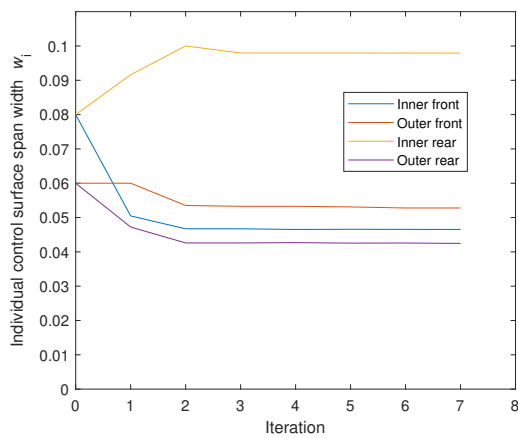


Figure A.7: CS span development for CPI 2

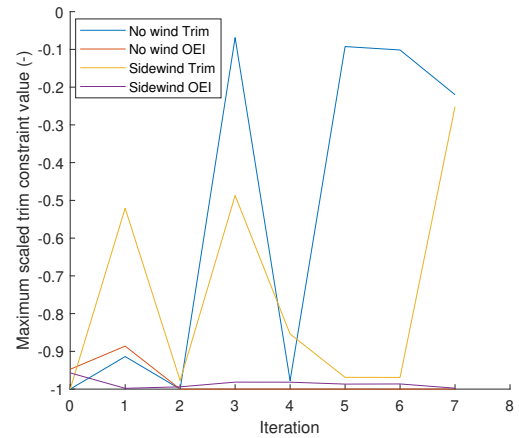


Figure A.8: Trim and OEI constraints for CPI 2

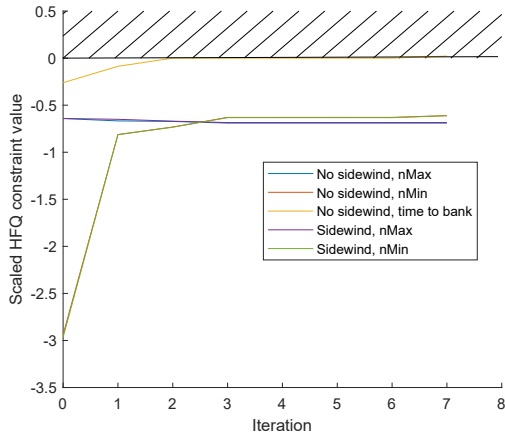


Figure A.9: HFQ constraints for CPI 2

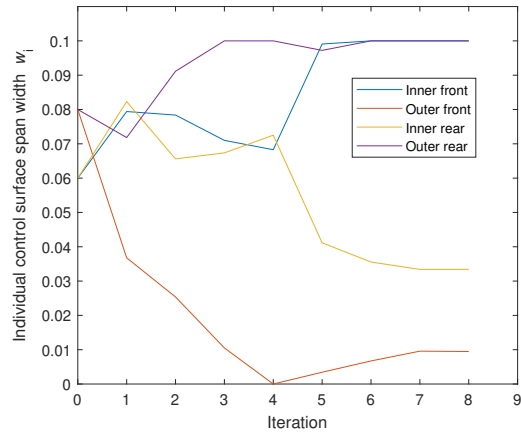


Figure A.10: CS span development for CPI 3

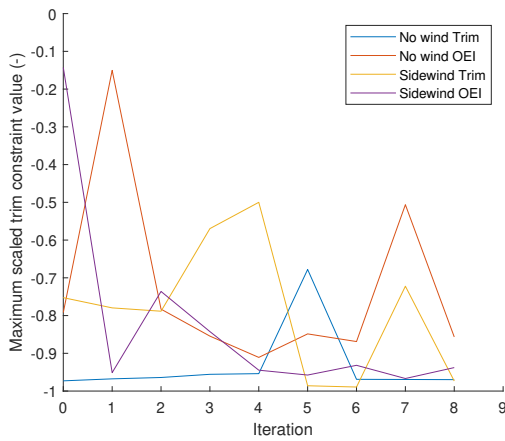


Figure A.11: Trim and OEI constraints for CPI 3

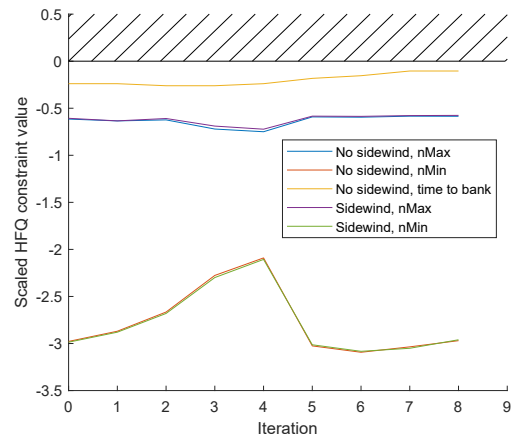


Figure A.12: HFQ constraints for CPI 3

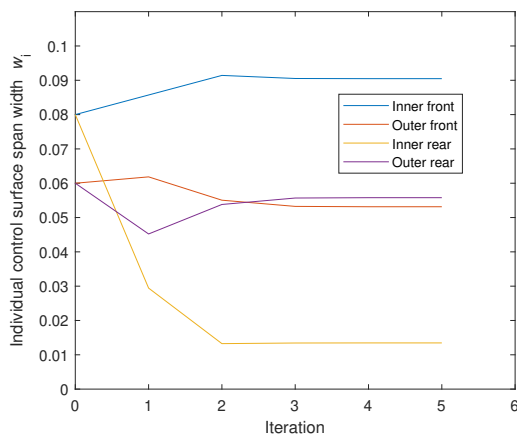


Figure A.13: CS span development for DA 2

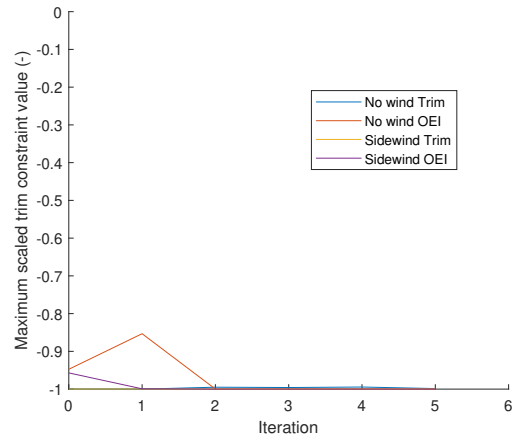


Figure A.14: Trim and OEI constraints for DA 2

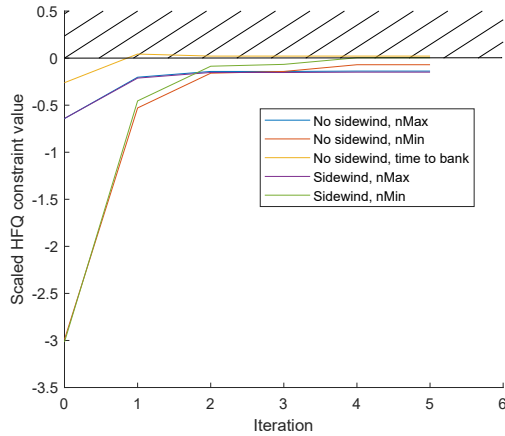


Figure A.15: HFQ constraints for DA 2

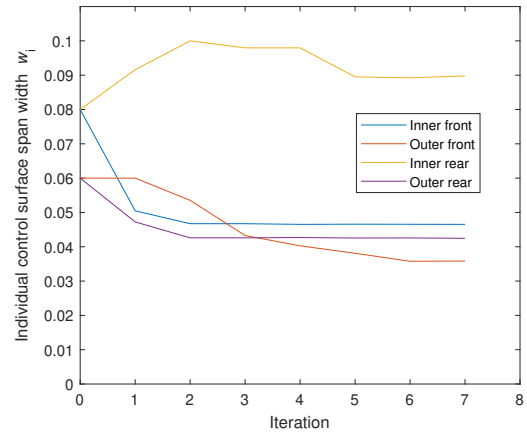


Figure A.16: CS span development for DA 3

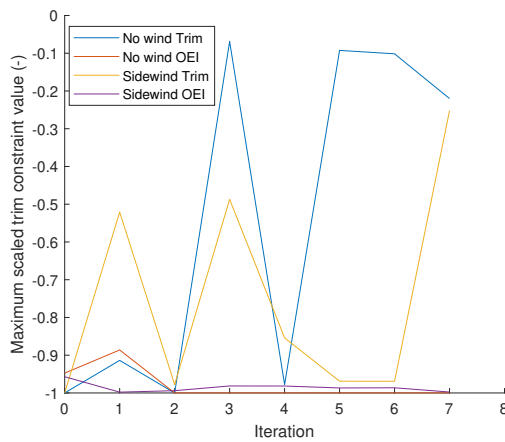


Figure A.17: Trim and OEI constraints for DA 3

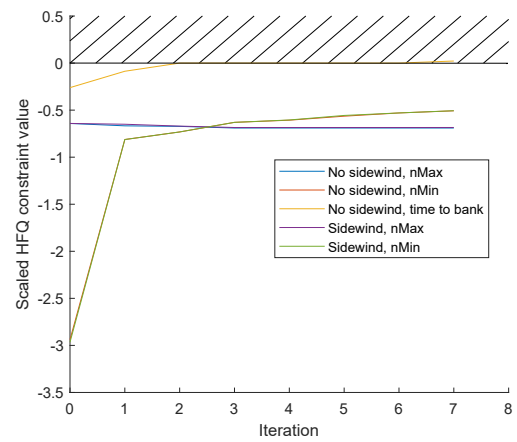


Figure A.18: HFQ constraints for DA 3

A.2. Detailed optimisation results for minimum area objective function

This section shows the optimisation plots for the optimisations using the minimum area objective function. It contains the iteration histories of the CS spans, and the constraint behaviours at every iteration of the optimiser for the three optimisation runs.

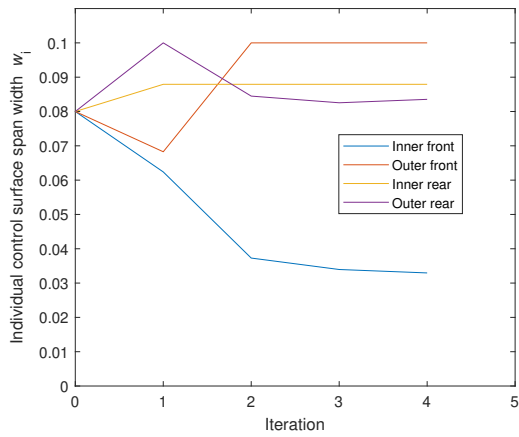


Figure A.19: CS span development for MG

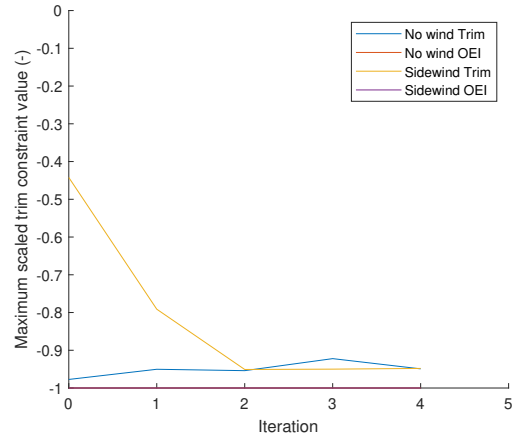


Figure A.20: Trim and OEI constraints for MG

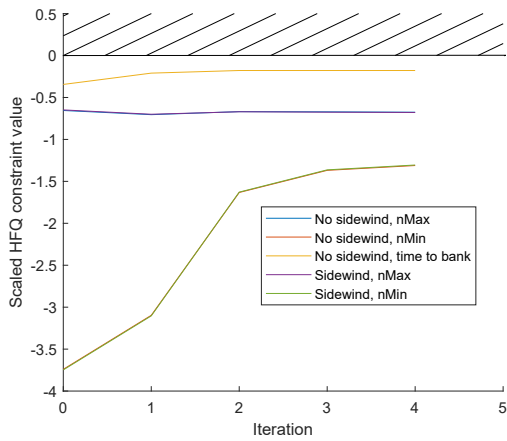


Figure A.21: HFQ constraints for MG

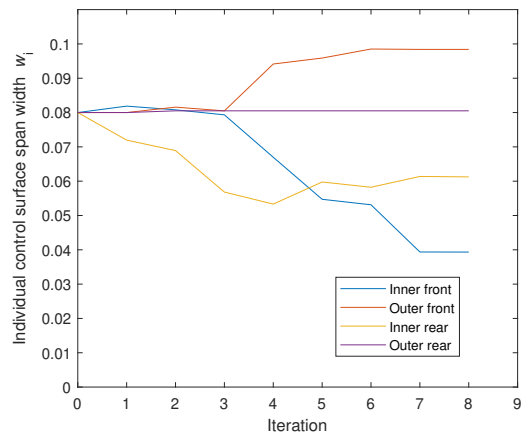


Figure A.22: CS span development for CPI

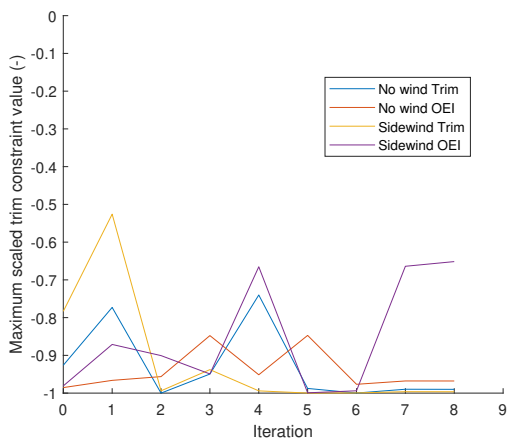


Figure A.23: Trim and OEI constraints for CPI

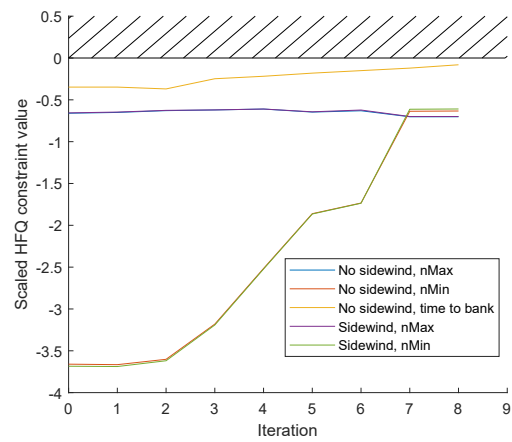


Figure A.24: HFQ constraints for CPI

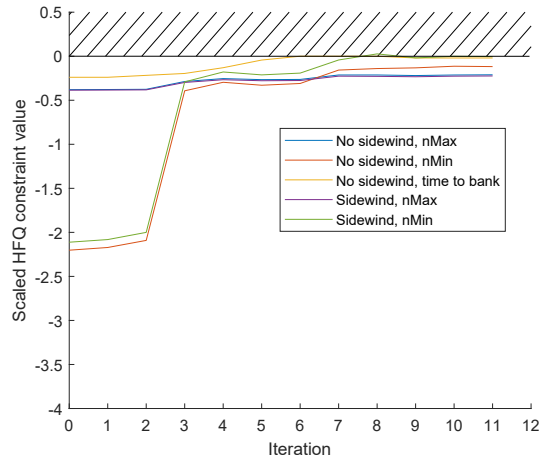


Figure A.27: HFQ constraints for DA

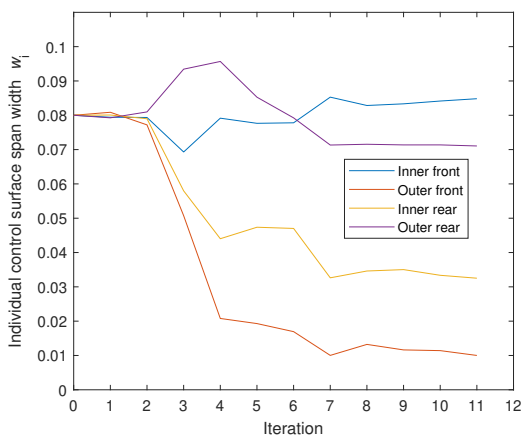


Figure A.25: CS span development for DA

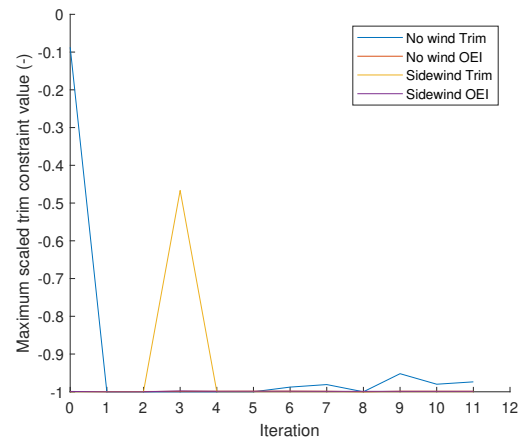


Figure A.26: Trim and OEI constraints for DA

A.3. Detailed optimisation results for improved rear CS placement minimum span objective function

This section shows the optimisation plots for the optimisations of the improved placement comparison using the minimum span objective function. It contains the iteration histories of the CS spans, and the constraint behaviours at every iteration of the optimiser for the two optimisation runs. The case B set-up has added another control surface further mid-wing. The case C set-up has only the mid-wing surface. The original inboard rear surface was removed.

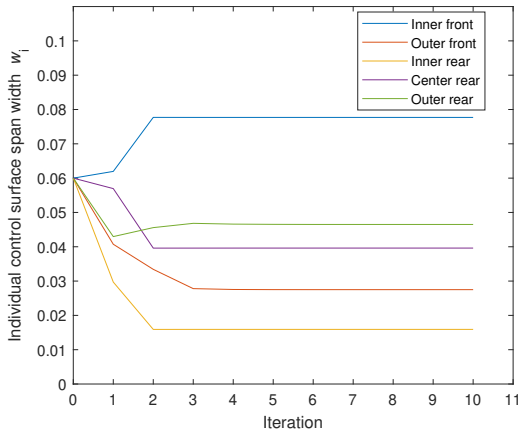


Figure A.28: CS span width development for case B

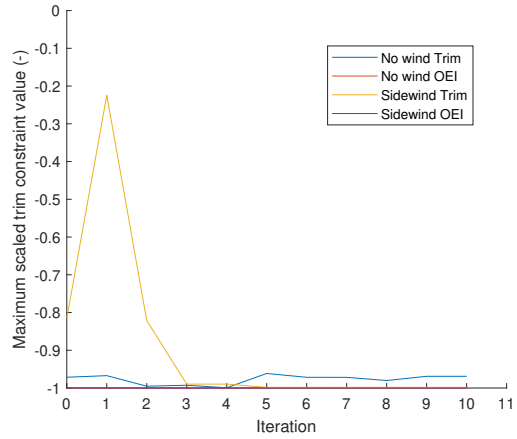


Figure A.29: Trim and OEI constraints for case B

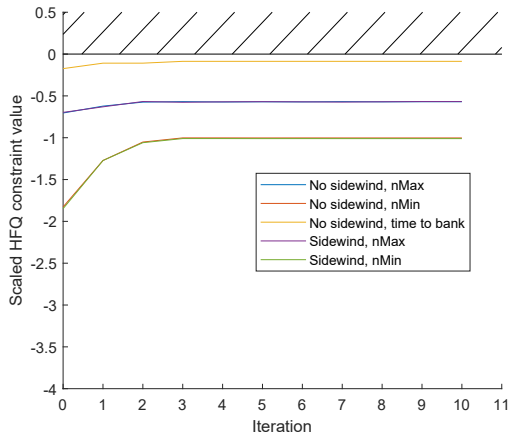


Figure A.30: HFQ constraints for case B

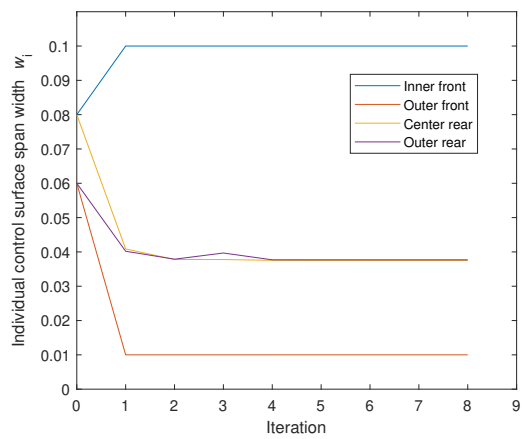


Figure A.31: CS span width development for case C

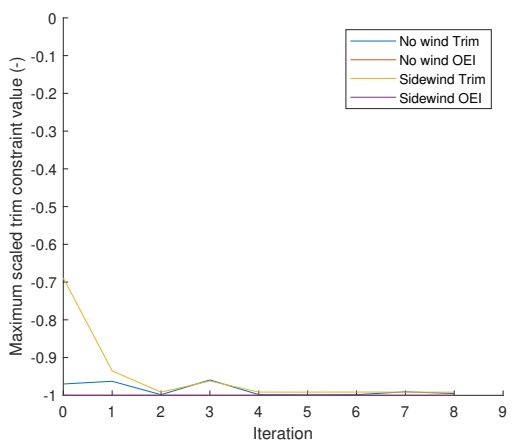


Figure A.32: Trim and OEI constraints for case C

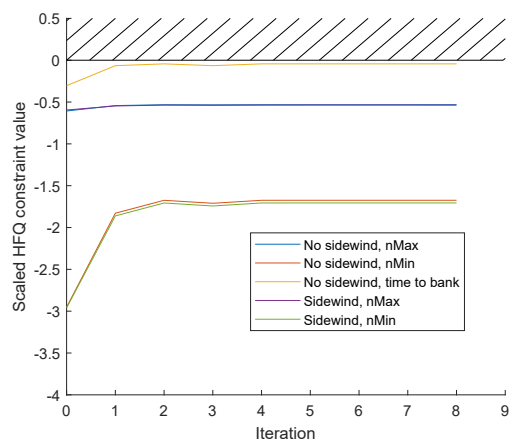
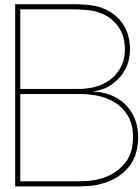


Figure A.33: HFQ constraints for case C



Exploring the effect of higher control surface numbers

The main study shows benefits of DA over MG. Theoretically, DA also offers additional design freedom. Especially, the question arises, whether more independent CSs and a free placement along the trailing edge may be advantageous. Hence, an exploratory investigation is performed to assess, whether three and four CSs per wing may result in smaller total required CS size, compared to the results above. For this, each CS is defined by the design variables inboard position η_i and CS width w_i .

The main goal of this exploratory analysis is not to provide a final design for an improved CS layout on the box wing, but to investigate the behaviour of the DA and the optimiser when they are given more freedom to find an optimal solution.

The additional design variables require the implementation of geometric constraints to avoid overlapping. Hence, if during the calculation two surfaces would intersect, the inner surface is constrained in width to the beginning of the outer surface by the system.

The free movement of the surfaces makes it impossible to define a sensible flap. So, the optimised control surfaces will also have to take over this role to achieve sufficient lift at the commanded approach speed. The goal of this preliminary investigation is thus not a direct comparison of additional CS compared to the main investigation, but to explore how resulting designs may differ in shape when the CS are allowed free movement. The exclusion of a flap in this analysis underlines that this is intended as an academic investigation, not specifically destined to yield a practical CS arrangement for a specific aircraft design.

The optimisation is performed using the DA algorithm and for two cases. One case uses three CS per wing, the other four. Figure B.1 shows the initial layout of the three CS case, with the initial points and bounds for all design variables shown in table 9. The four surface case uses the same bounds on its design variables, solely the initial values differ slightly to fit four surfaces on each wing. To retain a somewhat reasonable design, a lower limit of $w_{limit} = 0.01$ was imposed. If the CS shrink below this tolerance, the surface would be assumed to have a zero width for the aerodynamic and flight mechanic analysis.

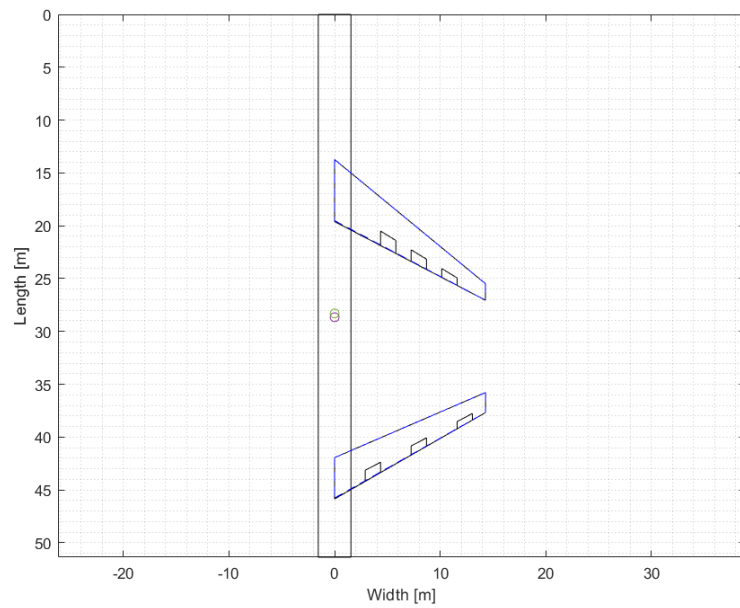


Figure B.1: Initial layout for the three CS investigation

Table B.1: Initial value and bounds for three surface individual optimisation

Wing	Control surface	Symbol	Initial value	Lower bound	Upper bound
Front wing	CS 1	η_1	0.15	0.1	0.45
		w_1	0.05	0	0.3
	CS 2	η_2	0.3	0.1	0.45
		w_2	0.05	0	0.3
CS 3	η_3	0.4	0.1	0.45	
	w_3	0.05	0	0.3	
Rear wing	CS 4	η_4	0.15	0.005	0.45
		w_4	0.05	0	0.4
	CS 5	η_5	0.3	0.005	0.45
		w_5	0.05	0	0.4
	CS 6	η_6	0.4	0.005	0.45
		w_6	0.05	0	0.4

Figures B.2 and B.3 show the results of the optimisations utilising direct allocation (DA) with a minimum area objective function. Two things can be observed from these results. First, the final result always optimised at least one control surface to have zero area, hence removing the surface from the wings. Some of the remaining control surfaces have shrunk to very small levels, such that from an engineering point of view, this design is not viable anymore. This is especially visible in the optimisation results with four initial surfaces, in figures B.3.

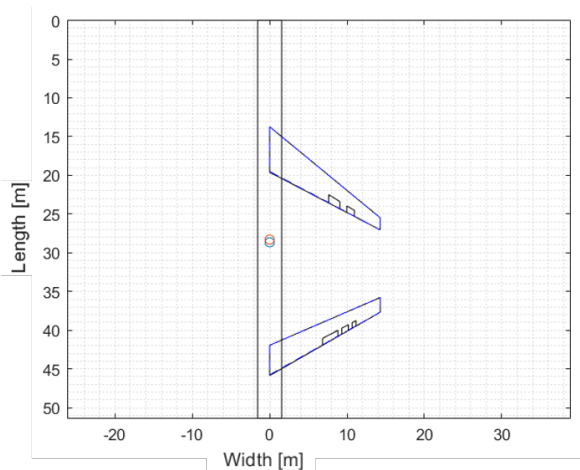


Figure B.2: Resulting layout of three individual CS using DA for minimum area

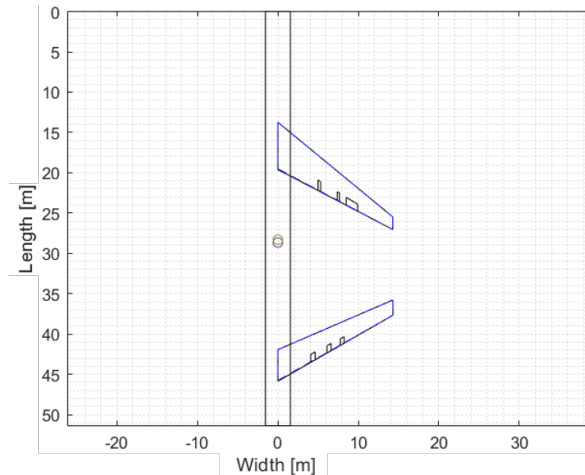


Figure B.3: Resulting layout of four individual CS using DA for minimum area

AVL as linear aerodynamic solver is still able to solve for the control effectiveness of these small surfaces, however, in reality nonlinearities will play a dominant role for these shapes and hence the practical control effectiveness of these small surfaces will be near zero. The linear nature of AVL's results are shown in figure B.4, where it is shown that even for small surfaces ($0.01 b_{wing}$), the CS effectiveness decreases to zero in a smooth manner for all aerodynamic coefficients.

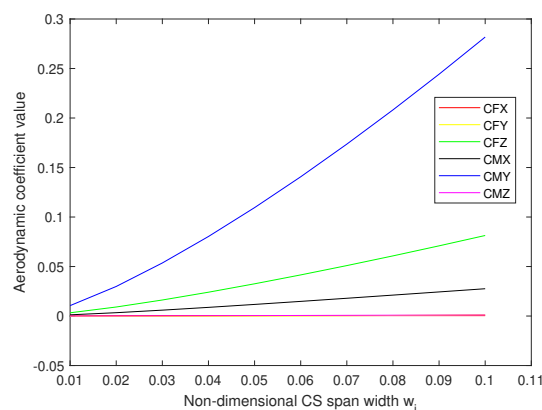


Figure B.4: Aerodynamic moment coefficients from AVL for a CS at ± 30 degrees deflection as function of non-dimensional span width

The calculations gave some insight that with multiple control surfaces, an optimal solution seems to reduce to less individual surfaces, especially visible on the front wing. Additionally, when comparing the objective function results with the main study, the results now are considerably smaller. This may have two major reasons: the removal of the flap reduces the required control power to counteract the pitching moment of an aircraft with extended flaps. Hence, the CS can be smaller. Secondly, the optimised locations may result in better effectiveness of the individual CS. However, this investigation is intended as an exploration and not a comparison to the main study, hence the results should be considered as trends, not absolute CS positions or sizes.

The optimisation behavior of the three surface case using DA is shown in figures B.5 to B.8. Figures B.5 and B.6 show how both the width and location of every CS changed sig-

nificantly over the course of the optimisation, and shows overall more variability compared to the main study results. The most interesting fact arises from the HFQ behavior in figure B.8. Removing the flap significantly reduces the pitching moment of the aircraft. Now, the CS have optimised to a point where the maximum pull up acceleration is the limiting constraint whereas the banking is not limiting. This is the exact opposite compared to the main study results.

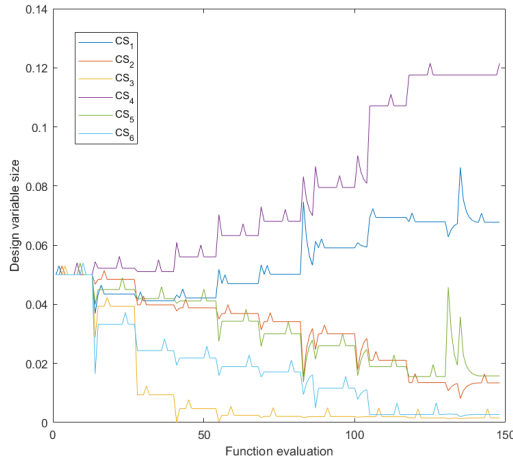


Figure B.5: CS span width development for three individual CS per wing

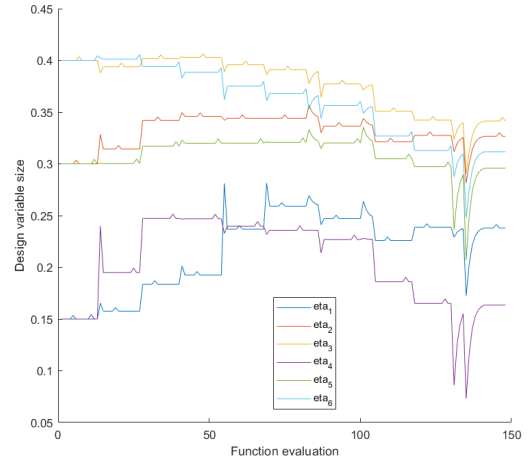


Figure B.6: CS inboard position development for three individual CS per wing

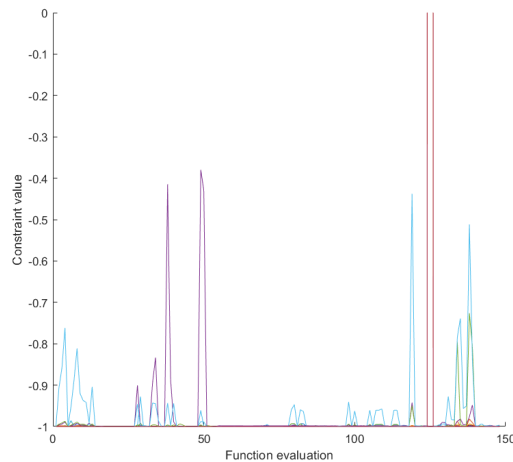


Figure B.7: Trim and OEI constraints for three individual CS per wing

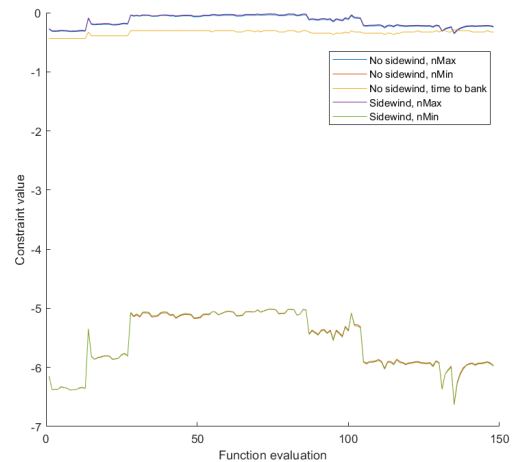


Figure B.8: HFQ constraints for three individual CS per wing

Following the observations, that the inclusion of η_i as design variables leads to infeasible results from an engineering perspective, the test case was amended to chain the CS together such that all surfaces will remain attached to each other at all times. Only the location of the inboard beginning of the control surface chain is kept as a position design variable ($\eta_{front}, \eta_{rear}$), and control surfaces are simplified to a width-only (w_i) optimisation. This investigation uses a minimum size of $w_{min} = 0.01$ for each surface to retain the initial number of CS on the wing.

The results for the three surface case are shown in figure B.9 and table B.2, for the four surface case they are shown in figure B.10 and table B.3.

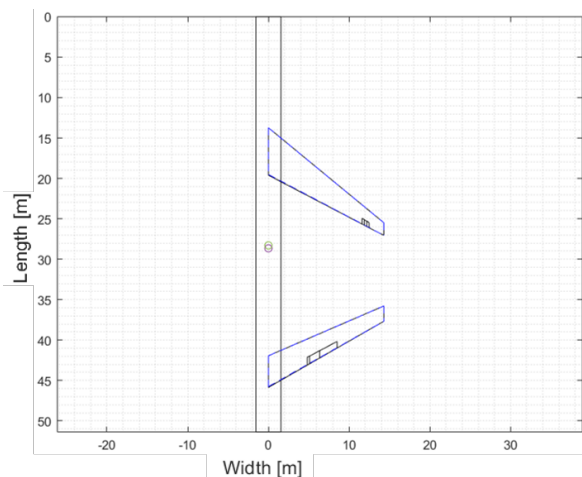


Figure B.9: Resulting layout of three connected CS using DA for minimum area

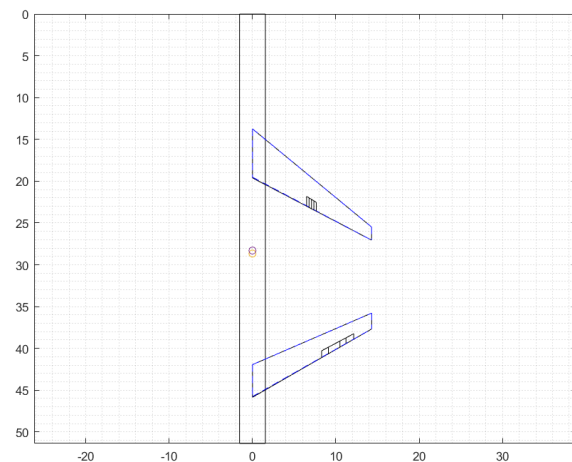


Figure B.10: Resulting layout of four connected CS using DA for minimum area

Table B.2: Resulting CS position and sizes as fraction of span of three connected surfaces for minimum area

Algorithm	Obj. (m^2)	η_{front}	w_1	w_2	w_3	η_{rear}	w_4	w_5	w_6
Initial	5.8019	0.25	0.04	0.04	0.04	0.2	0.04	0.04	0.04
DA	3.8796	0.40	0.01	0.01	0.01	0.166	0.01	0.044	0.074

Table B.3: Resulting CS position and sizes as fraction of span of four connected surfaces for minimum area

Alg.	Obj. (m^2)	Front	CS 1	CS 2	CS 3	CS 4	Rear	CS 5	CS 6	CS 7	CS 8
Initial	7.9422	0.3	0.04	0.04	0.04	0.04	0.1	0.04	0.04	0.04	0.04
DA	4.1352	0.224	0.01	0.01	0.01	0.01	0.286	0.028	0.048	0.025	0.032

These results show that the chaining of the CS leads to designs with a small total CS size on the front wing and a large total CS size on the rear wing. On the rear wing, the CS are not located specifically inboard and or outboard, but mainly mid-wing. The main difference in shape between the three and four CS calculations is that in the latter the front wing surfaces are placed further inboard, while the rear surfaces are placed further outboard. This is probably not an effect of the number of CS but again shows that multiple local minima concerning the optimum distribution for pitch and roll effectors may exist for a box wing design. This is similar to the two surface analyses where different layouts lead to comparable objective function results. It may also be a consequence of having removed flaps, which invalidates any reasonable comparison to the main studies or engineering evaluation

The optimisation behavior of the three connected surface case using DA is shown in figures B.11 to B.14. The overall shape is very similar to the three individual surface results. Interesting to note is that the CS on the front wing did not reduce right away, but only in the third iteration, when a rear surface was significantly enlarged. The HFQ results again show the impact of the missing flap on the constraints. Here, both pull and bank constraints are limiting.

The results of this exploratory investigation with free floating combined CS can be a hint for further studies, that more midwing positions with small surfaces on the front wing and large surfaces on the rear wing could be advantageous over the original inboard-outboard

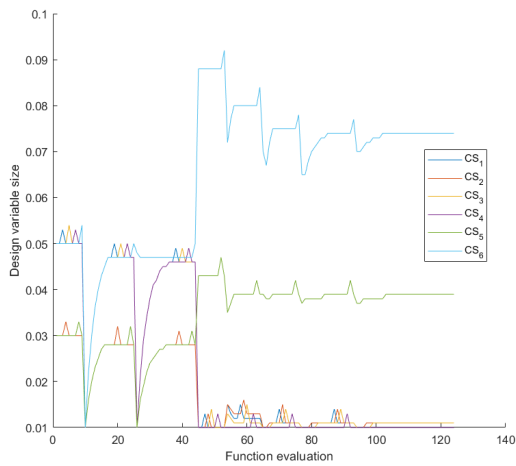


Figure B.11: CS span width development for three connected CS per wing

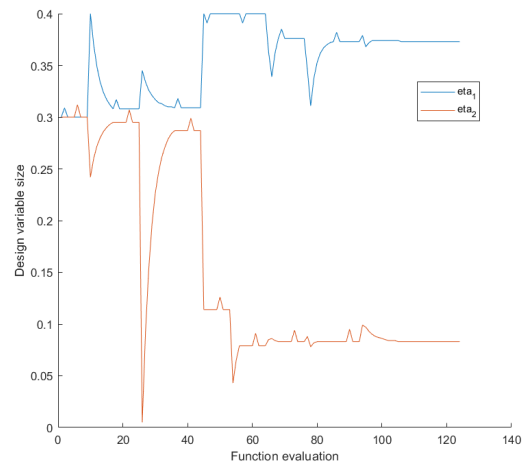


Figure B.12: CS inboard position development for three connected CS per wing

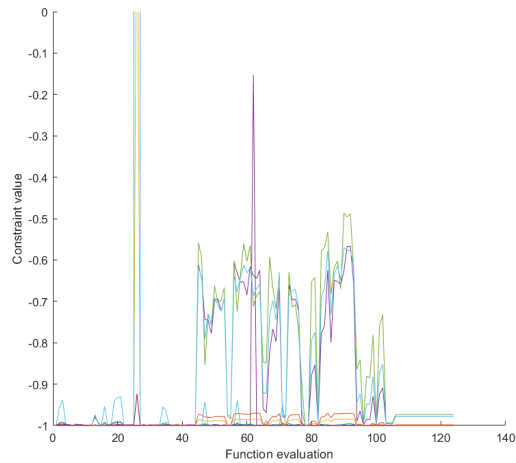


Figure B.13: Trim and OEI constraints for three connected CS per wing

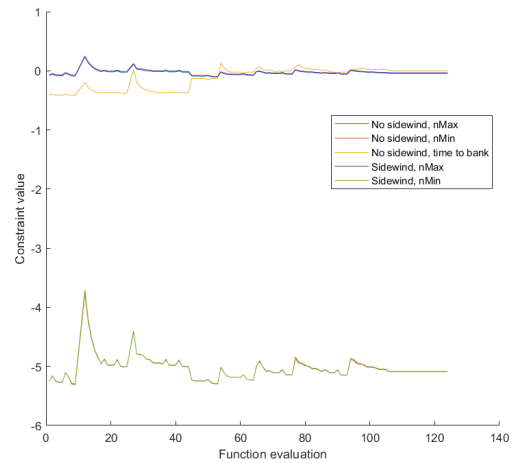


Figure B.14: HFQ constraints for three connected CS per wing

configuration. The three CS case here shows a more practical result, as the remainder of the front wing can be designated as a flap for a real design, with the rear wing CS distribution and size staying the same.